

Aus dem Leibniz Institut für Neurobiologie in Magdeburg

**Die Rolle der Zellen des angeborenen Immunsystems nach zerebraler
Ischämie**

D I S S E R T A T I O N

zur Erlangung des Doktorgrades

Dr. med.

(doctor medicinae)

an der Medizinischen Fakultät
der Otto-von-Guericke-Universität Magdeburg

vorgelegt von

Jens Neumann

aus

Magdeburg

Magdeburg

2011

DOKUMENTATIONSBLATT

Neumann, Jens:

Die Rolle der Zellen des angeborenen Immunsystems nach zerebraler Ischämie.

- 2011. – 12 S., 3 Anl.

Kurzreferat:

Der Schlaganfall ist in den Industrienationen die dritthäufigste Todesursache und eine der führenden Ursachen für eine dauerhafte Behinderung. Seit einiger Zeit wird auch der postischämischen immunologischen Reaktion Beachtung geschenkt. Nach wie vor wird darüber diskutiert, ob die immunologische Reaktion einen positiven oder negativen Einfluss auf die Schwere des Schlaganfalls hat. In Experimenten in denen eine Migration von Mikroglia (Immunzellen des Gehirns) zum Ort der Ischämie simuliert wurde, konnte gezeigt werden, dass Mikroglia in der Lage waren, innerhalb eines bestimmten Zeitfensters Nervenzellen vor dem Absterben zu schützen. Hingegen zeigten Experimente mit neutrophilen Granulozyten (Rekrutierung aus dem Blut), dass diese nach einem Schlaganfall den neuronalen Schaden sogar vergrößern. Wurden Mikroglia und neutrophile Granulozyten simultan zu ischämisch geschädigten Nervenzellen gegeben, konnte eine Reduktion der Neurotoxizität der Granulozyten erzielt werden. In weiteren Experimenten wurde beobachtet, dass Mikroglia die potenziell toxischen neutrophilen Granulozyten phagozytieren und somit die Nervenzellen indirekt nach einer Ischämie schützen. Daraus lässt sich schlussfolgern, dass die postischämische Immunreaktion different auf die Schwere des Schlaganfalls Einfluss nimmt und eine antiinflammatorische Behandlung aufgrund der auch positiven Eigenschaften der Immunantwort nicht unmittelbar zu einer Neuroprotektion führen muss.

INHALTSVERZEICHNIS

Einführung und Zusammenfassung.....	3
Referenzen.....	8
Publikationen.....	9
Danksagung.....	10
Lebenslauf.....	11

EINFÜHRUNG UND ZUSAMMENFASSUNG

Der Schlaganfall ist in den Industrienationen die dritthäufigste Todesursache und eine der führenden Ursachen für eine dauerhafte Behinderung. Die Grundlage eines Schlaganfalls stellt eine vorübergehende oder dauerhafte Durchblutungsstörung von Teilen des Gehirns dar. Dafür ursächlich sind Thromboembolien markoangiopathisch veränderter hirnzuführender und intrakranieller Gefäße, kardiogene Embolien oder mikroangiopathische Veränderungen. Die Behandlungsoptionen des Schlaganfalls sind limitiert. Kommt ein Patient mit entsprechenden Schlaganfall-Symptomen, wie z.B. akuten Lähmungen, Störungen der Sensibilität oder Sprachstörungen, steht innerhalb von 3 - 4,5 Stunden nach Einsetzen der Symptomatik medikamentös ausschließlich die Lyse-Therapie zur Rekanalisierung des verschlossenen Gefäßes als Behandlungsoption zur Verfügung. Im Folgenden besteht die Therapie darin, die relevanten Parameter, wie beispielsweise Blutdruck, Blutzucker und Elektrolyte optimal zu führen. Im Anschluss ist eine sekundärprophylaktische Therapie anzustreben, die an die Ursache des Schlaganfalls angepasst wird, z. B. die orale Antikoagulation bei absoluter Arrhythmie oder endovaskuläre Versorgung mit Gefäßdilatation und ggf. Implantation einer Gefäßstütze bei Gefäßverengungen.

Die Optionen in der akuten Schlaganfallbehandlung konnten auch nach jahrzehntelanger Forschung nicht erweitert werden. Seit einiger Zeit ist in der experimentellen Schlaganfallforschung die Beteiligung des Immunsystems in den Fokus gerückt.

Das hirneigene Immunsystem in Form der Mikroglia wird im Rahmen einer zerebralen Ischämie aktiviert. Mikroglia, die in gesundem Gewebe stark ramifiziert vorliegen, nehmen nach einer Ischämie eine „aktivierte“ amöboide Form an und migrieren zum Ort des ischämischen Schadens (Kreutzberg 1996).

Des Weiteren werden aus dem Blut 6 Stunden nach der Ischämie neutrophile Granulozyten und nach 12 - 24 Stunden Monozyten zum Ort des Schadens rekrutiert (Prestigiacomo 1999). Die Zellen des adaptiven Immunsystems hingegen sind erst nach etwa drei Tagen an der Randzone des ischämischen

Schadens zu finden (Liesz 2009). Wie sich die Immunzellen auf die Entwicklung des neuronalen Schadens auswirken, ist nach wie vor Gegenstand intensiver Diskussionen (del Zoppo 2001; Feuerstein 2001). Im Rahmen meiner Promotionsarbeit habe ich mich mit folgenden Fragen auseinandergesetzt:

1. Welchen Einfluss haben die Zellen des angeborenen Immunsystems (Mikroglia, neutrophile Granulozyten, Monozyten/Makrophagen) auf den neuronalen Schaden nach experimenteller zerebraler Ischämie?
2. Wie interagieren diese Immunzellen nach einer Ischämie?

Um diese Fragen adäquat zu bearbeiten, wurde ein postischämisches Entzündungsmodell etabliert. Als neuronales Modell kamen organotypische hippocampale Schnittkulturen (OHC) mit intakter dreidimensionaler Struktur zum Einsatz. Die zerebrale Ischämie wurde durch einen Sauerstoff- und Glukoseentzug (OGD) induziert. Um das Einwandern der Mikroglia in das geschädigte Areal und die Rekrutierung der neutrophilen Granulozyten sowie Monozyten aus dem Blut zu simulieren, wurden diese Zellen nach einer OGD auf die hippocampalen Schnittkulturen appliziert. Zur Beurteilung des neuronalen Schadens wurde 24 Stunden nach der OGD Propidiumjodid in das Kulturmedium gegeben. Propidiumjodid interkaliert in der DNA von Zellen mit zerstörter Membranintegrität und zeigt sich bei entsprechender Anregung rot fluoreszierend. Im Anschluss wurde die Intensität dieser Rotfärbung in den neuronalen Zellbändern des Hippokampus (Cornu Amonis 1-3) gemessen und damit der neuronale Zelltod erfasst. Es zeigte sich, dass exogen applizierte Mikroglia in einem Zeitfenster von 1 - 4 Stunden nach OGD neuroprotektiv wirken (Neumann 2006). Eine Applikation 6 Stunden nach OGD blieb wirkungslos. Des Weiteren stellte sich die Protektion durch die Mikroglia stimulusabhängig dar, denn eine vorausgehende Stimulation der Mikroglia mit einem bakteriellen Agens (Lipopolysaccharide) zeigte, dass sich die neuroprotektive Wirkung der Mikroglia aufhob.

Im Anschluss wurde das Verhalten der Mikroglia zu den Neuronen auf zellulärer Ebene untersucht. Dazu wurden hippocampale Schnittkulturen von transgenen Mäusen hergestellt, die unter dem Thy-1 Promotor das gelb fluoreszierende

Protein exprimieren. Dieses Protein wird selektiv von den Pyramidenzellen im Gehirn der Mäuse exprimiert und damit auch in den Pyramidenzellen des Cornu Amonis im Hippokampus. Zudem wurden die exogenen Mikroglia mit einem roten Farbstoff markiert. Im Anschluss wurden die gefärbten Mikroglia auf den organotypischen Schnitt appliziert. Mittels 2-Photonen-Mikroskopie konnte eine Ischämie-induzierte Migration der Mikroglia in die Schnittkultur beobachtet werden. Unter Kontrollbedingungen zeigte sich keine mikrogliale Migration. Darüber hinaus konnte eine Stimulus-(Ischämie)-abhängige Zell-Zell Interaktion zwischen Mikroglia und Neuron identifiziert werden (Neumann 2006).

Im Anschluss wurden die neutrophilen Granulozyten und Monozyten/Makrophagen hinsichtlich ihres Einflusses auf den neuronalen Schaden nach einer zerebralen Ischämie untersucht. Hier zeigte sich eine starke Neurotoxizität bei Applikation von neutrophilen Granulozyten nach der Ischämie, wohingegen die Monozyten/Makrophagen weder protektiv noch toxisch waren (Neumann 2008). Die Neurotoxizität der neutrophilen Granulozyten war nur nach Ischämie präsent. Unter Kontrollbedingungen hingegen waren die neutrophilen Granulozyten nicht toxisch, selbst die sensible Langzeitpotenzierung (LTP) wurde unter Kontrollbedingungen nicht beeinflusst. Auch hier erfolgte eine Untersuchung der migratorischen Eigenschaften. Neutrophile Granulozyten durchdrangen schon nach kurzer Zeit (ca. 30 Minuten – eine Stunde) die gesamte Tiefe des Hirnschnittes (ca. 200 µm). Es fand sich hinsichtlich der migratorischen Eigenschaften, anders als bei den Mikroglia, kein Unterschied zwischen Kontrollbedingungen und Ischämie. Zusammenfassend kann konstatiert werden, dass Mikroglia in den ersten 24 Stunden nach einer OGD neuroprotektiv, neutrophile Granulozyten neurotoxisch und Monozyten/Makrophagen neutral wirken.

Im Anschluss wurde das Modell erweitert, indem die Kombination der Immunzelltypen auf den neuronalen Schaden untersucht wurde. In diesen Experimenten stellte sich überraschenderweise heraus, dass die kombinierte Applikation von Mikroglia und neutrophilen Granulozyten die Neurotoxizität der Granulozyten signifikant reduziert. Eine Ko-Applikation von Monozyten/Makrophagen mit neutrophilen Granulozyten führte zu keiner signifikanten Reduzierung der granulozytären Neurotoxizität.

Um dieses Phänomen zu erklären, wurden Mikroglia und neutrophile Granulozyten zusammen kultiviert und mittels Zeitraffermikroskopie beobachtet. Dabei konnte eine Phagozytose der neutrophilen Granulozyten durch die Mikroglia beobachtet werden. Interessanterweise wurden nicht nur apoptotische, sondern auch vitale, sich bewegende Granulozyten phagozytiert. Aus der Peripherie ist bereits bekannt, dass Makrophagen apoptotische neutrophile Granulozyten phagozytieren. Jedoch gibt es keine Hinweise, dass Makrophagen vitale neutrophile Granulozyten aufnehmen. In einer Kultur aus Makrophagen und neutrophilen Granulozyten konnte keine Phagozytose von vitalen Granulozyten beobachtet werden. Das bedeutet, dass die Phagozytose von vitalen neutrophilen Granulozyten mikroglia-spezifisch zu sein scheint. Um herauszufinden, ob dieser Mechanismus eine indirekte Neuroprotektion darstellt, wurden die Experimente mit simultaner Applikation von Mikroglia und Granulozyten auf ischämisch geschädigte Hirnschnitte und Gabe von Phagozytoseinhibitoren durchgeführt. Die Inhibition von Integrin- und Lektinstrukturen führte zu einer signifikanten Abnahme der phagozytierten Granulozyten und hob die durch Mikroglia vermittelte Protektion auf. Daraus ist abzuleiten, dass die Phagozytose der neurotoxischen neutrophilen Granulozyten durch die Mikroglia einen indirekten neuroprotektiven Mechanismus darstellt (siehe Schema).

Zusammenfassend konnten folgende Erkenntnisse während der Promotionsarbeit gewonnen werden:

1. Mikroglia sind in den ersten 24 - 48 Stunden protektiv, wenn sie innerhalb von 4 Stunden am Ort der Ischämie sind.
2. Monozyten/Makrophagen sind in den ersten 24 - 48 Stunden nach Ischämie weder neuroprotektiv noch neurotoxisch.
3. Neutrophile Granulozyten sind neurotoxisch nach Ischämie, jedoch nicht unter Kontrollbedingungen.
4. Mikroglia migrieren stimulusabhängig im neuronalem Gewebe zum Ort des Schadens.
5. Neutrophile Granulozyten migrieren stimulus-unabhängig im neuronalen Gewebe.

6. Die durch Mikroglia vermittelte Protektion ist abhängig von der Art der Stimulus (ischämischer Stimulus – Mikroglia protektiv, bakterieller Stimulus – Mikroglia nicht protektiv).
7. Durch eine Ischämie kommt es zu einer Zell-Zell Interaktion zwischen Mikroglia und Neuronen.
8. Mikroglia reduzieren signifikant die neurotoxische Wirkung der neutrophilen Granulozyten nach einer Ischämie durch selektive Phagozytose von vitalen und proapoptotischen neutrophilen Granulozyten. Diese Phagozytose wird durch Integrin- und Lectinstrukturen vermittelt.

Aus diesen Ergebnissen ist folgendes postischämisches Szenario ableitbar:

Nach einer zerebralen Ischämie erfolgt eine Aktivierung der lokalen Mikroglia und die Attraktion der peripheren Mikroglia zum Ort des ischämischen Schadens. Mikroglia sind in der Lage, postischämisch geschädigte Neurone unter bestimmten Bedingungen vor weiterem Schaden (vor dem Tod) zu schützen. Durch die beobachtete Zell-Zell-Interaktion zwischen Mikroglia und Neuronen kann spekuliert werden, dass die Mikroglia die Fähigkeit besitzt, zwischen Neuronen zu differenzieren, die möglicherweise noch gerettet werden können oder bereits so stark geschädigt sind, dass eine Rettung nicht mehr möglich ist. Im Umkehrschluss könnte eine Beschleunigung des Sterbeprozesses eingeleitet werden, sodass mit konsekutiver Phagozytose die Freisetzung weiterer Entzündungsstimuli verhindert werden kann. Des Weiteren kommt es nach einer Ischämie zu einer Infiltration (Extravasion) von neutrophilen Granulozyten in das geschädigte Areal. Aufgrund der vorliegenden Ergebnisse kann spekuliert werden, dass Mikroglia infiltrierende neutrophile Granulozyten erkennen und spezifisch phagozytieren. Damit reduzieren Mikroglia die Neurotoxizität der neutrophilen Granulozyten im zerebralen Gewebe. Zusammenfassend können den Mikroglia unter experimentellen Bedingungen zwei neuroprotektive Eigenschaften zugeschrieben werden: einerseits die direkte Neuroprotektion über die Zell-Zell-Interaktion, andererseits die indirekte Neuroprotektion über die Phagozytose neurotoxischer neutrophiler Granulozyten.

REFERENZEN

Del Zoppo GJ, Becker KJ, Hallenbeck JM. (2001) Inflammation after stroke: is it harmful? Arch Neurol. Review.

Feuerstein GZ, Wang X (2001) Inflammation and stroke: benefits without harm? Arch Neurol.

Liesz A, Suri-Payer E, Veltkamp C, Doerr H, Sommer C, Rivest S, Giese T, Veltkamp R. (2009) Regulatory T cells are key cerebroprotective immunomodulators in acute experimental stroke. Nat Med.

Kreutzberg GW. (1996) Microglia: a sensor for pathological events in the CNS. Trends Neurosci. Review.

Prestigiacomo CJ, Kim SC, Connolly ES Jr, Liao H, Yan SF, Pinsky DJ. (1999) CD18-mediated neutrophil recruitment contributes to the pathogenesis of reperfused but not nonreperfused stroke. Stroke.

Neumann J, Sauerzweig S, Röncke R, Gunzer F, Dinkel K, Ullrich O, Gunzer M, Reymann KG. (2008) Microglia cells protect neurons by direct engulfment of invading neutrophil granulocytes: a new mechanism of CNS immune privilege. J Neurosci.

Neumann J, Gunzer M, Gutzeit HO, Ullrich O, Reymann KG, Dinkel K. (2006) Microglia provide neuroprotection after ischemia. FASEB J.

PUBLIKATIONEN

1. Neumann J, Gunzer M, Gutzeit HO, Ullrich O, Reymann KG, Dinkel K. *Microglia provide neuroprotection after ischemia*. FASEB J. 2006 Apr
2. Neumann J, Sauerzweig S, Rönicke R, Gunzer F, Dinkel K, Ullrich O, Gunzer M, Reymann KG. *Microglia cells protect neurons by direct engulfment of invading neutrophil granulocytes: a new mechanism of CNS immune privilege*. J Neurosci. 2008 Jun
3. Braun H, Bühnemann C, Neumann J, Reymann K. *Preparation of a tissue-like cortical primary culture from embryonic rats using Matrigel and serum free Start V Medium*. J Neurosci Methods. 2006 Oct
4. Niesner R, Andresen V, Neumann J, Spiecker H, Gunzer M. *Multifocal 2-photon microscopy for high-speed imaging deep in biological tissues*. Biophys J. 2007 Oct
5. Häke I, Schönenberger S, Neumann J, Reymann KG, Ismail G, Laily bin Din, Said IM, Zipp F, Ullrich O. *Neuroprotection and enhanced neurogenesis by extract from the tropical plant *Knema laurina* after inflammatory damage in living brain tissue*. J Neuroimmunol. 2009 Jan

DANKSAGUNG

An dieser Stelle möchte ich allen danken, die mich während der Anfertigung meiner Promotion begleitet haben und zum Gelingen dieser Arbeit entscheidend beigetragen haben:

Herrn Prof. Dr. KG. Reymann und Herrn Prof. Dr. Dr. O. Ullrich danke ich für die Überlassung des interessanten Promotionsthemas. Darüber hinaus danke ich ihnen dafür, dass mir während der Promotionsphase viele Freiheiten gewährt wurden und viel Vertrauen entgegen gebracht wurde.

Herrn Dr. Klaus Dinkel danke ich für die äußerst intensive Einführung in die wissenschaftliche Denkweise und die wissenschaftlichen und privaten Diskussionen, auch noch lange nachdem er die Arbeitsgruppe verlassen hatte.

Herrn Prof. Dr. Matthias Gunzer möchte ich dafür danken, dass auch er mir viel Vertrauen entgegen brachte, sodass er mir seine hochspezialisierte Technologie in kurzer Zeit für die Fragestellungen zur Verfügung stellte. Außerdem erinnere ich mich noch gerne an die exzellenten Diskussionen über unsere Manuskripte.

Ganz besonders möchte ich mich bei Frau Diane Mundil und Frau Susanne von Kenne für die herzliche Aufnahme in die Arbeitsgruppe und das Beibringen aller relevanten Arbeitsschritte für das Durchführen der Experimente bedanken.

Frau Dr. Claudia Bühnemann, Frau Dr. Monika Riek-Burchardt, Herrn Dr. Steven Sauerzweig, Herrn Dr. Holger Braun, Herrn Dr. Ullrich Schröder und Herrn Dr. Raik Rönicke danke ich für die hervorragenden Diskussionen beim Kaffee, für die netten Konferenzen und natürlich für die überaus kollegiale Interaktion und Kooperation bei wissenschaftlichen Fragestellungen.

Ganz besonders danke ich meinen Eltern, die mich während des gesamten Studiums und der Promotionsarbeit unterstützten, sowie meiner Frau Anneka, die aufgrund von vielen Experimenten viele Nächte alleine schlafen musste, dafür aber viel Verständnis aufbrachte.

LEBENS LAUF

Neumann, Jens

Geburtstag: 3. März 1980
Geburtsort: Magdeburg, Deutschland
Nationalität: deutsch
Familienstand: verheiratet, 2 Kinder
Anschrift: Junoweg 11, 39118 Magdeburg, Deutschland
Email: jens.neumann@sciencetoday.de
Phone: +49 (0) 1774666020

Ausbildung

1999 – 2000	Studium der Volkswirtschaftslehre Otto-von-Guericke-Universität Magdeburg
2000 – 2009	Studium der Medizin Otto-von-Guericke-Universität Magdeburg
2003	Physikum
2003 – 2005	Studium der Neurowissenschaften Otto-von-Guericke-Universität Magdeburg
09/2007 – 12/2007	Stanford Medical School, Depart. of Neurosurgery, USA Visiting Scientist (advisor: Prof. G. Steinberg, MD, PhD)
04/2009	Staatsexamen
seit 07/2009	Assistenzarzt Klinik für Neurologie, Universität Magdeburg
2004 – 2008	MD-Thesis: Institut für Immunologie/Leibniz Institut für Neurobiologie, Magdeburg (advisors: Prof. Dr. KG Reymann, Prof. Dr. M. Gunzer) - Die Rolle der Zellen des angeborenen Immunsystems nach zerebraler Ischämie. -

Jens Neumann
Junoweg 11
39118 Magdeburg

Ich erkläre, dass ich die der Medizinischen Fakultät der Otto-von-Guericke-Universität zur Promotion eingereichte Dissertation mit dem Titel

“Die Rolle der Zellen des angeborenen Immunsystems nach zerebraler Ischämie“

im Leibniz Institut für Neurobiologie

mit Unterstützung durch Prof. Dr. rer. nat. KG. Reymann,

ohne sonstige Hilfe durchgeführt und bei der Abfassung der Dissertation keine anderen als die dort aufgeführten Hilfsmittel benutzt habe.

Bei der Abfassung der Dissertation sind Rechte Dritter nicht verletzt worden.

Ich habe diese Dissertation bisher an keiner in- oder ausländischen Hochschule zur Promotion eingereicht. Ich übertrage der Medizinischen Fakultät das Recht, weitere Kopien meiner Dissertation herzustellen und zu vertreiben.

Magdeburg, den 21.02.2011

The FASEB Journal express article 10.1096/fj.05-4882fje. Published online February 10, 2006.

Microglia provide neuroprotection after ischemia

Jens Neumann,* Matthias Gunzer,[†] Herwig O. Gutzeit,[‡] Oliver Ullrich,[§] Klaus G. Reymann,*^{||} and Klaus Dinkel*

*Institute for Applied Neuroscience (FAN gGmbH), Leipziger Str. 44, D-39120, Magdeburg, Germany; [†]German Research Centre for Biotechnology, Research Group Immunodynamics, 38124 Braunschweig, Germany; [‡]Institute of Zoology, Technical University Dresden, Dresden, Germany; [§]Institute of Immunology, University Hospital Magdeburg, 39120 Magdeburg, Germany; ^{||}Leibniz Institute for Neurobiology, Project Group Neuropharmacology, Brenneckestr. 6, D-39118, Magdeburg, Germany

Corresponding author (current address): Klaus Dinkel, Jerini AG, Invalidenstr, 130 D-10115 Berlin, Germany. E-mail: dinkel@jerini.com

ABSTRACT

Many neurological insults are accompanied by a marked acute inflammatory reaction, involving the activation of microglia. Using a model of exogenous application of fluorescence-labeled BV2 microglia in pathophysiologically relevant concentrations onto organotypic hippocampal slice cultures, we investigated the specific effects of microglia on neuronal damage after ischemic injury. Neuronal cell death after oxygen-glucose deprivation (OGD) was determined by propidium iodide incorporation and Nissl staining. Migration and interaction with neurons were analyzed by time resolved 3-D two-photon microscopy. We show that microglia protect against OGD-induced neuronal damage and engage in close physical cell-cell contact with neurons in the damaged brain area. Neuroprotection and migration of microglia were not seen with integrin regulator CD11a-deficient microglia or HL-60 granulocytes. The induction of migration and neuron-microglia interaction deep inside the slice was markedly increased under OGD conditions. Lipopolysaccharide-prestimulated microglia failed to provide neuroprotection after OGD. Pharmacological interference with microglia function resulted in a reduced neuroprotection. Microglia proved to be neuroprotective even when applied up to 4 h after OGD, thus defining a “protective time window.” In acute injury such as trauma or stroke, appropriately activated microglia may primarily have a neuroprotective role. Anti-inflammatory treatment within the protective time window of microglia would therefore be counterintuitive.

Key words: neuroinflammation • stroke • organotypic cultures • two-photon microscopy • CD11a integrin

Abundant evidence exists that an inflammatory reaction is mounted within the central nervous system (CNS) following trauma, stroke, and seizure. The inflammation in response to acute brain injury is characterized by the infiltration of neutrophils and monocytes/macrophages into the respective brain parenchyma; activation of resident microglia; and expression of pro-inflammatory cytokines, adhesion molecules, and other inflammatory mediators (1, 2). A key issue regarding this well-described inflammation in brain injury is

whether this multifactorial reaction is beneficial or detrimental postischemia. Because of its complexity, the role of inflammation in acute brain injury remains a controversial subject (3, 4). Certain parts of inflammation may contribute to neuronal damage while other components of the inflammation may actually be beneficial in the recovery from brain damage.

To understand the complex process of neuroinflammation and to develop sensible therapeutic strategies, we sought to investigate the respective components individually. Since this is almost impossible to perform in vivo and the results obtained from dissociated cell cultures are obviously limited regarding their in vivo relevance, we chose organotypic interphase slice cultures as an experimental model. Organotypic hippocampal slice cultures (OHC) contain the different CNS cell types and retain the complex 3-D organization of the nervous tissue (5, 6). OHC are thus a useful model system to study the interaction of microglia and neurons (7, 8). Most importantly, OHC allowed us to analyze the effects of postischemic microglial inflammation excluding factors/cells from the peripheral inflammation such as granulocytes/monocytes.

Under normal conditions, microglia are quiescent and distributed throughout the CNS. One of the main characteristics of microglia is their rapid activation in response to a variety of stimuli. Several articles have reviewed reactive microglial responses in various pathologies such as axonal injury, ischemia, trauma, and neurodegenerative diseases (9–11). Hallmarks of activation are proliferation, change of morphology into an amoeboid shape, increased phagocytosis, up-regulation of MHC class I molecules, and the release of cytokines and growth factors (12, 13)

In this study, we investigated specific effects on neuronal damage exclusively mediated by microglia in OHC after ischemic injury by oxygen-glucose deprivation (OGD). Although OHC contain endogenous microglia, we performed exogenous application of the well characterized and widely used microglial cell line BV2 to the OHC. Our rationale for this was to be able to modify the microglia before application, increase the microglia numbers to pathophysiologically relevant levels, and enhance any microglial effects and ensure they were mediated exclusively by the microglia. This method represents a further development of the model previously established by our group (8, 14).

MATERIALS AND METHODS

OHC

Hippocampal interphase organotypic cultures were prepared as previously described (5, 15) from postnatal day 7–9 Wistar rats (Harlan Winkelmann GmbH, Borcheln, Germany). For two-photon microscopy experiments, hippocampal slice cultures were prepared from transgenic B6.Cg-TgN (Thy1-YFP)16Jrs mice (Jackson, distributed by Charles River, Wilmington, MA), which express EYFP at high levels in subsets of central neurons, including the pyramidal cells of the hippocampus (16). Hippocampi were dissected and transversely sliced into a 350 μm thickness on a McIlwain tissue chopper (The Mickle Laboratory Engineering, Surrey, UK). Slices were transferred to Millicell membranes (Millipore, Saint-Quentin-en-Yvelines, France). Cultures were maintained at 37°C in 1 ml of the serum-based medium containing 50% MEM-Hanks, 25% HBSS, 17 mM HEPES, 5 mM glucose (pH 7.8; Cell Concepts, Umkirch, Germany), 1 mM L-glutamine (Biochrom, Berlin, Germany), 25% horse serum (HS; Gibco, Eggenstein, Germany) and 0.5% Gentamycine (Biochrom) for 2–3 days. Cultures were then maintained in serum-free

medium (Neurobasal-A medium with B27 complement, glucose, 5 mM, L-glutamine, 1 mM). OHC were selected with propidium iodide (PI, 2 µg/ml; Sigma, St. Louis, MO) before the experiment ([Fig. 1A](#)).

OGD

The inserts with OHC were placed into 1 ml glucose-free medium (GFM) in sterile six-well culture plates (TPP). Before use, the GFM had been saturated with 5%CO₂/95%N₂ for 10 min. The six-well culture plates were transferred to a hypoxic chamber (Billups-Rothenberg). Then OHC were subjected to the OGD (40 min of OGD in a temperature-controlled hypoxic chamber; no glucose medium, N₂/CO₂ atmosphere). Cultures were kept in regular medium (plus glucose) under normoxic conditions. The cultures were analyzed 24 or 48 h after OGD.

Culture of microglia cell line BV2

The BV2 microglia were cultured in (D)MEM supplemented with 10% fetal calf serum (FCS) (Biochrom), 1% Pen/Strep (Biochrom), and 1% L-glutamine (Biochrom) at a density not exceeding 5 × 10⁵ cells/ml and maintained in 5% CO₂ at 37°C. To apply BV2 microglia, we trypsinated cells (trypsin/EDTA) (Biochrom) and then centrifuged them at 500g for 5 min and resuspended them in neurobasal medium (Gibco). Cell concentration was determined by counting cells in a “Neubauer” hemocytometer, and viability was assessed by trypan blue staining (0.4% trypan blue in PBS) (Sigma). BV2 microglia were applied directly onto 10-day-old OHSC in a volume of 2 µl neurobasal medium containing 8 × 10⁴ BV2 microglial cells, resulting in pathophysiologically relevant microglia numbers in the slice closely resembling those found in vivo after global ischemia. Viability of BV2 microglia after application onto the OHC was confirmed by prior staining with CMFDA (Molecular Probes, Leiden, The Netherlands).

BV2 microglia treatment

To stimulate BV2 microglia before application onto the OHCs, we either exposed them to OGD for 40 min or treated them with 50 µg/ml lipopolysaccharide (LPS; Sigma) for 4 h. To block protein synthesis in BV2 cells, we pretreated the microglia for 2 h with 10 µM anisomycin (Molecular Probes) before application. Microglia were either pretreated with 50 µM minocycline for 4 h before the application, or minocycline (25 µM; 50 µM) was applied simultaneously with the BV2 microglia at 1 h after OGD.

Culture and differentiation of cell line HL-60

Human acute promyelocytic leukemia HL-60 cells were cultured in RPMI-1640 (Biochrom) medium supplemented with 10% FCS (Biochrom) and 1% Pen/Strep (Biochrom) at a density up to 5 × 10⁵ cells/ml and maintained in 5% CO₂ at 37°C. To induce differentiation toward granulocytes, we treated HL-60 cells (2×10⁵ cells/ml) with 1 µM all-trans retinoic acid (ATRA) for 5 days. Before application, HL-60 cells were counted in a “Neubauer” hemocytometer, and viability was assessed by trypan blue staining (0.4% trypan blue in PBS) (Sigma).

Cloning of an antisense CD11a vector and transfection experiments

RNA was isolated from BV2 cells (RNeasy Maxi Kit, Qiagen, Valencia, CA) followed by a cDNA synthesis (cDNA Synthesis Kit, Clontech, Palo Alto, CA) with random hexamer primer

and amplification of the DNA of interest by PCR (MJ Research, Cambridge, MA). The ligation of the insert (antisense-CD11a) was made by using the Topo pCR 2.1 vector (Invitrogen, Carlsbad, CA) and the T4 DNA Ligase (New England BioLabs, Ipswich, MA). Competent *E. coli* cells (genotype TOP10F⁺) were transformed, and, in addition, the vector was isolated and sequenced. After cleavage of the antisense construct, the insert was ligated into the pcDNA3.1 vector (Invitrogen). Competent *E. coli* cells (genotype TOP10F⁺) were again transformed, and the vector was isolated for cell transfection experiments. Transfections of the pcDNA3.1-control vector and the asCD11a vector in BV2 microglial cells were performed by a lipofectin method (Rotifect, Carl-Roth). A stable cell line was established by selection with 100 µg/ml zeocin during 4 wk.

Analysis of cell death

Cell death was evaluated by cellular incorporation of propidium iodide (PI) 24 h and 48 h after OGD. Cultures were incubated with PI-containing medium (10 µM) for 2 h at 33°C. Fluorescent images were acquired semiautomatized (Nikon motorized stage; LUCIA software) and analyzed by densitometry to quantify necrotic cell death (LUCIA Image analysis software). Based on transmission light images, the area of analysis was determined excluding the dentate gyrus followed by conversion of the fluorescent image into a greyscale image. Background correction was performed automatically by a control square (150×150 µm) in the stratum moleculare outside the pyramidal cell layer. Damage was detected only in the CA area (CA1-CA2-CA3), thus representing neuronal damage. To combine data from individual experiments, the densitometric mean value of the respective insult of an individual experiment was set to 100% damage. All other data are given in % of insult damage. Nissl-staining was performed 24h after OGD. OHC were fixed with 4% PFA for 40 min at room temperature and were then maintained in 30% sucrose at 4°C for 2 days. OHC were then cryosectioned to 30 µm thick slices, and Nissl-staining was performed.

Two-photon microscopy

For two-photon microscopy, the microglial cell line was stained with cell tracker orange (CTO, 5 µM in PBS, 10 min, room temperature; Molecular Probes). At different time points after OGD induction, the microglia-brain slice cocultures were subjected to 3-D two-photon microscopy using an Olympus BX51WI stage equipped with a XLUMPL ×20, NA 0.95 water dipping lens and a multibeam scanhead (LaVision Biotech, Bielefeld, Germany) run at 16 beams with full laser power. Image detection was done with a cooled CCD camera (Imager Intense, LaVision, Goettingen, Germany). Brain slices were imaged in live modus at 800 and 920 nm wavelength of the laser (MaiTai, Spectra physics) using a scanning window of 90 × 150 µm to obtain the upper most as well as the lowest possible position within the slice. These positions defined the maximum cube of tissue available for imaging. Subsequently, this cube was scanned with a resolution in Z of 0.5 µm, first at 920 nm and then at 800 nm wavelength with no filter. The emission of EYFP at 800 nm was negligible as was the emission of CTO at 920 nm. Image stacks were exported as two independent 8-Bit multilayer TIFF stacks and subsequently reconstructed using the AMIRA software package (Berlin, Germany).

Statistical analysis

All data are given as mean \pm SD. Statistical analysis was performed by one-way ANOVA followed by post hoc comparison (Tukey test). $P < 0.05$ was considered statistically significant.

RESULTS

Microglia protect against OGD-induced neuronal damage

The focus of this study was to elucidate the role of microglial cells in a model of ischemic injury in vitro (see [Fig. 1A](#) for experimental setup). Direct application of the microglial cell line BV2 (up to 8×10^4 cells/slice in 2 μ l) onto otherwise untreated OHC had no effect on neuronal viability in the CA area after 24 h (control in [Fig. 1B](#), [1C](#)). For all the following experiments involving direct application, 2 μ l of 4×10^4 cells/ μ l was used. Since only ~20% of the applied microglia adhered to or invaded into the slice, this exogenous application resulted in in vitro microglia (OX-42+) numbers ($\sim 1.9 \times 10^3$) that are also found in vivo in the hippocampus after global ischemia ($\sim 2.3 \times 10^3$). When microglia were transferred directly 24 h before OGD, we observed a significant reduction ($P < 0.001$ vs. OGD) of the OGD-induced neuronal damage ([Fig. 1B](#)). Furthermore, this microglial neuroprotection was also effective when the microglia were added 1 h or 4 h after OGD ([Fig. 1B](#)). At 6 h after OGD, however, the application of microglia was not protective anymore ([Fig. 1B](#)). Representative fluorescent images for the densitometric quantification ([Fig. 1B](#)) are shown in [Fig. 1C](#). We could also confirm the neuroprotective effect of microglia by Nissl staining. At a $\times 20$ magnification, we observed a lower neuron density and a higher number of small shrunken neuronal cell bodies in OGD-treated cultures vs. cultures treated with OGD plus microglia ([Fig. 1D](#)). Microglia viability was monitored with CMFDA vital staining before application. On the slice border, viable (CMFDA+) microglia showed some PI uptake under control conditions, which was dramatically increased after OGD (see [Fig. 1C](#); arrowhead).

Granulocytes fail to provide neuroprotection after OGD

To investigate whether the observed neuroprotective effect was specific for microglia, we performed experiments using the granulocyte cell line HL-60. Undifferentiated HL-60 cells had no protective effect after OGD and did not alter neuronal viability under basal conditions ([Fig. 2A](#)). In contrast, when HL-60 cells had been differentiated into the granulocyte phenotype by treatment with ATRA they caused significant neuronal cell death under basal conditions ([Fig. 2A](#)). However, differentiated HL-60 cells did not exacerbate or ameliorate neuronal cell loss after OGD ([Fig. 2A](#)), thus confirming the specificity of the neuroprotective microglia effect. Representative fluorescent images for the densitometric quantification ([Fig. 2A](#)) are shown in [Fig. 2B](#). These results prompted us to investigate whether a specific interaction occurs between microglia and neurons in the slice cultures.

Microglia migrate into hippocampal slices and engage in close cell-cell contact with neurons after OGD

For the analysis of microglial migration and a possible microglia-neuron interaction in living organotypic slice cultures over time, we used 3-D time-resolved two-photon microscopy. Microglia were labeled with cell tracker orange (CTO) and then directly applied onto OHC

prepared from transgenic B6.Cg-TgN (Thy1-YFP)16Jrs mice. In these transgenic mice, a subset of neurons (particularly the CA1 area) is labeled by expression of EYFP. Two-photon microscopy was performed at 1, 7, and 20 h after OGD and 16 h after microglia application under basal conditions (Table 1). Representative images are shown as 3-D reconstruction and a 2-D collapsed side view of the individual confocal planes (Fig. 3). Under basal conditions, the majority of microglia stayed on the surface of the slice and rarely migrated into the slice (Fig. 3A, 3B). In very few cases, a cellular microglia-neuron interaction was observed on the surface of the slice. This interaction is best described as a “capping” of the neuron by the microglia (Fig. 3Aa).

One hour after OGD, the majority of microglia were still on the slice surface; however, most of these microglia showed the “capping” interaction with the first neuronal layer (Fig. 3C, 3D). Seven hours after OGD, microglia were detected frequently inside of the slice culture (~70 μm depth). The “capping” interaction could be observed at a majority of microglia on the surface and often inside of the slice (70 μm depth; Fig. 3E, 3F). The top neuronal layer (0–30 μm depth) was still detectable at this time point (Fig. 3D, 3E). At 20 h after OGD, the majority of microglia had migrated into the slice (80 μm depth) and the top neuronal layer was destroyed except for a few EYFP+ fragments (Fig. 3G, 3H). We could observe a “capping” interaction of microglia with these fragments on the surface, but the majority of “capping” was detected inside of the slice (80 μm depth; Fig. 3G, 3H).

Duration of the microglial neuroprotection after OGD

Next we wanted to assess how long the microglia protective effect lasted. Neuronal cell death in the CA area was analyzed by PI uptake densitometry at 24 and 48 h after OGD. Because of limitations of our experimental culture system, we were unable to analyze time points later than 48 h after OGD. We observed a significant protection against OGD-induced neuronal damage at 24 h and 48 h when the microglia were applied to the slice 1 h after OGD (Fig. 4).

CD11a-deficient microglia fail to provide neuroprotection

Based on the two-photon data, we suggested that microglial migration into the slice and subsequent interaction with neurons are necessary to provide neuroprotection. To elucidate the molecular basis for the microglia-mediated neuroprotective effect after OGD, we generated BV2 microglia that are unable to express the integrin CD11a. Antisense CD11a-transfected BV2 [asCD11a] were applied 1 h after OGD directly onto the OHC. We found that asCD11a microglia failed to provide neuroprotection after OGD ($P < 0.001$ BV2 [asCD11a] vs. BV2; $n = 7-18$ /bar). Representative fluorescent images for the densitometric quantification (Fig. 5A) are shown in Fig. 5B. We could further show by 3-D time-resolved two-photon microscopy that the [asCD11a] were still engaging in a “capping” interaction with the neurons on the slice surface 1 h after OGD (Fig. 6A). This suggested that the “capping” interaction occurred independently of CD11a expression and was not crucial for the neuroprotective effect. The migration of microglia deep into the slice culture after OGD was severely inhibited. The [asCD11a] microglia were unable to migrate deeper than 50 μm into the injured slice at 1, 7, and 20 h after OGD (Fig. 6B–D) and were not colocalized at that depth with neurons, whereas wt-microglia were found colocalized with neurons as deep as 80 μm in the slice (Fig. 3H). These data supported our hypothesis that CD11a-mediated microglial migration into the injured slice may be necessary for neuroprotection.

LPS-stimulated microglia fail to provide neuroprotection after OGD

We further addressed whether preactivation of microglia by OGD or LPS (50 μ g, 4 h) had an effect on neuroprotection after OGD. Microglia were therefore exposed to OGD or LPS before application. Under control conditions, the application of OGD-preactivated microglia had no significant neurotoxic effect in the CA1 area ([Fig. 7A](#)). LPS-preactivated microglia, however, caused a significant ($P < 0.001$ vs. control) neurotoxic effect on untreated control cultures ([Fig. 7A](#)). When OGD-preactivated microglia were applied onto slice cultures 1 h after the slice had been subjected to OGD, approximately the same neuroprotective effect as with naïve microglia was observed ($P < 0.01$ vs. OGD; [Fig. 7A](#)). In contrast, LPS-preactivated microglia failed to induce neuroprotection after OGD ([Fig. 7A](#)).

Representative fluorescent images for the densitometric quantification ([Fig. 7A](#)) are shown in [Fig. 7B](#). These data suggested that the observed neuroprotective microglial response required an injury-specific stimulus.

Pharmacological interference with microglial function causes reduced microglia-mediated neuroprotection

We investigated whether the observed microglial neuroprotective effect could be influenced by impairment of microglial function. Microglia were added directly onto the slice culture at 1 h after OGD. When microglia were pretreated with the protein-synthesis inhibitor anisomycin (2 h, 10 μ M), we observed a significant reduction ($P < 0.05$ vs. OGD/BV2) in neuroprotection compared with untreated microglia ([Fig. 8A](#)). This indicates that de novo protein synthesis seems to be necessary to achieve the highest neuroprotective microglia effect. The partial neuroprotection still observed with anisomycin-treated microglia seems to be independent of de novo protein synthesis or could be explained by the reversibility of protein synthesis inhibition by anisomycin. When microglia were pretreated with the monocyte inhibitor minocycline (4 h, 50 μ M), we observed a significant reduction ($P < 0.001$ vs. BV2) in neuroprotection compared with untreated microglia ([Fig. 8A](#)). The simultaneous application of microglia with 25 or 50 μ M minocycline at 1 h after OGD also caused a significantly lower ($P < 0.001$; $P < 0.01$ vs. OGD/BV2) neuroprotection compared with the protection with microglia alone ([Fig. 8A](#)). However, there was no dose-response effect detected. Representative fluorescent images for the densitometric quantification are shown in [Fig. 8B](#).

DISCUSSION

The role of inflammation (harmful or beneficial) in the pathogenesis of acute brain injury remains a controversial subject (3, 4). To investigate the complex process of neuroinflammation, we chose organotypic interphase slice cultures as an experimental model. The aim of this study was to investigate effects of microglia on neuronal death in OHC after ischemic injury. Our experimental design includes the exogenous application of the microglial cell line BV2 to the OHC. We could thus modify microglia before application, reach pathophysiologically relevant microglia numbers, and ensure that the observed effects were mediated exclusively by the microglia.

We first found that direct application of up to 8×10^4 BV2 microglia was well tolerated by OHC and did not cause any neuronal cell death, demonstrating that under normal conditions the BV2

cell line is not neurotoxic in our model. Only ~20% of the applied BV2 microglia adhered to the slice and had therefore direct contact to the tissue, while the majority of BV2 microglia accumulated on the border of the slice culture. We found that the exogenous application of 8×10^4 microglia resulted in pathophysiologically relevant microglia numbers inside/on top of the slice, resembling closely postischemic in vivo conditions (C. Pforte, personal communication). Under insult conditions, we observed that neuronal damage caused by OGD was significantly reduced by direct application of microglia onto OHC. The microglia were neuroprotective when applied 24 h before and up until 4 h after OGD, but not at 6 h after OGD. This is in line with data from our lab (unpublished observations) and others (17) showing that in this model significant neuronal cell death appeared at 6–9 h after OGD. Microglia seem to possess a protective time window after an ischemic insult.

We could further show that this neuroprotective effect was still evident until at least 48 h after OGD. We found that the observed neuroprotection was specific for microglia since the human granulocyte cell line HL-60 had no significant effect on neuronal damage after OGD. Under basal conditions, differentiated HL-60 granulocytes caused a significant increase in neuron death and there was also a tendency toward worsening injury-induced neuron death by HL-60 granulocytes. These results are in line with recent data showing the neurotoxic potential of granulocytes (18, 19)

These results indicated that the microglial neuroprotection might be based on a specific interaction between microglia and neurons in the slice cultures. Previous studies showed that exogenously applied microglia migrated into slice cultures under normal and NMDA-excitotoxic conditions (20, 21). We used a novel two-photon microscopy approach to study the interaction of fluorescence-labeled microglia with fluorescence-labeled neurons in living brain tissue of transgenic animals. We show for the first time that microglia migrated into the slice and engaged in close cell-cell contact with neurons (“capping”). Furthermore, the induction of migration and neuron-microglia interaction deep inside the slice were dramatically increased by OGD. Based on our 3-D reconstruction images, we propose the following “mode of action” for the microglia-mediated protection. Immediately after OGD, microglia are activated by injured neurons and engage in close cell-cell contact with the first neuronal layer (“capping”). Since these neurons die later on, this capping could ensure the early recognition and fast phagocytic removal of dying/dead neurons. This mechanism would provide protection for the neurons in the deeper layers of the slice by minimizing the exposure time and dose of these cells to cytotoxic cell contents/debris released from dead/dying neurons. At later time points, we detected microglia that had migrated ~80 μm into the slice. These microglia could provide trophic support by the release of growth factors to improve the survival of the neurons in the deeper layers of the slice. The close proximity of injured neurons to microglia may also facilitate the targeted delivery of neurotrophic growth factors such as BDNF, GDNF, NGF, or TGF- β (12, 22).

Here the question arises: which mechanism directs microglial cells to the region of injury neurons, facilitates their migration, and keeps them in close cell-cell contact with the damaged neurons? Since migration and adhesion of microglial cells is mediated at least partially by expression of the integrin CD11a (8), we tested the possibility that this molecule is also involved in the observed neuroprotective action. Indeed, we found that microglial cells with down-regulated CD11a expression failed to protect neurons after ischemic damage and showed that CD11a expression and therefore assembly of LFA-1 is involved in the protective innate immunity provided by invading microglial cells, by enabling migration (8). Direct microglia-

neuron cell-cell contact (23) could also play a role in the deeper layers of the slice; however, the “capping” interaction between microglia and neurons on the slice surface was also observed in the absence of CD11a expression and neuroprotection.

We could also show that LPS-prestimulated microglia in contrast to naïve and OGD-preactivated microglia failed to provide neuroprotection after OGD. This suggests that microglia are differentially activated by injury-specific stimuli and can in turn only be beneficial in the corresponding injury model. Consequently, it is not surprising that LPS activation of microglia did not result in neuroprotection but instead in an exacerbation of cerebral ischemic injury (24). A pharmacologically induced impairment of microglial function resulted in a reduced neuroprotective effect after OGD. This was demonstrated by pretreatment of microglia with the protein synthesis inhibitor anisomycin or the anti-inflammatory tetracycline derivative minocycline, which inhibits the p38 MAPK pathway. In contrast to our data, minocycline has been shown to be neuroprotective against excitotoxicity and brain ischemia (25, 26). In these studies, minocycline could exert effects not exclusively on microglia but also on all other cell types (e.g., neurons and/or astrocytes). Due to our experimental design (pretreatment of microglia with minocycline before exogenous application), we could exclude side effects of the respective compounds on cell types other than microglia.

The demonstrated neuroprotective effect of microglia seems to be in sharp contradiction to previous studies suggesting that activation of microglia contributes to ischemic and excitotoxic cell death (25, 27–31). However, much of the information on the neurotoxic properties of activated microglia is derived from in vitro studies using monolayer dissociated cell cultures (26, 32–34). As mentioned previously, individual investigation of specific components of neuroinflammation after ischemia is almost impossible using in vivo studies. Often, conclusions are drawn from in vivo studies about the role of microglia without differentiation between microglia, macrophages, and neutrophils and their individual effects and reactions to various treatments. Moreover, several lines of evidence suggesting that postischemic inflammation has deleterious effects on ischemic injury focus on the reduction of leukocyte infiltration as a therapeutic target and not on microglia inhibition (35, 36). As a consequence of this generalization, microglia suffer from a bad reputation as contributors of cell death in ischemic and neurodegenerative disorders. On the other hand, considerable evidence shows that microglial activation after acute CNS injury is triggered by injured/dying neurons and results in reduction of neuronal damage and tissue repair (37–46). In OHC, excitotoxic neuronal damage was increased by pharmacological depletion of microglia (47) whereas NMDA neurotoxicity was decreased by microglia overexpressing the macrophage colony-stimulating factor receptor (48). Nimmerjahn et al. showed that microglia interact with endothelial cells to shield a focal blood-brain barrier disruption, providing another example of how microglia protect the brain environment by direct cell interaction (49).

In summary, our results demonstrate for the first time that microglia in pathophysiologically relevant numbers protect against OGD-induced neuronal damage and engage in close contact with neurons in living brain tissue. There is also evidence for a protective time window of microglia after ischemia which should not be the target of anti-inflammatory intervention. There is no doubt that microglia can secrete potentially neurotoxic substances, but also factors to promote neuronal survival and tissue repair (39, 50). It seems likely that the type and degree of injury (e.g., stroke, acute ischemia, Alzheimer’s disease, and chronic neurodegeneration) activate microglia differently toward performing neuroprotective or neurodestructive effects.

ACKNOWLEDGMENTS

This work was supported by grants to KGR from the EU framework “Quality of Life Program” QLK3-CT-2001-00407 and from the State of Saxony-Anhalt 3594M/0405M. We thank C. Pforte for sharing her data on microglia numbers in the hippocampus after global ischemia in rats. We also thank Diane Schrader and Susanne v. Kenne for excellent technical assistance.

REFERENCES

1. Dirnagl, U., Iadecola, C., and Moskowitz, M. A. (1999) Pathobiology of ischaemic stroke: an integrated view. *Trends Neurosci.* **22**, 391–397
2. Feuerstein, G., Wang, X., and Barone, F. (1998) *Cerebrovascular Disease: Pathophysiology, Diagnosis and Management*, Blackwell Science, London
3. del Zoppo, G. J., Becker, K. J., and Hallenbeck, J. M. (2001) Inflammation after stroke: is it harmful? *Arch. Neurol.* **58**, 669–672
4. Feuerstein, G. Z., and Wang, X. (2001) Inflammation and stroke: benefits without harm? *Arch. Neurol.* **58**, 672–674
5. Stoppini, L., Buchs, P. A., and Muller, D. (1991) A simple method for organotypic cultures of nervous tissue. *J. Neurosci. Methods* **37**, 173–182
6. Gahwiler, B. H., Capogna, M., Debanne, D., McKinney, R. A., and Thompson, S. M. (1997) Organotypic slice cultures: a technique has come of age. *Trends Neurosci.* **20**, 471–477
7. Czapiga, M., and Colton, C. A. (1999) Function of microglia in organotypic slice cultures. *J. Neurosci. Res.* **56**, 644–651
8. Diestel, A., Aktas, O., Hackel, D., Hake, I., Meier, S., Raine, C. S., Nitsch, R., Zipp, F., and Ullrich, O. (2003) Activation of microglial poly(ADP-ribose)-polymerase-1 by cholesterol breakdown products during neuroinflammation: a link between demyelination and neuronal damage. *J. Exp. Med.* **198**, 1729–1740
9. Banati, R. B., and Graeber, M. B. (1994) Surveillance, intervention and cytotoxicity: is there a protective role of microglia? *Dev. Neurosci.* **16**, 114–127
10. Kreutzberg, G. W. (1996) Microglia: a sensor for pathological events in the CNS. *Trends Neurosci.* **19**, 312–318
11. Minghetti, L., and Levi, G. (1998) Microglia as effector cells in brain damage and repair: focus on prostanoids and nitric oxide. *Prog. Neurobiol.* **54**, 99–125
12. Batchelor, P. E., Liberatore, G. T., Wong, J. Y., Porritt, M. J., Frerichs, F., Donnan, G. A., and Howells, D. W. (1999) Activated macrophages and microglia induce dopaminergic sprouting in the injured striatum and express brain-derived neurotrophic factor and glial cell line-derived neurotrophic factor. *J. Neurosci.* **19**, 1708–1716
13. Hanisch, U. K. (2002) Microglia as a source and target of cytokines. *Glia* **40**, 140–155

14. Ullrich, O., Diestel, A., Eyupoglu, I. Y., and Nitsch, R. (2001) Regulation of microglial expression of integrins by poly(ADP-ribose) polymerase-1. *Nat. Cell Biol.* **3**, 1035–1042
15. Laskowski, A., Schmidt, W., Dinkel, K., Martinez-Sanchez, M., and Reymann, K. G. (2005) bFGF and EGF modulate trauma-induced proliferation and neurogenesis in juvenile organotypic hippocampal slice cultures. *Brain Res.* **1037**, 78–89
16. Feng, G., Mellor, R. H., Bernstein, M., Keller-Peck, C., Nguyen, Q. T., Wallace, M., Nerbonne, J. M., Lichtman, J. W., and Sanes, J. R. (2000) Imaging neuronal subsets in transgenic mice expressing multiple spectral variants of GFP. *Neuron* **28**, 41–51
17. Bonde, C., Noraberg, J., and Zimmer, J. (2002) Nuclear shrinkage and other markers of neuronal cell death after oxygen-glucose deprivation in rat hippocampal slice cultures. *Neurosci. Lett.* **327**, 49–52
18. Dinkel, K., Dhabhar, F. S., and Sapolsky, R. M. (2004) Neurotoxic effects of polymorphonuclear granulocytes on hippocampal primary cultures. *Proc. Natl. Acad. Sci. USA* **101**, 331–336
19. Petrault, O., Ouk, T., Gautier, S., Laprais, M., Gele, P., Bastide, M., and Bordet, R. (2005) Pharmacological neutropenia prevents endothelial dysfunction but not smooth muscle functions impairment induced by middle cerebral artery occlusion. *Br. J. Pharmacol.* **144**, 1051–1058
20. Hailer, N. P., Heppner, F. L., Haas, D., and Nitsch, R. (1997) Fluorescent dye prelabelled microglial cells migrate into organotypic hippocampal slice cultures and ramify. *Eur. J. Neurosci.* **9**, 863–866
21. Heppner, F. L., Skutella, T., Hailer, N. P., Haas, D., and Nitsch, R. (1998) Activated microglial cells migrate towards sites of excitotoxic neuronal injury inside organotypic hippocampal slice cultures. *Eur. J. Neurosci.* **10**, 3284–3290
22. Mallat, M., Houlgatte, R., Brachet, P., and Prochiantz, A. (1989) Lipopolysaccharide-stimulated rat brain macrophages release NGF in vitro. *Dev. Biol.* **133**, 309–311
23. Mizuno, T., Yoshihara, Y., Kagamiyama, H., Ohsawa, K., Imai, Y., Kohsaka, S., and Mori, K. (1999) Neuronal adhesion molecule telencephalin induces rapid cell spreading of microglia. *Brain Res.* **849**, 58–66
24. Lee, J. C., Cho, G. S., Kim, H. J., Lim, J. H., Oh, Y. K., Nam, W., Chung, J. H., and Kim, W. K. (2005) Accelerated cerebral ischemic injury by activated macrophages/microglia after lipopolysaccharide microinjection into rat corpus callosum. *Glia* **50**, 168–181
25. Yrjanheikki, J., Keinänen, R., Pellikka, M., Hokfelt, T., and Koistinaho, J. (1998) Tetracyclines inhibit microglial activation and are neuroprotective in global brain ischemia. *Proc. Natl. Acad. Sci. USA* **95**, 15769–15774

26. Tikka, T., Fiebich, B. L., Goldsteins, G., Keinanen, R., and Koistinaho, J. (2001) Minocycline, a tetracycline derivative, is neuroprotective against excitotoxicity by inhibiting activation and proliferation of microglia. *J. Neurosci.* **21**, 2580–2588
27. Giulian, D., Corpuz, M., Chapman, S., Mansouri, M., and Robertson, C. (1993) Reactive mononuclear phagocytes release neurotoxins after ischemic and traumatic injury to the central nervous system. *J. Neurosci. Res.* **36**, 681–693
28. Giulian, D., Vaca, K., and Corpuz, M. (1993) Brain glia release factors with opposing actions upon neuronal survival. *J. Neurosci.* **13**, 29–37
29. Kim, W. K., and Ko, K. H. (1998) Potentiation of N-methyl-D-aspartate-mediated neurotoxicity by immunostimulated murine microglia. *J. Neurosci. Res.* **54**, 17–26
30. Rogove, A. D., and Tsirka, S. E. (1998) Neurotoxic responses by microglia elicited by excitotoxic injury in the mouse hippocampus. *Curr. Biol.* **8**, 19–25
31. Yrjanheikki, J., Tikka, T., Keinanen, R., Goldsteins, G., Chan, P. H., and Koistinaho, J. (1999) A tetracycline derivative, minocycline, reduces inflammation and protects against focal cerebral ischemia with a wide therapeutic window. *Proc. Natl. Acad. Sci. USA* **96**, 13496–13500
32. Kauppinen, T. M., and Swanson, R. A. (2005) Poly(ADP-ribose) polymerase-1 promotes microglial activation, proliferation, and matrix metalloproteinase-9-mediated neuron death. *J. Immunol.* **174**, 2288–2296
33. Thery, C., Chamak, B., and Mallat, M. (1993) Neurotoxicity of brain macrophages. *Clin. Neuropathol.* **12**, 288–290
34. Banati, R. B., Gehrmann, J., Schubert, P., and Kreutzberg, G. W. (1993) Cytotoxicity of microglia. *Glia* **7**, 111–118
35. Matsuo, Y., Onodera, H., Shiga, Y., Nakamura, M., Ninomiya, M., Kihara, T., and Kogure, K. (1994) Correlation between myeloperoxidase-quantified neutrophil accumulation and ischemic brain injury in the rat. Effects of neutrophil depletion. *Stroke* **25**, 1469–1475
36. Jiang, N., Moyle, M., Soule, H. R., Rote, W. E., and Chopp, M. (1995) Neutrophil inhibitory factor is neuroprotective after focal ischemia in rats. *Ann. Neurol.* **38**, 935–942
37. Morioka, T., Kalehua, A. N., and Streit, W. J. (1991) The microglial reaction in the rat dorsal hippocampus following transient forebrain ischemia. *J. Cereb. Blood Flow Metab.* **11**, 966–973
38. Streit, W. J., Morioka, T., and Kalehua, A. N. (1992) MK-801 prevents microglial reaction in rat hippocampus after forebrain ischemia. *Neuroreport* **3**, 146–148
39. Streit, W. J. (2002) Microglia as neuroprotective, immunocompetent cells of the CNS. *Glia* **40**, 133–139

40. Dowding, A. J., Maggs, A., and Scholes, J. (1991) Diversity amongst the microglia in growing and regenerating fish CNS: immunohistochemical characterization using FL.1, an anti-macrophage monoclonal antibody. *Glia* **4**, 345–364
41. Rapalino, O., Lazarov-Spiegler, O., Agranov, E., Velan, G. J., Yoles, E., Fraidakis, M., Solomon, A., Gepstein, R., Katz, A., Belkin, M., et al. (1998) Implantation of stimulated homologous macrophages results in partial recovery of paraplegic rats. *Nat. Med.* **4**, 814–821
42. Shaked, I., Tchoresh, D., Gersner, R., Meiri, G., Mordechai, S., Xiao, X., Hart, R. P., and Schwartz, M. (2005) Protective autoimmunity: interferon-gamma enables microglia to remove glutamate without evoking inflammatory mediators. *J. Neurochem.* **92**, 997–1009
43. Kitamura, Y., Takata, K., Inden, M., Tsuchiya, D., Yanagisawa, D., Nakata, J., and Taniguchi, T. (2004) Intracerebroventricular injection of microglia protects against focal brain ischemia. *J. Pharmacol. Sci.* **94**, 203–206
44. Kitamura, Y., Yanagisawa, D., Inden, M., Takata, K., Tsuchiya, D., Kawasaki, T., Taniguchi, T., and Shimohama, S. (2005) Recovery of focal brain ischemia-induced behavioral dysfunction by intracerebroventricular injection of microglia. *J. Pharmacol. Sci.* **97**, 289–293
45. Lu, Y. Z., Lin, C. H., Cheng, F. C., and Hsueh, C. M. (2005) Molecular mechanisms responsible for microglia-derived protection of Sprague-Dawley rat brain cells during in vitro ischemia. *Neurosci. Lett.* **373**, 159–164
46. Kipnis, J., Avidan, H., Caspi, R. R., and Schwartz, M. (2004) Dual effect of CD4+CD25+ regulatory T cells in neurodegeneration: a dialogue with microglia. *Proc. Natl. Acad. Sci. USA* **101**, Suppl 2, 14663–14669
47. Kohl, A., Dehghani, F., Korf, H. W., and Hailer, N. P. (2003) The bisphosphonate clodronate depletes microglial cells in excitotoxically injured organotypic hippocampal slice cultures. *Exp. Neurol.* **181**, 1–11
48. Mitrasinovic, O. M., Grattan, A., Robinson, C. C., Lapustea, N. B., Poon, C., Ryan, H., Phong, C., and Murphy, G. M., Jr. (2005) Microglia Overexpressing the Macrophage Colony-Stimulating Factor Receptor are Neuroprotective in a Microglial-Hippocampal Organotypic Coculture System. *J. Neurosci.* **25**, 4442–4451
49. Nimmerjahn, A., Kirchhoff, F., and Helmchen, F. (2005) Resting microglial cells are highly dynamic surveillants of brain parenchyma in vivo. *Science* **308**, 1314–1318
50. Polazzi, E., and Contestabile, A. (2002) Reciprocal interactions between microglia and neurons: from survival to neuropathology. *Rev. Neurosci.* **13**, 221–242

Received August 25, 2005; accepted December 7, 2005.

Table 1**Microglia migration and interaction with neurons in organotypic hippocampal slice culture^a**

	Microglia		Neurons (depth)	Interaction “Capping”	
	Surface	Inside		Surface	Inside
Basal 16 h	++	(-)	0–30 μ m: 1st layer	(+)	-
OGD 1 h	++	(+)	0–30 μ m: 1st layer	++	-
OGD 7 h	++	++ 30 μ m	0–30 μ m: 1st layer	++	++ 65 μ m
OGD 20 h	+	++ 70 μ m 80–100 μ m	0–30 μ m: gone, fragments >30 μ m: present	+ fragments	++ 80 μ m

^aMicroglia were labeled with CTO (red) and then directly applied onto organotypic hippocampal cultures prepared from transgenic B6.Cg-TgN (Thy1-YFP)16Jrs mice. Two-photon microscopy live image acquisition was performed at indicated timepoints (-, not detected; +), rarely detected; +, frequently detected; ++, majority of cells).

Fig. 1

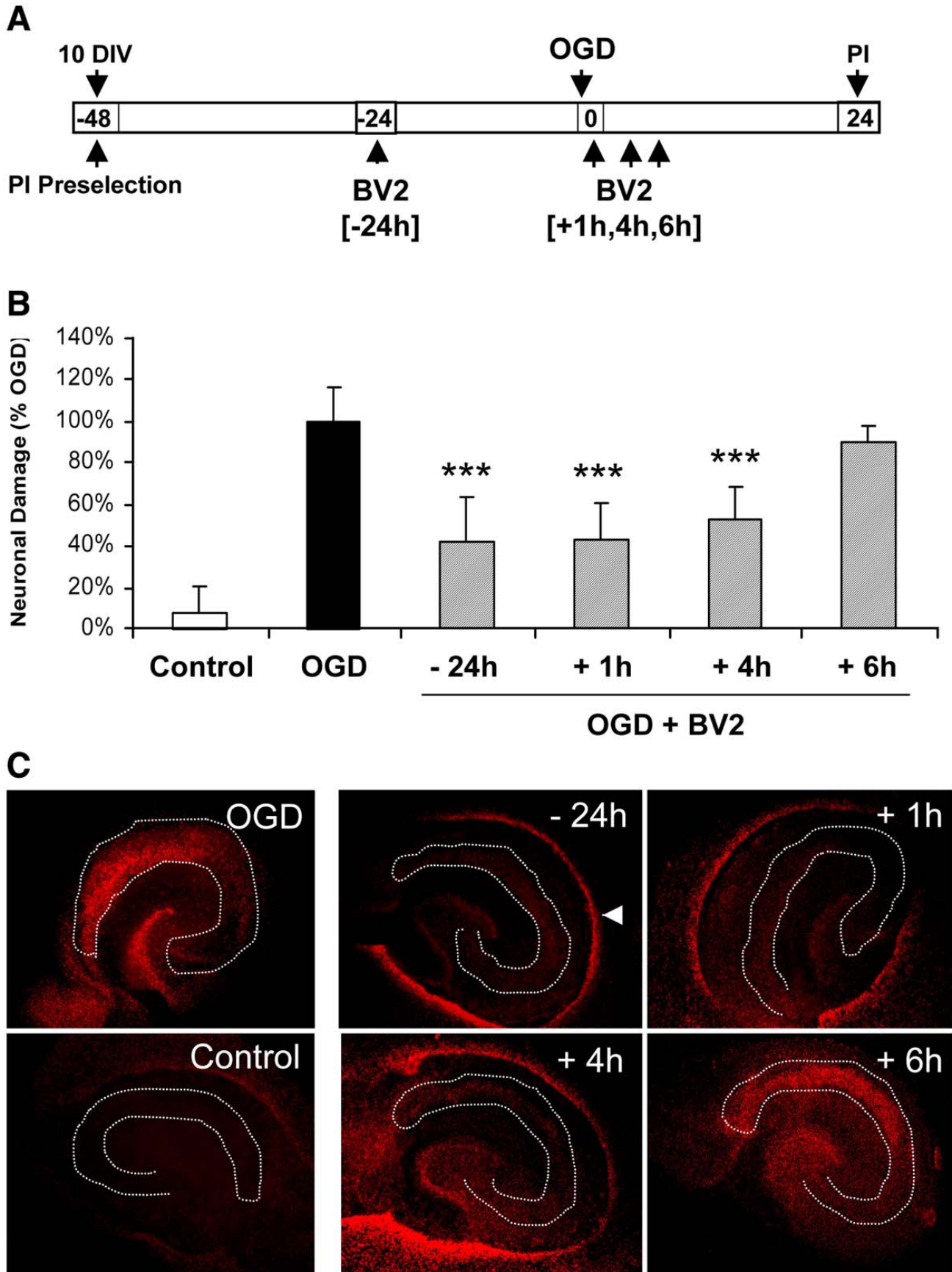


Fig. 1 (cont)

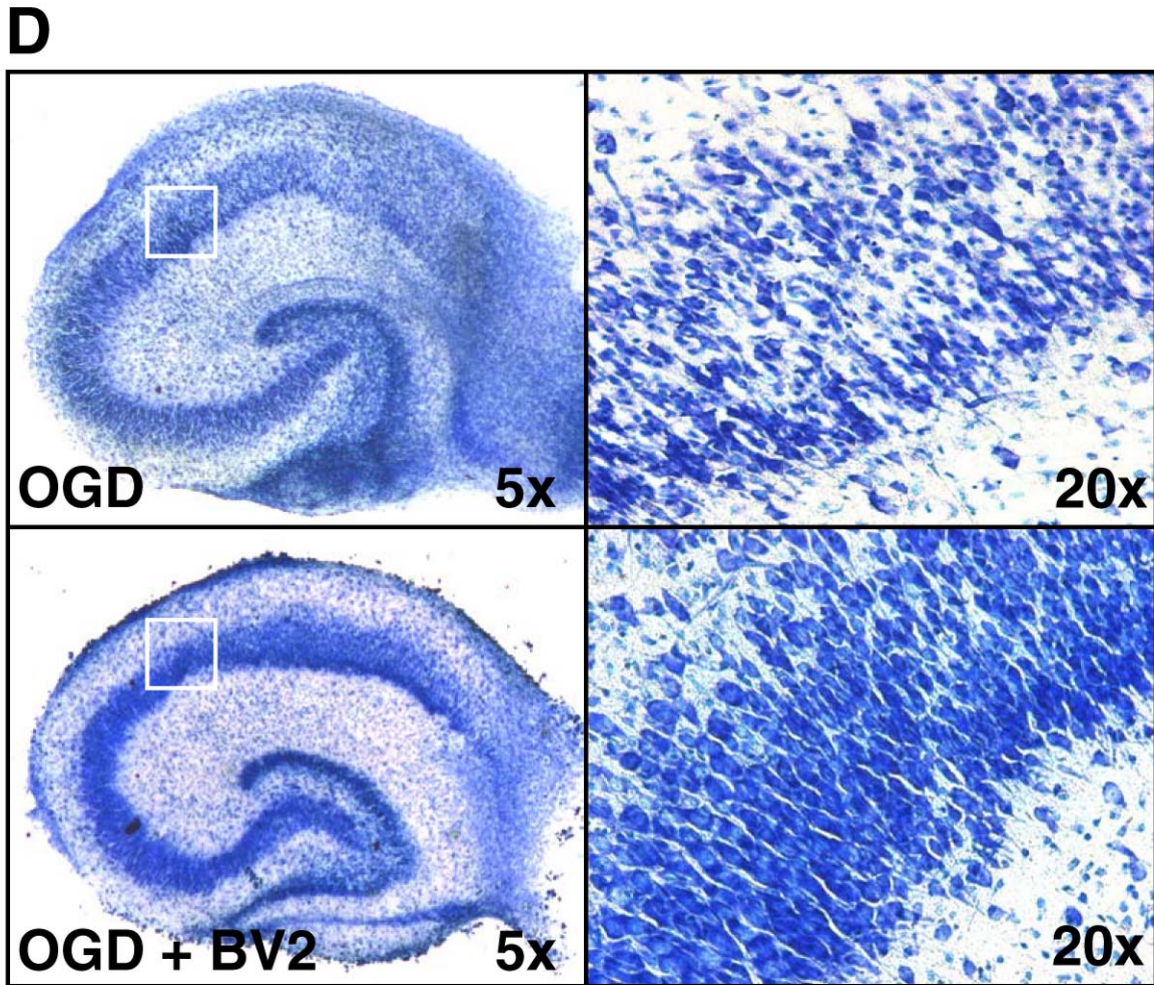


Figure 1. Protection against oxygen-glucose deprivation (OGD)-induced neuronal damage by microglia directly applied onto hippocampal slice cultures. **A)** BV2 microglia were applied onto the OHCs 24 h before or 1, 4, or 6 h after OGD. **B)** Quantification of neuronal death in cornu amonis (CA) by propidium iodide (PI) incorporation was determined after 24 h ($***P < 0.001$ vs. OGD; $n = 6-8/\text{bar}$). **C)** Representative PI fluorescent images showing neuronal death in CA. Arrowhead indicates PI-positive microglia on the slice border. **D)** Nissl staining was performed to confirm the PI data. The white box in the left panels ($\times 5$) indicates the position of the right panels ($\times 20$) in the CA1 area.

Fig. 2

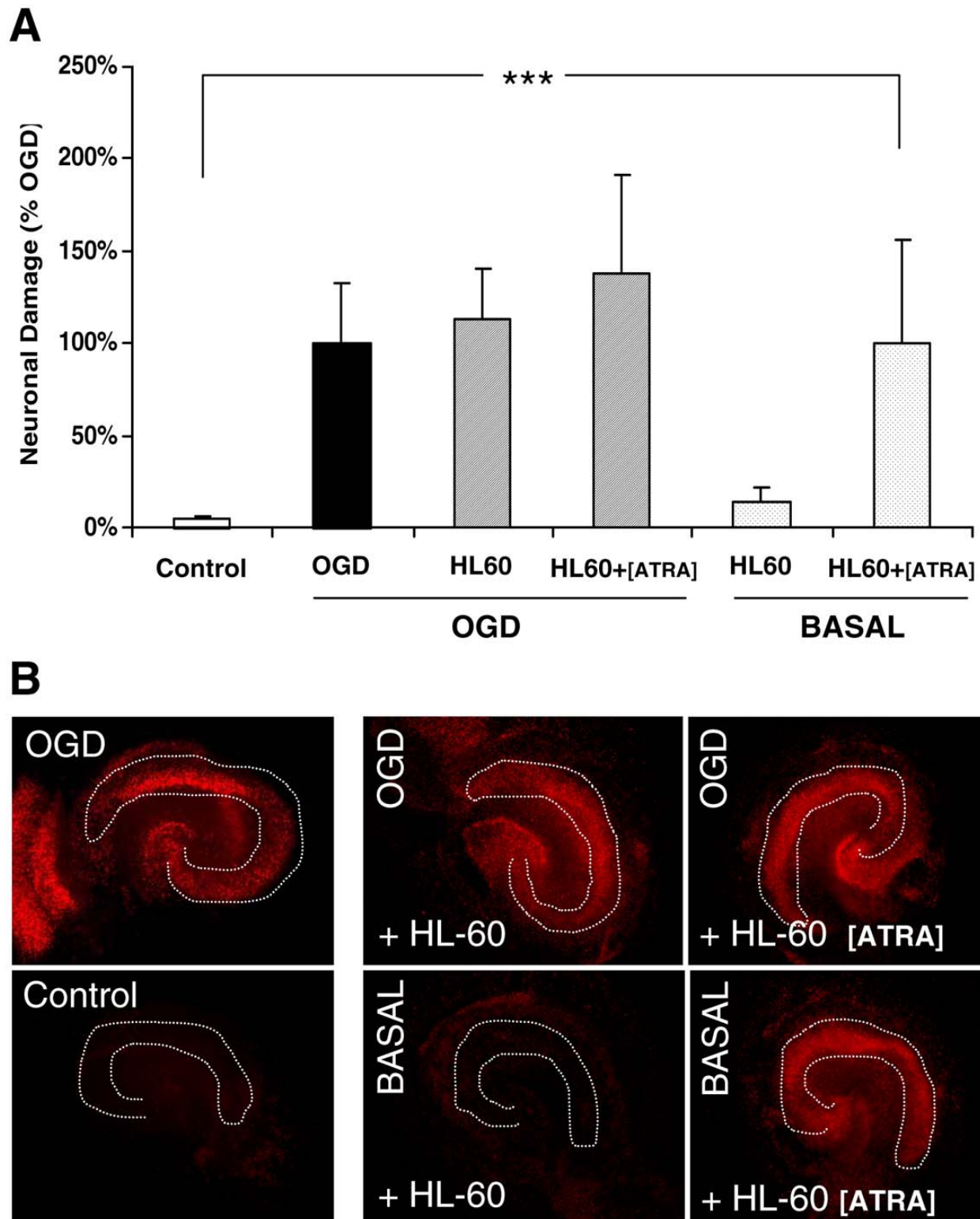


Figure 2. HL-60 neutrophils fail to provide neuroprotection after OGD-induced damage. Undifferentiated HL-60 cells or ATRA-differentiated HL-60 cells were applied directly onto untreated (basal) hippocampal slice cultures 1 h after OGD. Quantification of neuronal death in the CA region by PI incorporation was determined after 24 h ($***P < 0.001$ control vs. basal + HL-60 [ATRA]; $n = 6-7/\text{bar}$). **A**) Brackets indicate the differentiation pretreatment with ATRA (all-trans-retinoic acid). **B**) Representative PI fluorescent images showing neuronal death in CA 1-3.

Fig. 3

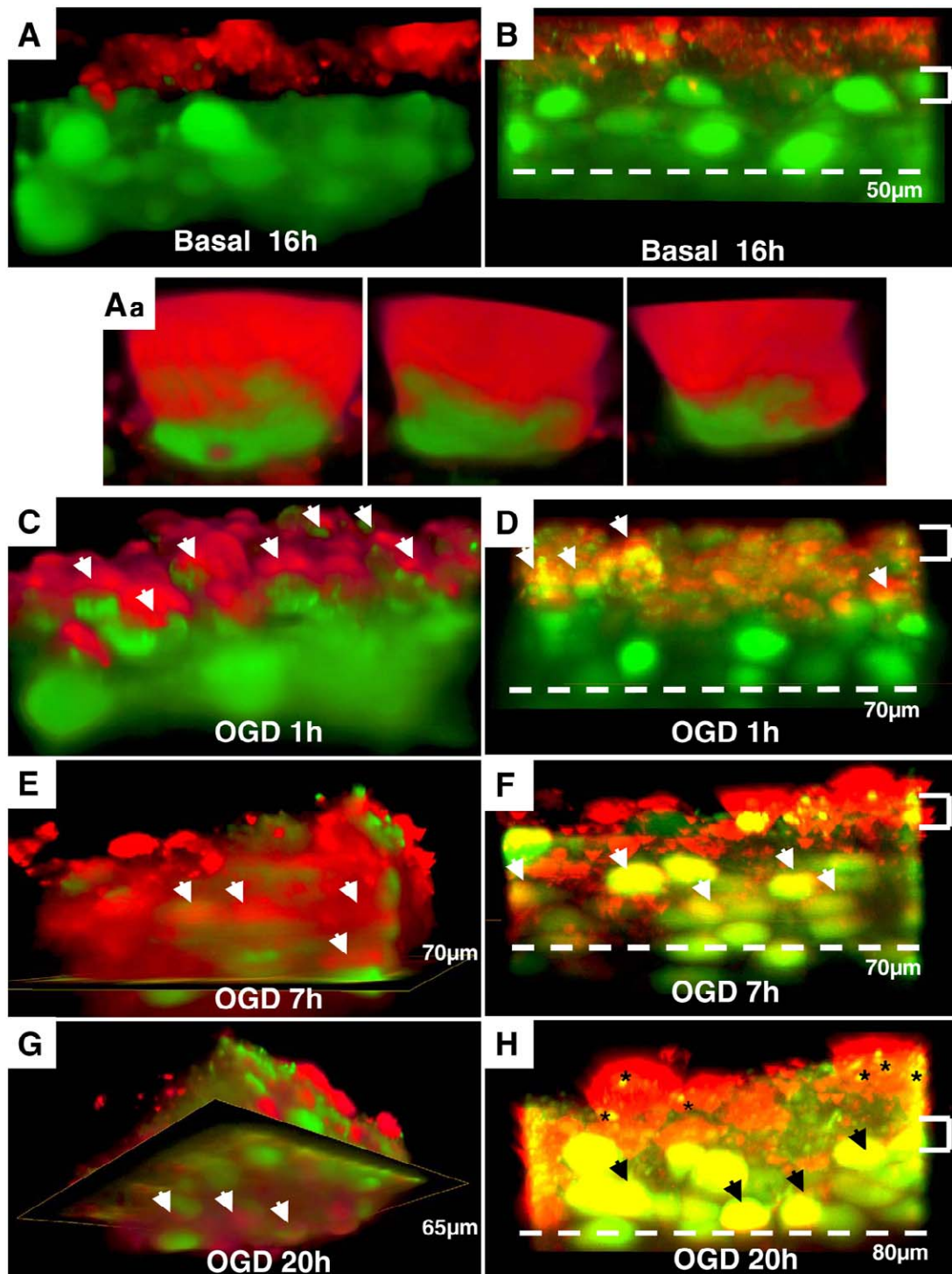


Figure 3. Migration of microglia into organotypic hippocampal cultures and “capping” interaction with neurons under normal and ischemic conditions. BV2 microglia were labeled with CTO (red) and then directly applied onto organotypic hippocampal cultures (OHCs) prepared from transgenic B6.Cg-TgN (Thy1-YFP)16Jrs mice (neurons: green). At indicated time points (Basal+ 16 h, OGD+ 1 h, 7 h, 20 h) Z-stacks were performed from living OHCs using two-photon microscopy. Images show 3-D reconstruction (*A*, *Aa*, *C*, *E*, *G*) and 2-D collapsed side view of the individual confocal planes (*B*, *D*, *E*, *F*). *Aa*) Images show a 180° view of a “capping” interaction between a neuron (green) and a BV2 microglia (red). *C*, *E*, *G*) “Capping” is marked by arrows. *D*, *F*, *H*) “Capping” is marked by arrows showing double labeling (yellow). White brackets indicate the “first neuronal layer,” and white dashed lines indicate “depth in the slice.” *H*) Asterisks indicate neuronal fragments.

Fig. 4

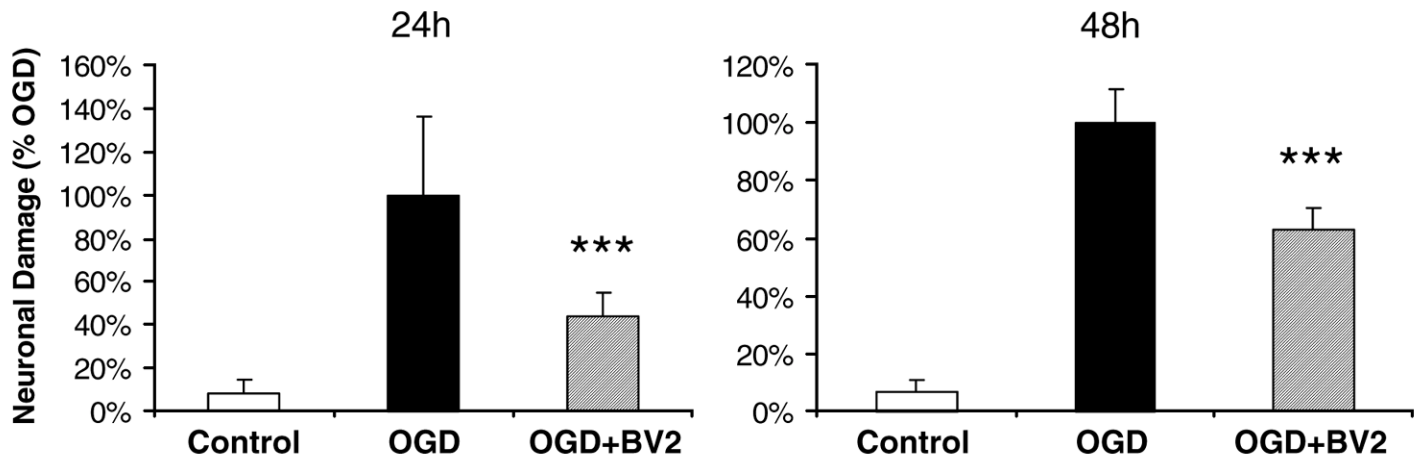


Figure 4. Duration of neuronal protection provided by microglia. Determination of neuronal death after 24 h and 48 h. BV-2 microglia were applied directly to the organotypic hippocampal cultures (OHCs) 1 h after oxygen-glucose deprivation (OGD). Quantification of neuronal death in CA over 48 h was determined by propidium iodide incorporation (***) $P < 0.001$ vs. OGD; $n = 6-8$ /bar).

Fig. 5

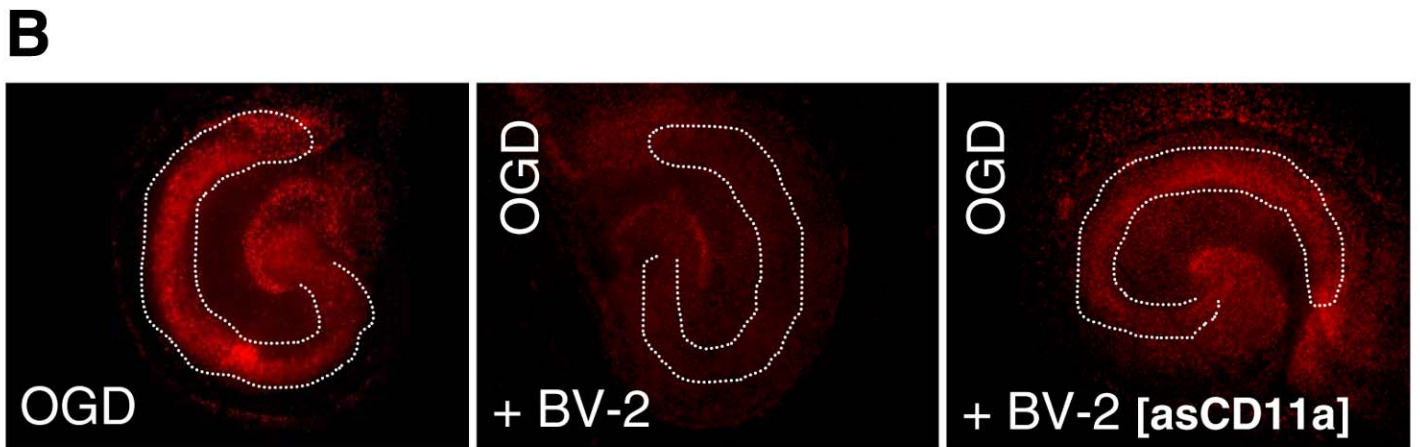
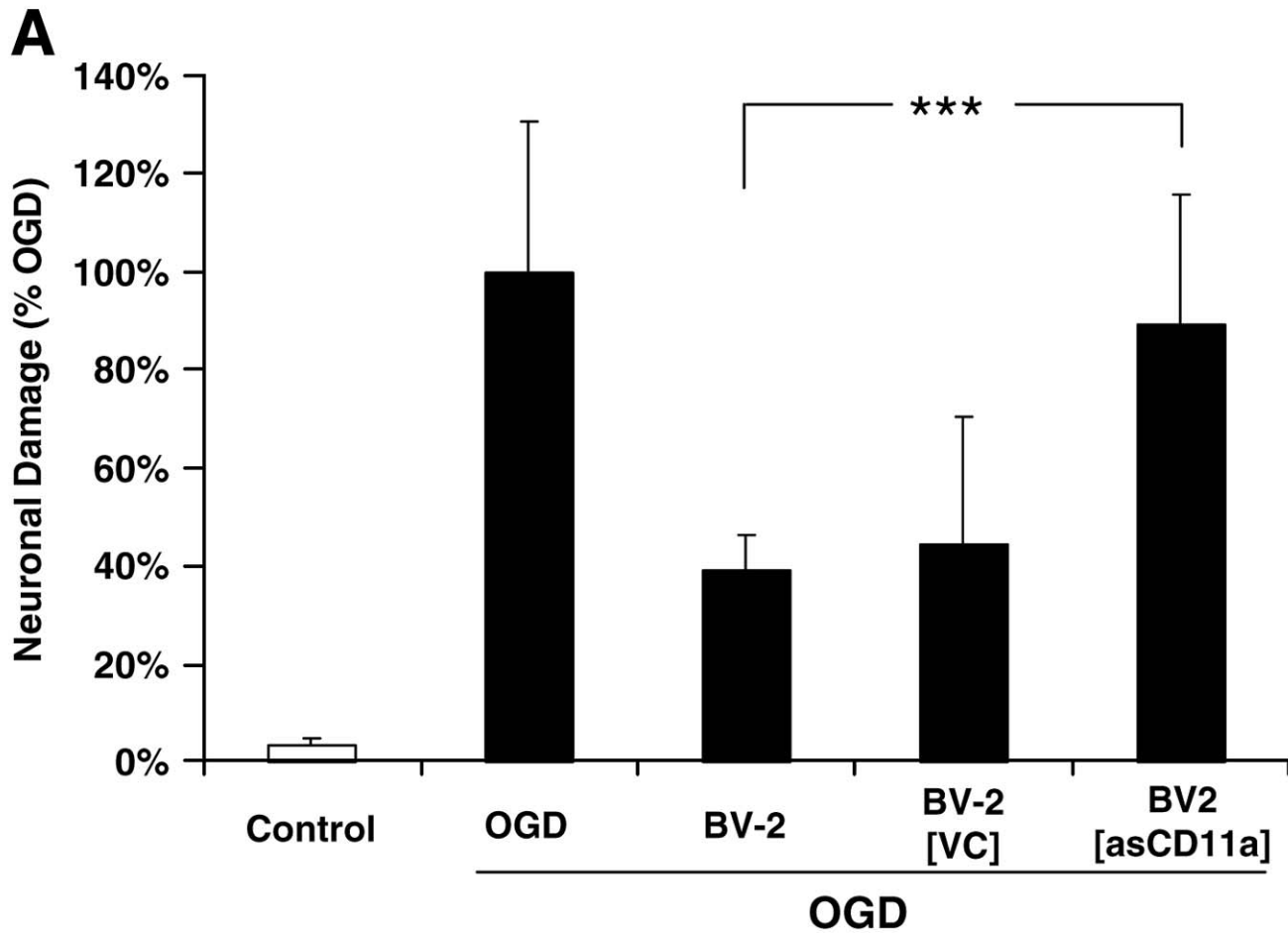


Figure 5. Antisense CD11a-transfected BV2 fail to provide neuroprotection after OGD-induced damage. Antisense CD11a-transfected BV-2 [asCD11a] were applied directly onto untreated (basal) hippocampal slice cultures 1 h after OGD. **A)** Quantification of neuronal death in the CA region by PI incorporation was determined after 24 h (***) $P < 0.001$ BV-2 [asCD11a] vs. BV-2; $n = 7-18$ /bar). VC = vector control. **B)** Representative PI fluorescent images showing neuronal death in CA 1-3.

Fig. 6

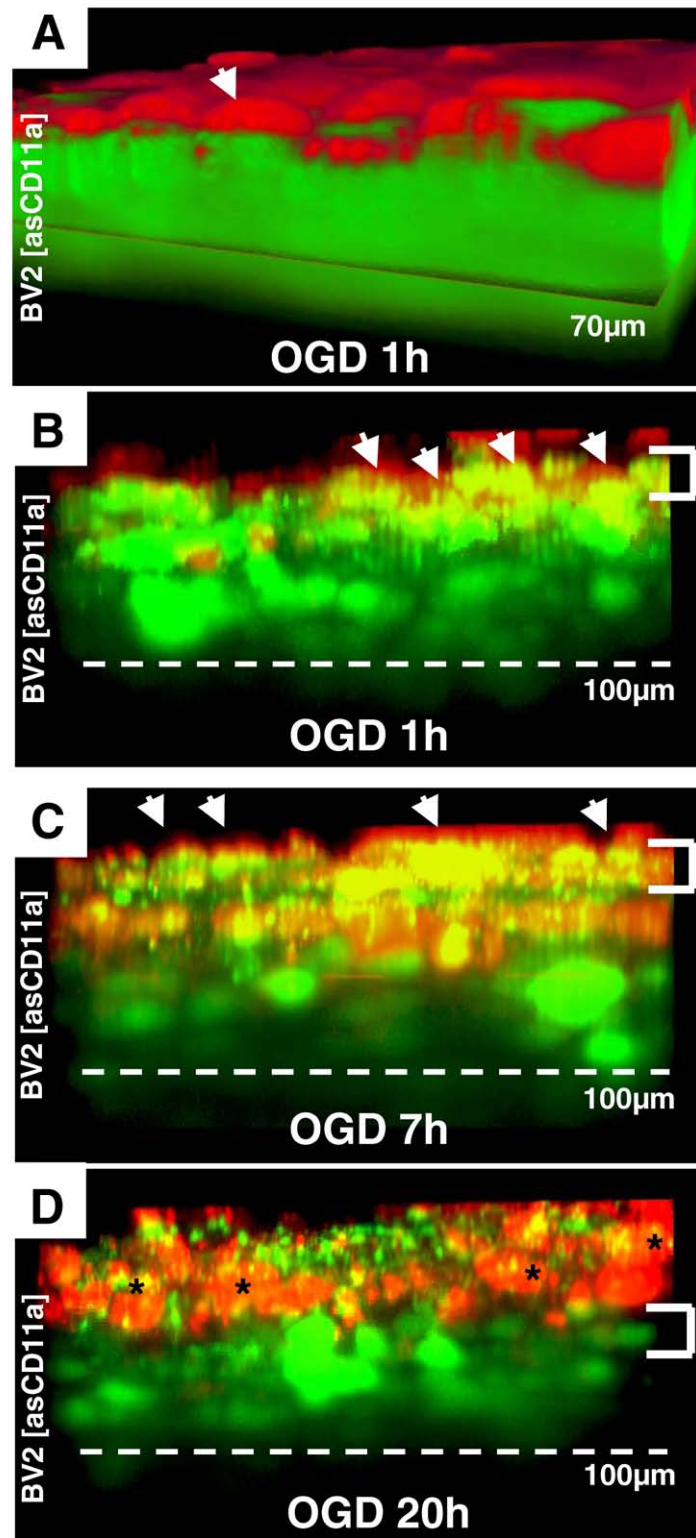


Figure 6. Antisense CD11a-transfected BV2 fail to migrate into organotypic slice cultures after OGD-induced damage. Antisense CD11a-transfected BV-2 [asCD11a] were labeled with CTO (red) and then directly applied onto organotypic hippocampal cultures (OHCs). At indicated time points (OGD+ 1 h, 7 h, 20 h), Z-stacks were performed from living OHCs using two-photon microscopy. Images show 3-D reconstruction (A) and 2-D collapsed side view of the individual confocal planes (B, C, D). A) “Capping” is marked by arrows. B, C) “Capping is marked by arrows showing double labeling (yellow). B, C, D) White brackets indicate the “first neuronal layer,” and white dashed lines indicate “depth in the slice.”

Fig. 7

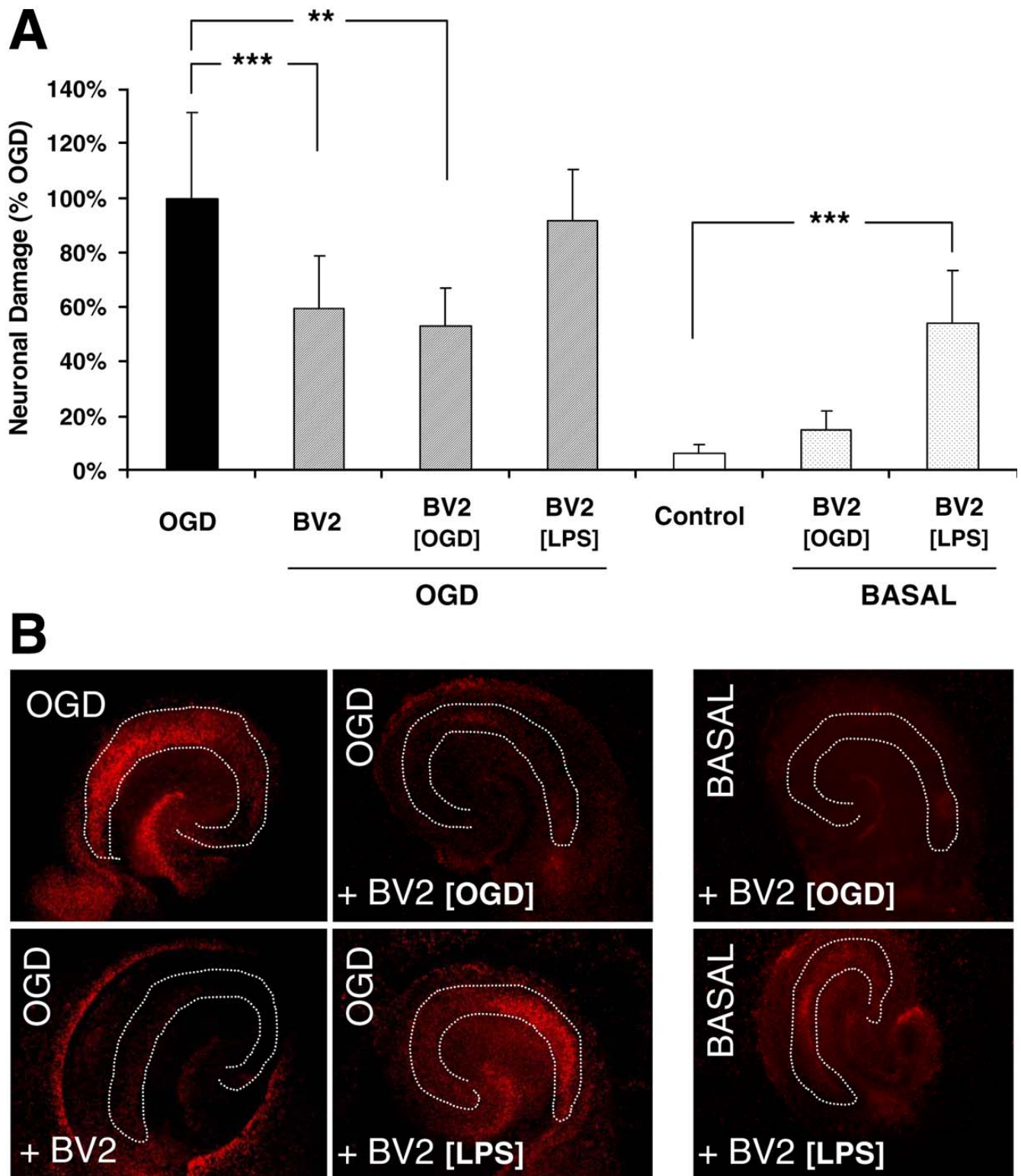


Figure 7. LPS-stimulated microglia fail to provide neuroprotection after oxygen-glucose deprivation (OGD). Microglia were preactivated by LPS (4 h; 50 $\mu\text{g}/\text{ml}$) or OGC (40 min) before they were applied onto organotypical hippocampal cultures (OHCs). Application of differently activated BV2 microglia was performed onto OHCs under basal conditions or after exposition of OHCs to OGC. **A**) Quantification of neuronal death in CA determined by propidium iodide (***) $P < 0.001$; **) $P < 0.01$; $n = 6-8/\text{bar}$). **B**) Representative PI fluorescent images showing neuronal death in CA.

Fig. 8

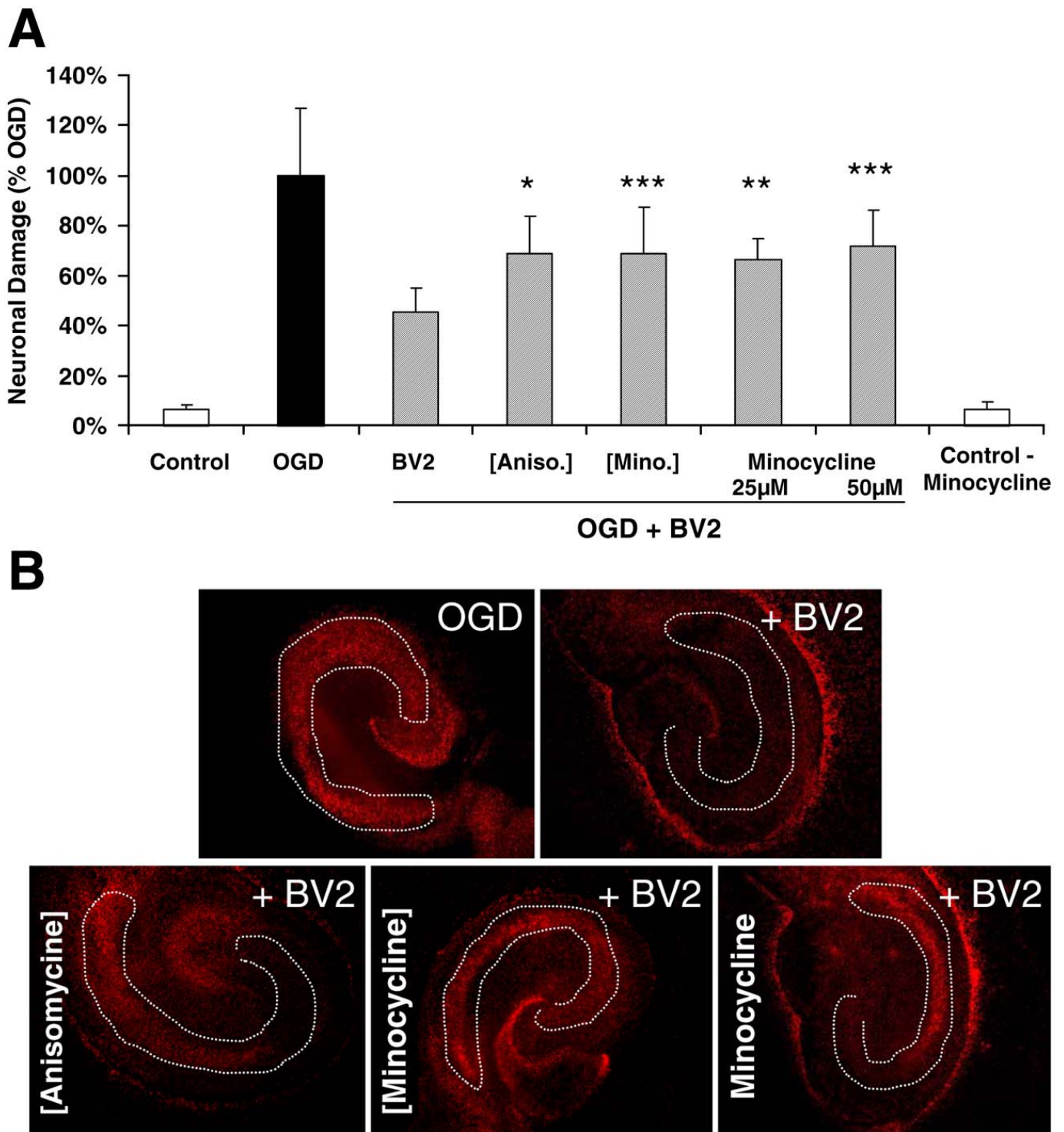


Figure 8. Anisomycine and minocycline reduce BV2 microglia-mediated neuroprotection. To block protein synthesis, we pretreated microglia with 10 μM anisomycine for 2 h before application onto organotypic hippocampal cultures (OHCs). To inhibit the p38-MAPK signal pathway, either microglia were pretreated with 50 μM minocycline for 4 h before the application or minocycline (25 μM ; 50 μM) was applied simultaneously with the BV2 microglia at 1 h after oxygen-glucose deprivation (OGD). Brackets indicate the respective pretreatment. **A**) Quantification of neuronal death in CA was performed by densitometric analysis of PI incorporation ($***P < 0.001$; $**P < 0.01$; $*P < 0.05$ vs. OGD/BV2; $n = 6-8/\text{bar}$). **B**) Representative PI fluorescent images showing neuronal death in CA.

Microglia Cells Protect Neurons by Direct Engulfment of Invading Neutrophil Granulocytes: A New Mechanism of CNS Immune Privilege

Jens Neumann,¹ Steven Sauerzweig,¹ Raik Röncke,¹ Frank Gunzer,³ Klaus Dinkel,¹ Oliver Ullrich,^{2,4} Matthias Gunzer,^{2,5*} and Klaus G. Reymann^{1,6*}

¹Leibniz Institute for Neurobiology, Project Group Neuropharmacology, and ²Institute of Immunology, Otto von Guericke University Magdeburg, 39118 Magdeburg, Germany, ³German University in Cairo, 11771 Cairo, Egypt, ⁴Institute of Anatomy, Faculty of Medicine, University Zurich, CH-8057 Zurich, Switzerland, ⁵Helmholtz Centre for Infection Research, Junior Research Group Immunodynamics, 38124 Braunschweig, Germany, and ⁶Institute for Applied Neuroscience (Institute für Angewandte Neurowissenschaften FAN gGmbH), 39120 Magdeburg, Germany

Microglial cells maintain the immunological integrity of the healthy brain and can exert protection from traumatic injury. During ischemic tissue damage such as stroke, peripheral immune cells acutely infiltrate the brain and may exacerbate neurodegeneration. Whether and how microglia can protect from this insult is unknown. Polymorphonuclear neutrophils (PMNs) are a prominent immunologic infiltrate of ischemic lesions *in vivo*. Here, we show in organotypic brain slices that externally applied invading PMNs massively enhance ischemic neurotoxicity. This, however, is counteracted by additional application of microglia. Time-lapse imaging shows that microglia exert protection by rapid engulfment of apoptotic, but, strikingly, also viable, motile PMNs in cell culture and within brain slices. PMN engulfment is mediated by integrin- and lectin-based recognition. Interference with this process using RGDS peptides and *N*-acetyl-glucosamine blocks engulfment of PMNs and completely abrogates the neuroprotective function of microglia. Thus, engulfment of invading PMNs by microglia may represent an entirely new mechanism of CNS immune privilege.

Key words: neuroinflammation; stroke; microglia; polymorphonuclear granulocytes; PMN; phagocytosis; time-lapse imaging

Introduction

Abundant evidence exists that an inflammatory response is mounted within the CNS after cerebral ischemia. Postischemic inflammation comprises the infiltration of polymorphonuclear granulocytes and monocytes/macrophages into the injured brain parenchyma, activation of microglia, and expression of proinflammatory cytokines, adhesion molecules, and other inflammatory mediators (Feuerstein et al., 1998; Dirnagl et al., 1999). Despite these well described inflammatory events after ischemia, the main impact of postischemic inflammation (beneficial or detrimental) is controversially discussed (del Zoppo et al., 2001; Feuerstein and Wang, 2001).

There is striking evidence that the infiltration of activated

polymorphonuclear neutrophils (PMNs) (Kochanek and Haltenbeck, 1992; Jean et al., 1998; Prestigiacomo et al., 1999) into the injured parenchyma and the activation of microglia (Banati and Graeber, 1994; Kreutzberg, 1996; Minghetti and Levi, 1998) are playing an important role in the pathology of cerebral ischemia.

It is suggested that activated PMNs contribute to tissue damage by the release of oxygen radicals, proteases, and proinflammatory cytokines like TNF α (tumor necrosis factor α) (Barone et al., 1991; Jordan et al., 1999). As evidence, experimental strategies by avoiding PMN infiltration into the injured parenchyma are neuroprotective (Heinel et al., 1994; Beray-Berthat et al., 2003b; Miljkovic-Lolic et al., 2003). However, other studies failed to provide clear evidence of a cause–effect of PMN contribution to neuronal damage after ischemia (Hayward et al., 1996; Fassbender et al., 2002; Beray-Berthat et al., 2003a; Harris et al., 2005).

Similarly controversial findings exist regarding the role of microglia after ischemia. Several studies demonstrated the neurotoxic properties of activated microglia after ischemic or excitotoxic damage (Giulian et al., 1993; Kim and Ko, 1998; Rogove and Tsirka, 1998; Yrjanheikki et al., 1999), whereas considerable evidence shows that microglia triggered by injured/dying neurons mediate a reduction of neuronal damage and induction of tissue repair (Morioka et al., 1991; Rapalino et al., 1998; Streit, 2002; Kohl et al., 2003; Kitamura et al., 2004; Shaked et al., 2005; Hayashi et al., 2006; Lalancette-Hebert et al., 2007).

Received Jan. 7, 2008; revised Feb. 28, 2008; accepted April 1, 2008.

This work was supported by grants from the State of Saxony-Anhalt (3594M/0405M) (K.G.R., O.U.), the German Research Community (Deutsche Forschungsgemeinschaft) (GU 769/2-1) (M.G.), and the German Federal Ministry for Science and Education (01G00504-CAI). We thank Susanne v. Kenne and Cornelia Garz for excellent technical assistance and Gabriella Orlando for critical reading of this manuscript. We also thank Roland Hartig for help with differential interference contrast microscopy.

*M.G. and K.G.R. contributed equally to this work.

Correspondence should be addressed to one of the following: Klaus G. Reymann or Jens Neumann, Leibniz Institute for Neurobiology, Project Group Neuropharmacology, Brenneckerstrasse 6, D-39118 Magdeburg, Germany, E-mail: reymann@fan-neuroscience.com or jens.neumann@sciencetoday.de; or Matthias Gunzer, Institute of Clinical and Molecular Immunology, Otto von Guericke University Magdeburg, Leipziger Strasse 44, D-39120 Magdeburg, Germany, E-mail: matthias.gunzer@med.ovgu.de.

DOI:10.1523/JNEUROSCI.0060-08.2008

Copyright © 2008 Society for Neuroscience 0270-6474/08/285965-11\$15.00/0

Considering these controversial findings on the role of PMNs and microglia during transient ischemia, strikingly few studies have evaluated the direct effect of these immune cells on neuronal survival/damage (Dinkel et al., 2004; Mitrasinovic et al., 2005). Despite that, although the combined recruitment of both cell types to tissue sites affected by cerebral ischemia is well established, a potential direct interaction of both immune cell types has not been investigated in depth. Two recent studies demonstrated a possible microglia–PMN interaction. By histology, microglia with engulfed PMNs were observed in zones of focal cerebral ischemia *in vivo* (Denes et al., 2007; Weston et al., 2007).

To better understand the complexity of cellular inflammation after experimental ischemia, we investigated the individual impact of PMNs, microglia, and macrophages on neuronal survival after ischemia and studied how these cells interact during the inflammatory response. To achieve this, we used an inflammation model that comprises oxygen–glucose deprivation (OGD) in organotypic hippocampal slice cultures (OHCs) as ischemic model and the application of immune cells onto the OHCs as simulation of the postischemic immune cell infiltration into the injured parenchyma.

Materials and Methods

Induction of focal cerebral ischemia by middle cerebral artery occlusion with endothelin-1

Focal cerebral ischemia was induced by occlusion of the left middle cerebral artery (MCA) via intracerebral microinjection of endothelin-1 (ET-1), following Sharkey and Butcher (1995) and Baldauf and Reymann (2005). Briefly, anesthesia was induced with halothane in a mixture of nitrous oxide and oxygen (50:50), and maintained with 2–3% halothane (Sigma-Aldrich) via a rat anesthetic mask (Störling). A 29 gauge cannula was inserted through the brain close to the MCA. Ischemia was induced by injection of 376 pmol of ET-1 (Sigma-Aldrich). The animals were killed by an overdose of chloral hydrate (Sigma-Aldrich) after 1 d. Frozen brains were cut coronally and 30 μ m slices were taken for additional staining.

Organotypic hippocampal slice cultures

Hippocampal interface organotypic cultures were prepared as previously described (Stoppini et al., 1991; Neumann et al., 2006) from postnatal day 7–9 Wistar rats (Harlan Winkelmann). For two-photon microscopy experiments, hippocampal slice cultures were prepared from transgenic B6.Cg-TgN(Thy1-YFP)16Jrs mice (The Jackson Laboratory; distributed by Charles River), which express enhanced yellow fluorescent protein (EYFP) at high levels in subsets of central neurons, including the pyramidal cells of the hippocampus (Feng et al., 2000). Hippocampi were dissected and transversely sliced at 350 μ m thickness with a McIlwain tissue chopper (The Mickle Laboratory Engineering). Slices were transferred to Millicell membranes (Millipore). Cultures were maintained at 37°C in 1 ml of serum-based medium containing 50% MEM-Hanks, 25% HBSS, 17 mM HEPES, 5 mM glucose, pH 7.8 (Cell Concepts), 1 mM L-glutamine (Biochrom), 25% horse serum (Invitrogen), and 0.5% gentamycin (Biochrom) for 2–3 d. Cultures were then maintained in serum-free medium (Neurobasal A medium with B27 complement, 5 mM glucose, 1 mM L-glutamine). The OHCs were selected by adding a nontoxic concentration of propidium iodide (PI) (2 μ g/ml; Sigma-Aldrich) 12 h before the experimental start. PI-negative slices were considered to be healthy, and only these slices were used for the experiments.

Isolation of polymorphonuclear granulocytes (PMNs)

Human PMNs were prepared from venous blood (8 ml) of healthy volunteers. The rat PMNs were prepared from blood of Wistar rats (Harlan Winkelmann). Briefly, anesthesia in rats was induced with chloral hydrate followed by opening the thorax. The left ventricle of the heart has been punctured under direct visualization, and 10–12 ml of blood was obtained per rat. The blood was collected in a vacutainer containing EDTA (BD Biosciences). The anticoagulated whole blood was carefully layered over 5 ml of the density gradient Polymorphprep (Axis-Shield).

Samples were centrifuged for 35 min at 500 \times g. After centrifugation, two leukocyte bands were visible. The top band contained the fraction of mononuclear cells, and the lower band contained the fraction of PMNs. The fraction of PMNs was collected by pipetting. PMNs were washed with PBS. Contaminating erythrocytes were removed by hypotonic lyses in plain H₂O for 20 s followed by addition of the same volume of 2 \times PBS to restore osmolarity. PMNs were pelleted and resuspended in DMEM/10% fetal calf serum (FCS). Cell yield (1.5 \times 10⁷ cells per preparation) was determined by counting cells in a “Neubauer” hemocytometer, and viability (>99%) was assessed by trypan blue staining (0.4% trypan blue in PBS; Sigma-Aldrich). PMN preparations contained >95% neutrophils assessed by hematoxylin/eosin staining on smears, whereas only a few basophil and eosinophil granulocytes could be detected. No monocytes or lymphocytes contaminated the preparation.

Isolation of rat primary microglia

Primary microglia cultures were prepared from postnatal day 2–3 Wistar rats (Harlan Winkelmann) and cultured in DMEM supplemented with 10% FCS (Biochrom), 1% Pen/Strep (Biochrom), and 1% L-glutamine (Biochrom). After 6 or 7 d of primary cultivation, microglia cells were separated from other cell types by shaking, placed in a 25 ml flask (TPP) at a density not exceeding 5 \times 10⁵ cells/ml and maintained in 5% CO₂ at 37°C for 2 d. Cultures consisted of 95% microglia cells as determined by staining with Alexa 568-conjugated *Griffonia simplicifolia* isolectin B4 (Invitrogen).

Culture of macrophage cell line RAW 264.7

The macrophage cell line RAW 264.7 was cultured in DMEM supplemented with 10% FCS (Biochrom), 1% Pen/Strep (Biochrom), and 1% L-glutamine (Biochrom) at a density not exceeding 1 \times 10⁶ cells/ml and maintained in 5% CO₂ at 37°C.

Application of cells onto OHCs

Isolated primary microglia or macrophages were trypsinated (trypsin/EDTA; Biochrom), centrifuged at 500 \times g for 2 min, and finally resuspended in Neurobasal medium (Invitrogen). PMNs were freshly prepared shortly before the experimental start. PMNs were also resuspended in Neurobasal medium. The cells were applied directly onto 10-d-old OHCs in a volume of 1 μ l of Neurobasal medium containing 8 \times 10⁴ microglia, macrophages, or 1 \times 10⁵ PMNs. Viability of microglia, macrophages, and PMNs after application onto the OHC was confirmed in initial experiments by previous staining with 5-chloromethylfluorescein diacetate (CMFDA) (Invitrogen) and by time-lapse microscopy of these cells (data not shown). As indicated, OHCs were fixed with 4% paraformaldehyde (PFA) and mounted with 3:1 PBS/glycerol. OHCs were then further analyzed with the indicated microscopy approach.

Oxygen–glucose deprivation

The membrane inserts carrying up to three OHCs were placed into 1 ml of glucose-free medium in sterile six-well culture plates (TPP) that had previously been saturated with 5% CO₂/95% N₂ for 10 min. Then OHC were subjected to the OGD [40 min of OGD in a temperature-controlled hypoxic chamber (Billups-Rothenberg); no glucose medium; N₂/CO₂ atmosphere] before retransfer into normal conditions. Control cultures were kept in regular medium (plus glucose) under normoxic conditions. The cultures were analyzed as indicated by individual experiments 24 or 48 h after OGD.

Analysis of cell death

Cell death was evaluated by cellular incorporation of PI at 24 or 48 h after OGD. Cultures were incubated with PI-containing medium (10 μ M) for 2 h at 33°C. Fluorescent images were acquired in a semiautomatic manner (Nikon motorized stage; LUCIA software) and analyzed by densitometry to quantify necrotic cell death (LUCIA Image analysis software). Based on transmission light images, the area of analysis was determined such that only the CA area (CA1–3) was analyzed, whereas the dentate gyrus was excluded. Background correction was performed automatically by a control square (150 \times 150 μ m) in the stratum moleculare outside the pyramidal cell layer. To combine data from individual experiments, the densitometric mean value of the respective insult of an indi-

vidual experiment was set to the value of 1 and given as relative fluorescence intensity. All other data are given as relative fluorescence intensity of the insult damage.

Electrophysiology

Wistar rats (25 d old) (Harlan Winkelmann) were killed by a blow on the neck. After decapitation, the brain was quickly removed and placed into ice-cold artificial CSF (ACSF) having the following composition (in mM): 124 NaCl, 4.9 KCl, 1.3 MgSO₄, 2.5 CaCl₂, 1.2 KH₂PO₄, 25.6 NaHCO₃, 10 D-glucose, saturated with 95% O₂ and 5% CO₂, pH 7.4. Transverse hippocampal slices (350 μm thickness) with adjacent subicular and entorhinal cortices were prepared using a vibratome (microm HM 650V). The slices were placed on Millicell membranes in a six-well cluster dish (Sigma-Aldrich) with 1 ml of high K⁺ culture media [25% horse serum (Invitrogen); 40% Eagle's Basal Essential Media (BME) (Sigma-Aldrich); 25% Earle's balanced salt solution (Sigma-Aldrich); 10% 250 mM Na-HEPES in BME, pH 7.3; 0.5 mM L-glutamine (Sigma-Aldrich); 28 mM glucose, pH 7.32]. One hour after preparation, 2 μl of high K⁺ culture media containing 4 × 10⁵ PMNs and 2 μl of cell-free media for control experiments, respectively, were applied on top of the slices and incubated overnight at 33°C in a humidified carbogen atmosphere (95% O₂/5% CO₂). Then, the slices were transferred into an interface-type recording chamber saturated with carbogen at 33 ± 1°C and constantly superfused with ACSF. Synaptic responses were elicited by stimulation of the Schaffer collateral–commissural fibers in the stratum radiatum of the CA1 region using lacquer-coated stainless-steel stimulating electrodes. Glass electrodes (filled with ACSF, 1–4 MΩ) were placed in the apical dendritic layer to record field EPSPs (fEPSPs). The initial slope of the fEPSP was used as a measure of this potential. The stimulus strength of the test pulses was adjusted to 30% of the EPSP maximum. During baseline recording, three single stimuli (10 s interval) were averaged every 5 min. After tetanization, recordings were taken as indicated in Figure 1C. Once a stable baseline had been established, long-term potentiation was induced by application of four times two-paired pulses in intervals of 200 ms (theta burst). The interval between the paired pulses was 10 ms, and the width of a single pulse was 0.2 ms.

Two-photon microscopy

For two-photon microscopy, PMNs were labeled with Cell Tracker Orange [5-(and-6)-((4-chloromethyl)benzoyl)-amino]tetramethylrhodamine (CMTMR) (7.5 μM in PBS, 10 min, room temperature; Invitrogen). At different time points after OGD induction, the OHCs were fixed with 4% PFA, subsequently mounted and subjected to three-dimensional two-photon microscopy. In other experiments, viable OHCs were analyzed. PMNs were labeled with CMFDA and microglia with CMTMR and both applied onto OHCs. Two hours after experimental start, the OHCs were placed in a custom-built chamber supplied with 37°C and 5% CO₂ directly under the microscope. The two-photon microscope setup was used exactly as previously described (Neumann et al., 2006). OHCs prepared from transgenic B6.Cg-TgN(Thy1-YFP)16Jrs mice (Feng et al., 2000) were imaged in a modus at 800 and 920 nm wavelength of the laser (MaiTai; Spectra Physics) using a scanning window of 90 × 150 μm size. With a resolution in Z of 1 μm, the entire thickness of the OHC was scanned, first at 920 nm and then at 800 nm wavelength with no filter. The emission of EYFP at 800 nm was negligible as was the emission of Cell Tracker Orange at 920 nm. Image stacks were exported as two independent 16-bit multilayer TIFF stacks and subsequently reconstructed using the Volocity software package (Improvision).

Confocal microscopy

Cultures were examined with a confocal microscope equipped with a 40× magnification Plan Neofluar 0.75 objective, an argon laser emitting at 488 nm, and a helium/neon laser emitting at 543 nm. Multitracking was used to avoid cross talk between channels. Images were analyzed with Carl Zeiss software (Pascal; Carl Zeiss).

Time-lapse video microscopy

The cellular dynamics of PMN–microglia interaction were investigated using OHCs or an *in vitro* PMN–microglia coculture.

Time-lapse microscopy of OHCs. Fluorescently labeled PMNs [7-amino-4-chloromethylcoumarin (CMAC)] and microglia (CMTMR) were applied onto OHCs. Two hours after start of the experiment, the OHCs were placed in a custom-made chamber (Incubator S-M; Pecon) adjusted to 37°C and 5% CO₂ (CTI-Controller 3700 digital; Tempcontrol 37–2 digital; Pecon).

Time-lapse microscopy of PMN–microglia coculture. Primary microglia were cultured onto Matrigel-coated surfaces in a 12-well plate (Falcon; BD Biosciences Discovery Labware). Matrigel basement membrane matrix (BD Biosciences), containing laminin as a major component, was diluted in ice-cold DMEM (ratio, 1:20) and polymerized at 37°C for 30 min. Thereafter, 2 × 10⁵ microglia/well were placed and recovered for 1 d. Freshly prepared human PMNs were applied to the primary microglia culture. If indicated, PMNs were CMFDA labeled prior to application. Thirty minutes after the experimental start, the coculture was placed into the chamber as described above. The time-lapse microscope was based on an Axiovert 200M (Carl Zeiss) stage equipped with a 10×, numerical aperture (NA) 0.3 lens or a 32×, NA 0.5 lens (Carl Zeiss) and a CCD camera (AxioCam MRm; Carl Zeiss). Images were recorded at defined time intervals. The data were subsequently analyzed with the Carl Zeiss software (AxioVs40 V4.5).

Statistical analysis

All data are given as mean ± SEM. Statistical analysis was performed by one-way ANOVA followed by *post hoc* comparison (Tukey's test). A value of *p* < 0.05 was considered statistically significant.

Results

PMNs infiltrate the brain parenchyma after focal ischemia

Given the heterogeneity of the data concerning the relevance of peripheral immune cells for ischemia-induced neuronal damage, we first wanted to investigate which type of peripheral immune cell was initially recruited into the injured brain parenchyma after transient ischemia. To this end, endothelin was injected directly above the MCA. Endothelin as vasoconstrictor occluded the MCA for ~30 min. We found that, 1 d after injection, endothelin-mediated transient focal ischemia induced a cellular infiltrate that was mainly composed of PMNs as detectable from the characteristic lobulated nuclei of infiltrating cells in immunohistological sections of the damaged area (Fig. 1A). We found no marked infiltration with other peripheral immune cells such as macrophages or lymphocytes. Thus, the acute cellular infiltrate of the ischemia-injured brain *in vivo* was dominated by PMNs, suggesting a prominent role of this immune cell type for the additional development of neuronal damage.

Application of human PMNs onto organotypic hippocampal cultures does not influence neuronal survival

Following the results of the *in vivo* ischemia-induced recruitment of PMNs (Fig. 1A), one goal of this study was to clarify the role of PMNs for the development of neuronal viability. To this end, we chose a well established model of ischemic injury *in situ* using OHCs that maintain many characteristics of true brain–parenchyma, especially the complex three-dimensional structure of neuronal circuits, yet allow for precise control of cellular or humoral factors impacting on neuronal viability as described previously (Neumann et al., 2006). The first step was to evaluate whether PMNs as such had a detrimental effect on neuronal viability in healthy OHCs. Because of the very limited availability of primary rat PMNs, we chose to use human PMNs throughout this study and performed only key experiments with primary rat PMNs. Direct application of up to 2 × 10⁵ human PMNs onto control OHCs had no effect on neuronal viability in the cornu ammonis (CA1–CA3) area after 24 h (Fig. 1B). Additionally, we investigated the effect of PMNs on neuronal function by electro-

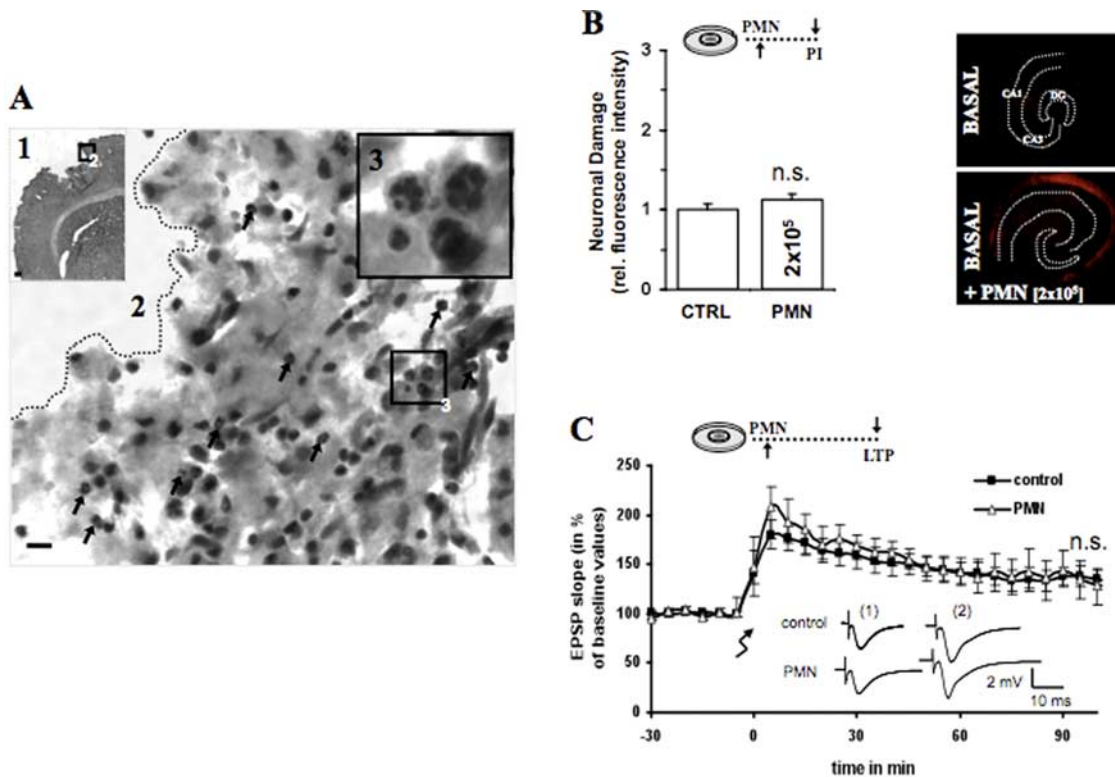


Figure 1. PMNs infiltrate the brain parenchyma 1 d after *in vivo* focal ischemia. **A1**, Hematoxylin/eosin staining of a coronal section shows an ischemic lesion in the cortex 1 d after focal ischemia. **A2**, Higher magnification from the edge of the ischemic lesion shows polymorphonuclear cells pointed by black arrows. **A3**, The black box in **A2** is enlarged in **A3** and demonstrates the occurrence of PMNs shown by the polymorphous nucleus. Scale bar: **A1**, 200 μm ; **A2**, 20 μm ; **A3**, 10 μm . **B**, A total of 2×10^5 PMNs was applied in 1 μl onto untreated OHCs. Quantification of neuronal death in CA1–3 was determined by PI incorporation after 24 h [control (CTRL) vs PMNs, nonsignificant (n.s.); $n = 9$ /bar]. In the panel next to the bar chart are representative PI fluorescent images showing neuronal death in CA1–3 after 24 h. **C**, Because of the nearly twice greater surface of 25-d-old slices, we applied 4×10^5 PMNs in 2 μl onto 1 DIV slices. The recording shows that applied PMNs did not influence EPSP signal nor the amount and persistence of LTP (CTRL vs PMNs, n.s.; CTRL = 11; PMNs, $n = 6$). Analogous traces represent typical recordings of single experiments taken 10 min before tetanization and 60 min after tetanization. Error bars indicate SEM.

physiological EPSP recording with subsequent LTP induction in 1 d *in vitro* (DIV) hippocampal slices. This approach provides two critical parameters of neuronal health. First, the shape and value of the synaptic signal reflects the quantity and integrity of the involved synapses. Second, the amount and persistence of the synaptic potentiation represents a highly sensitive marker for neuronal viability and functionality. According to the EPSP signal, neither the persistence nor the amount of the LTP was disturbed by application of 4×10^5 PMNs onto the 1 DIV hippocampal slices (Fig. 1C). These experiments indicated that PMNs derived from healthy human volunteers did not cause neuronal cell loss or neuronal electrophysiological disturbance in rat OHCs.

PMNs exacerbate neuronal damage after oxygen–glucose deprivation

To examine the effect of PMNs on CNS cells after ischemia, we simulated the PMN infiltration into the brain parenchyma by direct application of PMNs onto post-OGD OHCs (Fig. 2A). Application of increasing numbers of PMNs onto the OHCs after OGD resulted in a significant exacerbation of neuronal damage compared with OGD-induced neuronal damage alone (Fig. 2B). Representative fluorescence images of the densitometric quantification (Fig. 2B) are shown in Figure 2C. These data suggest that PMNs can aggravate the outcome of ischemic neurological insults after 24 h. For all the following experiments involving direct application of PMNs onto OHCs, 1×10^5 PMNs were used.

PMNs migrate rapidly into hippocampal slices independent of OGD-induced neuronal damage

We had previously shown that microglia can migrate deeply into OGD-damaged OHCs to provide neuroprotection (Neumann et al., 2006). Thus, we speculated that also PMNs might immigrate into OHCs, albeit with a neurotoxic effect after OGD. To test this assumption directly, we subjected cocultures of OGD-treated OHCs and PMNs to two-photon microscopy as previously described (Neumann et al., 2006). In this model, OHCs are made from mice that express EYFP under a specific Thy-1 promoter that leads to strong expression of the transgene in hippocampal neurons (Feng et al., 2000). We observed the rapid migration of PMNs into the brain tissue after 1 h under basal conditions. However, the PMN immigration rate into OGD-damaged slices was indistinguishable from that observed under control conditions (Fig. 3A,B). Also, at later time points, we detected a uniform distribution of PMNs within the slice and no differences between OGD conditions and basal conditions were observed (Fig. 3A–F). Additionally, we studied the morphology of EYFP-positive neurons within the OHCs after PMN application. The application of PMNs onto hippocampal slices without OGD showed morphologically intact neurons (neuronal body, dendrites, axons) at all analyzed time points (Fig. 3A,C,E). In contrast, OGD slices containing PMNs were characterized by a severe loss of axons and dendrites after 6 h (Fig. 3D) and an almost complete loss of EYFP-positive neurons associated with the appearance of subcellular granular material, presumably stemming

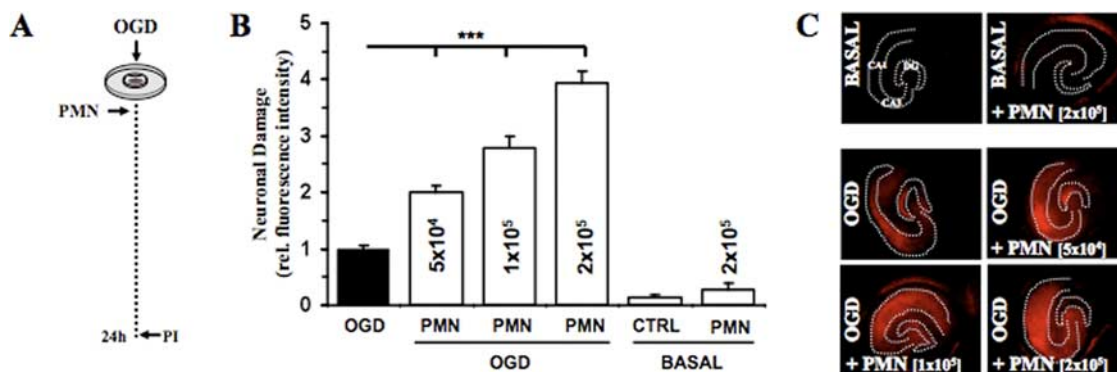


Figure 2. Polymorphonuclear granulocytes (PMNs) exacerbate neuronal damage after OGD. **A**, Different numbers of PMNs (0.5×10^5 , 1×10^5 , 2×10^5) were applied onto OHCs after OGD. **B**, Quantification of neuronal death in CA1–3 was determined by PI incorporation after 24 h ($***p < 0.001$ vs OGD; $n = 7$ /bar). Error bars indicate SEM. CTRL, Control. **C**, Representative PI fluorescent images showing neuronal death in CA1–3 after 24 h.

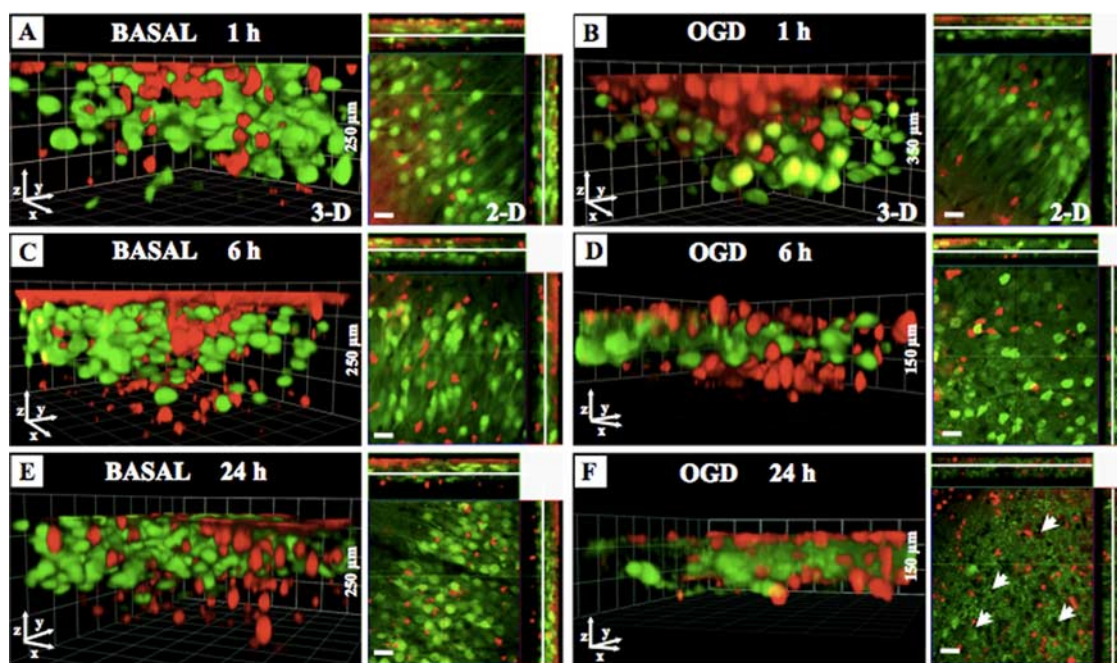


Figure 3. The migration of PMNs into the OHCs under basal and OGD conditions. PMNs (1×10^5) were labeled with CMTMR (red) and then directly applied onto OHCs prepared from B6.Cg-TgN(Thy1-YFP)16Jrs mice (neurons: green). At indicated time points (basal, 1, 6, 24 h; OGD, 1, 6, 24 h), slices were fixed with 4% PFA and subsequently Z-stacks through the whole OHCs were performed by using two-photon microscopy. **A–F**, Images show three-dimensional reconstruction of the OHCs and the representative focal plane (middle of OHCs) in the CA1 neuronal layer at the indicated time points after PMN application under basal conditions (**A**, **C**, **E**) or after OGD (**B**, **D**, **F**). Scale bars, 20 μ m.

from neuronal apoptosis and necrosis, in the CA1 area after 24 h (Fig. 3F). We also noted the appearance of holes in the otherwise homogenous layer of intact neuronal somata (Fig. 3F, arrowheads), which probably showed the loss of cell bodies in the respective areas. Thus, although PMNs have the ability to invade OHCs under normal conditions, they do not cause neuronal damage, unless this process is initiated by OGD.

Exogenous microglia counteract the neurotoxicity of PMNs

We previously showed that microglia can have a neuroprotective function in the OGD-induced neuronal damage within OHCs (Neumann et al., 2006). We next asked whether this might also hold true for the PMN-induced neurotoxicity. The direct application of PMNs (Fig. 4A), microglia, or macrophages (RAW264.7) to control OHCs had no effect on neuronal viability in the CA area after 48 h (Fig. 4B,C). However, although the presence of PMNs in OGD-treated OHCs showed a strong exacer-

beration of OGD-induced neuronal damage after 24 and 48 h (Fig. 4B,C), microglia application resulted in a significant reduction of OGD-induced neuronal damage after 48 h but not after 24 h (Fig. 4B,C). No significant effect on neuronal death was observed after application of macrophages (Fig. 4B,C). We next wanted to analyze whether microglia were also able to counteract the massive neurotoxicity induced by PMNs. Therefore, we applied PMNs (1×10^5) in combination with microglia or macrophages (0.8×10^5 each) directly onto the OHCs (Fig. 4D). The combined application of PMNs and microglia resulted in a significant reduction of PMN-caused exacerbation of neuronal damage after OGD (Fig. 4E). In contrast, no significant effect was detected by simultaneous application of PMNs and macrophages. These data suggested that there might be a direct interaction between microglia and PMNs, which significantly attenuated the deleterious effects of PMNs on neuronal survival.

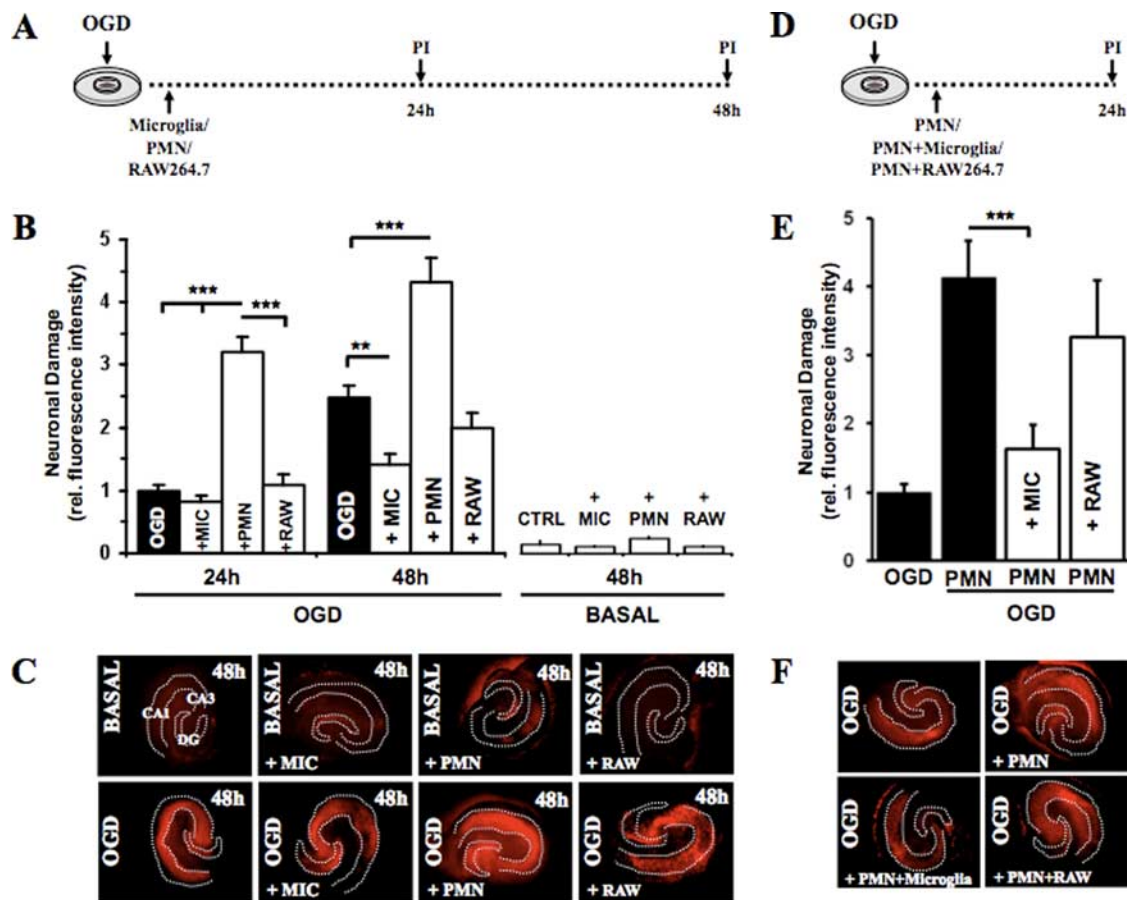


Figure 4. Exogenous microglia counteract PMN neurotoxicity. In *A–C*, the effects of PMNs, microglia, and macrophages (RAW264.7) were examined individually. *A*, PMNs (1×10^5), microglia (0.8×10^5), and macrophages (0.8×10^5) were applied directly onto the OHCs after OGD. *B*, Quantification of neuronal death in CA1–3 was determined by PI incorporation after 24 and 48 h (24 h: $***p < 0.01$ vs PMNs; 48 h: $***p < 0.001$ PMNs vs OGD, $**p < 0.01$ MIC vs OGD; $n = 9$ /bar). *C*, Representative PI fluorescent images showing neuronal death in CA1–3 48 h after OGD. In *D–F*, the effect of combined application of PMNs/microglia or PMNs/RAW264.7 was studied. *D*, PMNs were applied directly onto the OHCs together with microglia or macrophages after OGD. *E*, Quantification of neuronal death in CA1–3 was determined by PI incorporation after 24 h ($***p < 0.001$ PMNs vs PMNs/MIC; $n = 9$ /bar). Error bars indicate SEM. *F*, Representative PI fluorescent images showing neuronal death in CA1–3 24 h after OGD. MIC, Microglia; RAW, RAW264.7.

Microglia engulf PMNs within the OHCs

Based on these findings, we investigated a possible direct microglia–PMN interaction in OGD-damaged OHCs. Therefore, we applied fluorescently labeled PMNs and microglia onto the OHCs. Confocal microscopy analyses revealed that exogenous microglia had engulfed PMNs in OGD-treated OHCs (Fig. 5*A*). By means of two-photon microscopy and three-dimensional reconstruction of individual microglia, we found that endogenous as well as newly applied microglia were able to fully incorporate single or multiple PMNs within the OHCs (Fig. 5*B*). To investigate the cellular dynamics of such an engulfing process in more detail, we applied fluorescently labeled PMNs and microglia onto OHCs and recorded their migratory behavior by time-lapse microscopy. Surprisingly, we observed that, in addition to inactive (immotile and presumably apoptotic) PMNs, microglia were able to also engulf active (motile and viable) PMNs (Fig. 5*C*; supplemental movie 1, available at www.jneurosci.org as supplemental material).

Microglia engulf viable, motile, nonapoptotic PMNs

The previous experiments suggested that the microglia was able to engulf fully viable PMNs. However, although the phagocytosis of apoptotic cellular material by microglia is a relatively common process (Stolzing and Grune, 2004; Takahashi et al., 2005; Chan et al., 2006), the capture of active and viable cells by microglia was

not been observed before. Phototoxicity and bleaching prevented us from performing hour-long time-lapse sequences on individual OHCs. However, in several instances, we were able to document the uptake of live PMNs by parenchymal microglia within the brain slices in a manner very similar to the one observed before for isolated microglia (supplemental movie 6, available at www.jneurosci.org as supplemental material), which suggests that the behavior of the externally added microglia was similar to the parenchymal cells. The related low frequency of phagocytosis events in individual image sequences did not allow performing a thorough quantitative analysis of PMN phagocytosis in this *ex vivo* model system. We therefore performed cell culture experiments *in vitro*. PMNs (3×10^5) were cocultured with primary microglia (0.75×10^5) *in vitro*. These experiments allowed to clearly visualize the engulfing process of motile PMNs by individual microglia (Fig. 6*A,B*) and demonstrated that before being engulfed and phagocytosed PMNs could exhibit profound motility over long time periods (Fig. 6*A,A**).

We frequently observed that microglia adopted a “chasing behavior” while attempting to engulf PMNs, either including cellular protrusions (supplemental movie 2, available at www.jneurosci.org as supplemental material) or the whole cell bodies (Fig. 6*B*; supplemental movie 3, available at www.jneurosci.org as supplemental material). Because also immotile (presumably apoptotic or preapoptotic) PMNs were engulfed by microglia

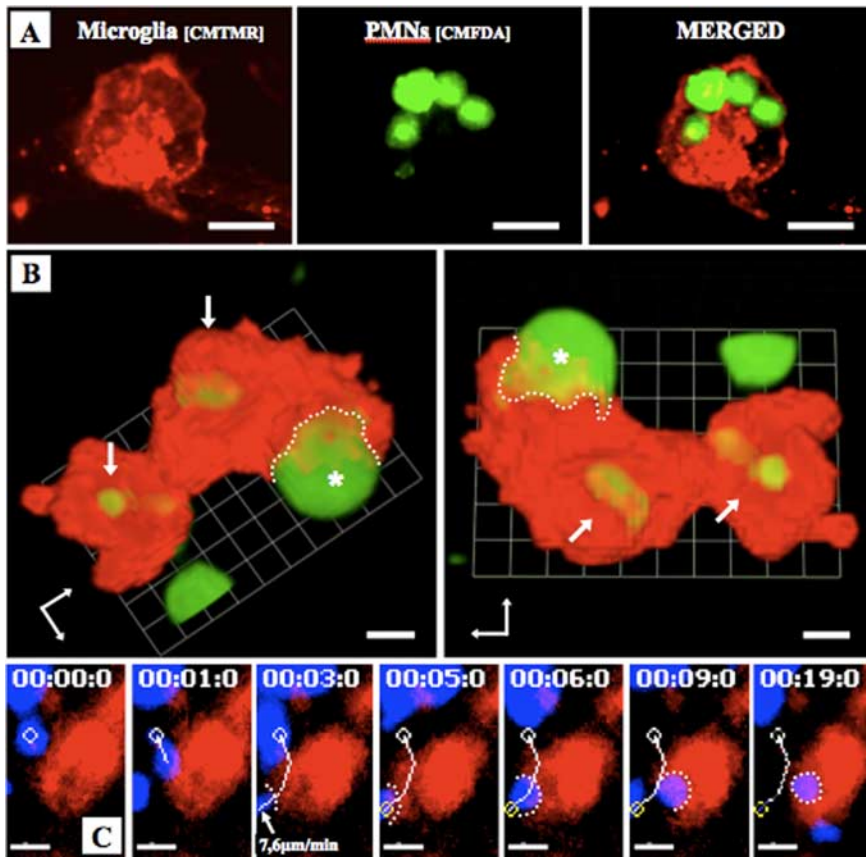


Figure 5. Microglia phagocytose PMNs within the OHCs. PMNs (1×10^5) were labeled with CMFDA (green) (*A*, *B*) or CMAC (blue) (*C*) and microglia with CMTMR (red) and then directly applied onto OHCs. *A*, OHC was fixed with 4% PFA and subsequently investigated using confocal microscopy. *B*, The images from a living slice show the three-dimensional reconstruction of one microglia that had already phagocytosed two PMNs (arrows) and was in progress to phagocytose another PMN (asterisk). The dotted line indicates the contact between microglia and PMNs. *C*, Time-lapse video microscopy was performed 4 h after experimental onset. Images show the engulfing of a motile PMN by the microglia. The white line indicates the migration pathway of the PMN. The microglia contacted the PMN at the time (3 min after start of time-lapse imaging) at which the PMN showed a velocity of $7.6 \mu\text{m}/\text{min}$. The white dotted line shows the contact point between microglia and PMN (supplemental movie 1, available at www.jneurosci.org as supplemental material). Scale bars: *A*, $20 \mu\text{m}$; *B*, $5 \mu\text{m}$; *C*, $10 \mu\text{m}$.

(Fig. 6*B*; supplemental movie 4, available at www.jneurosci.org as supplemental material), we next addressed the question of whether engulfed PMNs always exhibited signs of proapoptosis. Therefore, we transferred PMNs to primary microglia and added FITC-labeled Annexin V to the coculture. Annexin V binds to phosphatidylserine on the outer side of the membrane of cells that have already initiated the apoptotic cascade (Fadok et al., 1992). Thus, in our coculture system, proapoptotic cells (especially PMNs) were detectable by an increased FITC signal (Fig. 7). This set of experiments revealed that microglia indeed engulfed both proapoptotic PMNs and healthy PMNs (Fig. 7; supplemental movie 5, available at www.jneurosci.org as supplemental material). Our experimental setup required a 48 h resting period of primary microglia before use. Attempts to apply microglia directly shaken from the culture were not successful because these cells were not very active and partially died during the first hour of investigation. Thus, it could not be excluded that microglia were activated by the necessary culture conditions. Microscopic analysis of the cells showed that untreated microglia were very adhesive to plastic but, in the presence of supernatant of OGD-treated OHC or PMNs, detached from the plastic surface and obtained a motile morphology (supplemental Fig. 1, available at www.jneurosci.org as supplemental material), which suggested,

that indeed the microglia was activated by the presence of PMNs or the supernatant of OGD-treated OHC. Thus, it was possible that the observed phagocytosis behavior was a general phenomenon of activated macrophage-like cells and not specific for microglia. To test this assumption, we compared the ability of primary microglia with peritoneal macrophages freshly isolated from rats by peritoneal lavage with PBS. Analysis showed that despite being motile and frequently touching or dragging PMNs in the culture peritoneal macrophages never engulfed PMNs, whether apoptotic or alive (supplemental movie 7, available at www.jneurosci.org as supplemental material), whereas microglia cocultured in the same experiment phagocytosed on average 2.6 PMNs per cell (supplemental Fig. 2 and movie 8, available at www.jneurosci.org as supplemental material). Thus, the ability to phagocytose live or dead PMNs seemed to be specific for microglia activated by the presence of PMNs or the supernatant of OGD-treated OHC and was not observed with peripheral macrophages, at least from the peritoneum.

Blocking the engulfment process of PMNs by microglia worsens the outcome of neuronal viability after OGD

Next, we investigated whether the engulfment of PMNs by microglia had any consequence on neuronal viability after OGD. It has been shown that apoptotic PMN cells can be internalized by binding to the $\alpha_v\beta_3$ -integrin receptor on macrophages. In addition, lectin-like receptors have been

shown to be involved in this process (Fadok et al., 1998; Meszaros et al., 1999). Thus, we evaluated the potential of the integrin-blocking tetrapeptide RGDS (Arg-Gly-Asp-Ser) and the lectin inhibitor *N*-acetyl glucosamine (GlcNAc) to block the engulfing process by preincubating primary microglia with the reagents before adding PMNs to the culture. We distinguished between engulfment of motile or immotile PMNs by time-lapse microscopy. RGDS and GlcNAc blocked the engulfing of both immotile and, interestingly, also motile PMNs, highly significantly (Fig. 8*A*). Thereby GlcNAc was more efficient than RGDS (Fig. 8*A*). We also noted a slight synergistic effect on the blockage of the engulfment process when both substances were combined. This synergistic effect was more pronounced in the engulfment of nonmotile cells (Fig. 8*A*). Additionally, we always observed altered microglia–PMN interaction patterns in the presence of RGDS and GlcNAc. Whereas untreated microglia bound and engulfed PMNs, treated microglia bound several PMNs but mostly failed to ingest them (Fig. 8*B*).

An important question was whether interfering with the engulfment process affected the neuronal viability after OGD. To test this, we applied PMNs and microglia simultaneously onto the OHCs after OGD. Microglia and OHCs were also preincubated with RGDS/GlcNAc before application. Indeed, the presence of

RGDS or GlcNAc alone, and, more efficiently, in combination strongly reduced the neuroprotective function of coapplied microglia in this model (Fig. 8C). In addition, we obtained similar results by using primary rat PMNs, confirming that the observed behavior was specific for PMNs (Fig. 8C).

Thus, blocking the engulfment of PMNs by microglia severely compromised the neuroprotective function that microglia exerted on neurons on OGD exposure pointing to a physiological role of this cellular function of microglia.

Discussion

This study was designed to determine the role of individual cell types of the innate immune system that contribute to the postischemic inflammation after cerebral ischemia. Taking advantage of our neuroinflammation model, we were able to simulate the migration and infiltration of these cells to the site of damage in the neuronal tissue. It is generally accepted that the main immune cells involved in the inflammation-induced secondary neuronal damage are PMNs, microglia, and macrophages, which all are recruited as early as the postischemic inflammation is initiated. However, PMNs and local microglia are the first cells present on site, followed by peripheral microglia and monocytes/macrophages. Although all three cell types potentially exhibit cytotoxicity by releasing noxious substances such as cytokines, oxygen radicals, and proteases (Hallenbeck et al., 1986; Barone et al., 1991; Minghetti and Levi, 1998), their individual contribution to the overall damage remains unclear.

There is still an ongoing debate as to the importance of the individual cell types in brain ischemia. In an attempt to overcome this limitation, we chose to use a well established *ex vivo* model of neuroinflammation (Ullrich et al., 2001; Mitrasinovic et al., 2005; Neumann et al., 2006). Using this model, we were now able to demonstrate that indeed only PMNs sharply increased neuronal damage associated with transient ischemia. This was not a general phenomenon of infiltrating phagocytes, because neither local nor externally added microglia nor macrophages appeared to be neurotoxic after cerebral ischemia. In fact, we and others previously showed that local (Kohl et al., 2003) or externally added (Neumann et al., 2006) microglia may even be neuroprotective in this model. Our data provide strong evidence that PMNs are a critical innate immune cell type that is responsible for the increase of neuronal damage associated with ischemia. This finding is well in line with previous studies showing enhanced neuronal death after ischemia in a dissociated neuronal culture (Dinkel et al., 2004). Moreover, *in vivo* studies strongly correlate the degree of PMN infiltration to the size of the neuronal damage (Beray-Berthat et al., 2003b; Weston et al., 2007). Another study found a positive correlation between the intensity of myeloperoxidase staining, a hallmark of PMN activity, and the degree of neuronal damage in the area of ischemia (Matsuo et al., 1994). This finding also

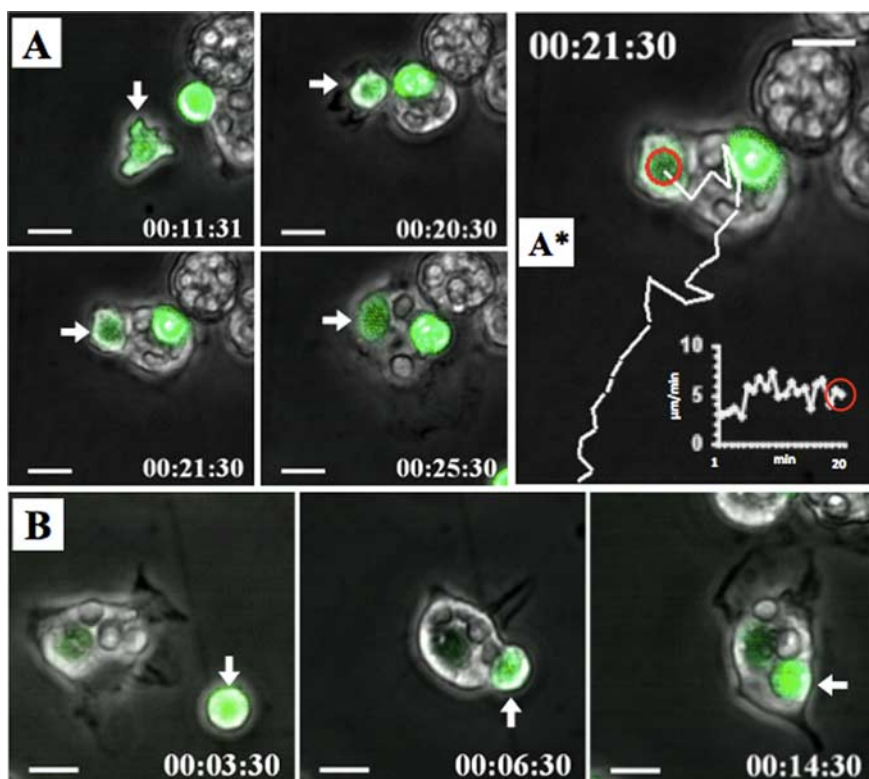


Figure 6. Microglia engulf motile PMNs. The panels show CMFDA (green)-labeled PMNs (3×10^5) cocultured with primary microglia (0.75×10^5). Cell movements were recorded by time-lapse microscopy. **A**, The panel displays a microglia that engulfed a motile CMFDA-labeled PMN (arrow). **A***, The image depicts the PMN migration path (white line) before the microglia contacted and engulfed the PMN (red circle). The integrated white graph shows the PMN velocity of $5 \mu\text{m}/\text{min}$ at the time the microglia had touched the PMN (supplemental movie 2, available at www.jneurosci.org as supplemental material). **B**, Images show the engulfment of an immotile CMFDA-labeled PMN (arrow) (supplemental movie 4, available at www.jneurosci.org as supplemental material). Scale bars, $10 \mu\text{m}$.

strongly supports the view that PMNs are critically involved in the progress of postischemic neuronal damage.

Interestingly, the inhibition of reactive oxygen species (ROS) production by NAD(P)H-oxidases, one of the key actions of inflammatory PMNs (Segal, 2005), results in strong neuroprotective effects in rodent models of ischemic stroke (Wang et al., 2006; L. L. Tang et al., 2007). Moreover, interfering with the homing of immune cells by an antiadhesive therapy has been shown to be neuroprotective (Connolly et al., 1996; Yanaka et al., 1996). However, because this approach affects indiscriminately all immune cell types, it did not provide any suggestions as to whether PMNs might play a specific role in this context. In addition, it is assumed that also cells of the adaptive immune system can invade areas of ischemia-induced neuroinflammation (Arumugam et al., 2005). Because their contribution is still unclear, our model is well suited to examine this matter in the future. In summary, in the line of these previous data and our study, it seems likely that PMNs constitute an important neurotoxic cell type under ischemic conditions. Because we did not find evidence that microglia and macrophages were neurotoxic, at least 48 h after ischemia, we assume that interfering with the function of PMNs might be a particularly promising option to limit the extent of neuronal damage after stroke.

A major conclusion from our study is that there seems to be a natural mechanism aiming precisely at this goal. After coapplying microglia and PMNs onto ischemically damaged OHCs, we found a strong decrease of neuronal damage compared with the application of PMNs alone. This was a rather unexpected finding, because numerous studies demonstrated that microglia preacti-

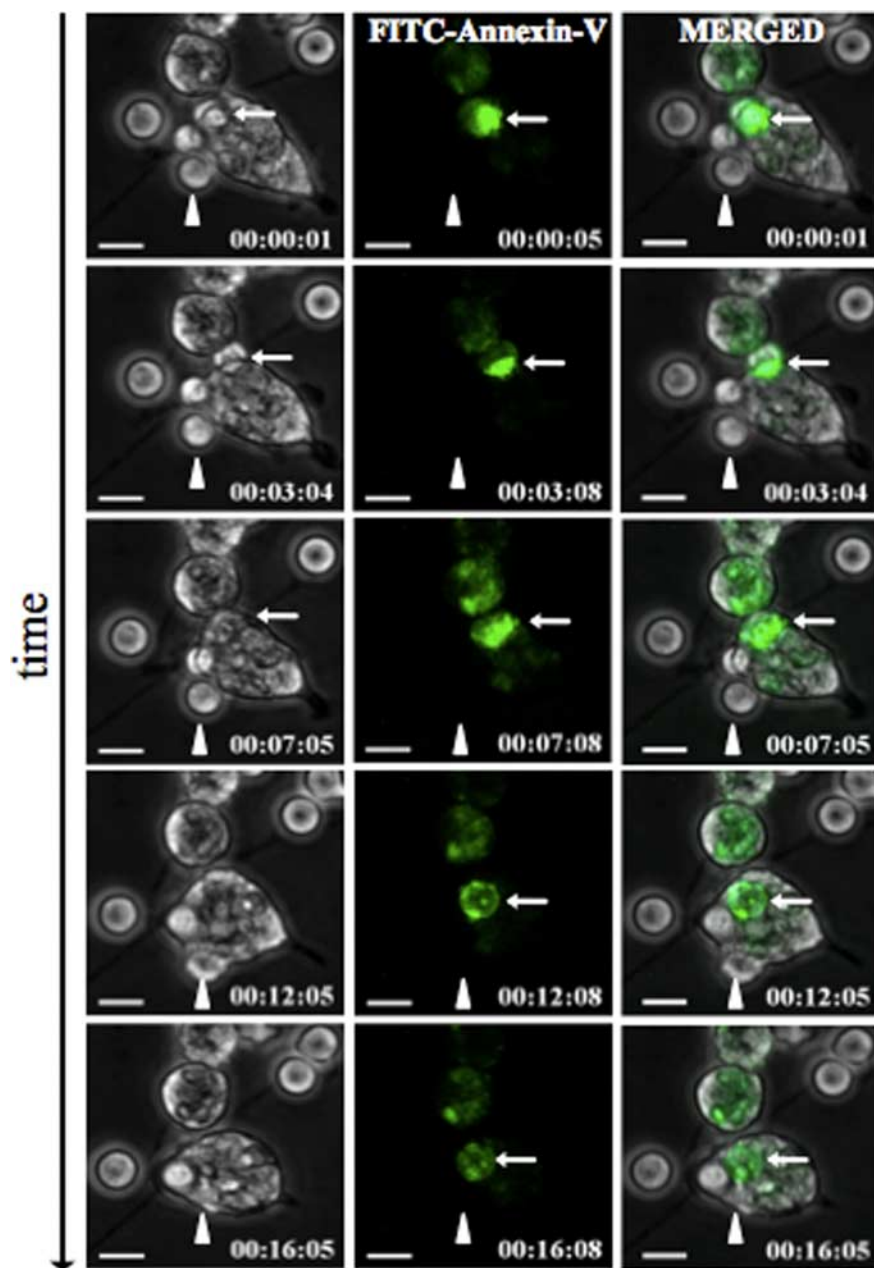


Figure 7. Microglia engulf preapoptotic and nonapoptotic PMNs. FITC-conjugated Annexin V was added to the microglia–PMN coculture, and thus preapoptotic cells were visualized by an increased FITC signal. The white thin arrow points on an Annexin V-positive PMN that was fully engulfed after 12 min. The arrowhead shows a PMN that was engulfed without exhibiting a FITC signal at any time point of the engulfment process (supplemental movie 5, available at www.jneurosci.org as supplemental material). Scale bars, 10 μ m.

vated by inflammatory mediators are strongly neurotoxic (Arai et al., 2004; Minghetti et al., 2004; Qin et al., 2004; Fordyce et al., 2005; Huang et al., 2005). However, a close inspection of these studies shows that microglial activation was achieved by exposure to microbial products (Arai et al., 2004; Qin et al., 2004; Huang et al., 2005) or viral particles (Lim et al., 2003; Minghetti et al., 2004). Lipopolysaccharide (LPS) or viral particles are well known to trigger a massive immune cell reaction via Toll-like receptors (TLRs) (Kawai and Akira, 2006). Recent evidence suggests that, even in the situation of stroke, which constitutes a sterile inflammation, Toll-like mediated pathways can be triggered on microglia (Lehnardt et al., 2007) or even directly on neurons (S. C. Tang et al., 2007) and that this response increases neuronal damage after

stroke. However, the signaling induced by bacterial TLR triggers might well be different from the one induced by endogenous inflammatory mediators because neurons, which express both TLR-2 and -4 do not respond to classical triggers of these receptors such as peptidoglycan or LPS (S. C. Tang et al., 2007). It might, therefore, be possible that also microglia are able to distinguish between microbial and other inflammatory stimuli of the TLR system. In this concept, microglia activated by nonmicrobial inflammation might exert neuroprotective effects, whereas microbial activation of microglia preferentially triggers neurotoxicity.

Our study also provides insights into the mechanism whereby this protection is accomplished. We demonstrate that microglia were very effective in phagocytosing invading PMNs. Macrophage-like cells are well known to clear the inflamed tissue from cell debris, such as apoptotic PMNs. Two recent histological studies have also demonstrated brain-resident microglia associated with PMN-related debris in areas of ischemia-induced neuronal damage (Denes et al., 2007; Weston et al., 2007). However, our data show that, in addition to proapoptotic PMNs, also fully viable, Annexin V-negative, PMNs were effectively engulfed by microglia.

In contrast, we have never observed microglia engulfing other types of immune cells such as freshly prepared lymphocytes and monocytes, and in addition we did not find engulfing of PMNs by macrophage lines or freshly prepared peritoneal macrophages. These findings underscore the specificity of the microglia–PMN engagement. By time-lapse microscopy, we observed microglia exerting a PMN chasing behavior, either including cellular protrusions or the whole cell bodies. To the best of our knowledge, the phagocytosis of active and viable immune cells by other immune cells has not been described so far and therefore might represent an entirely novel way of immune control. This is probably attributable to the fact that such a mechanism can only be revealed by life cell imaging, which is technically chal-

lenging, especially with the cell types investigated in the current study.

Given the fact that phagocytosis was inhibitable by RGDS peptides and GlcNAc, we assumed that integrins such as vitronectin receptors (Ruoslahti, 1996) or lectins mediated the engulfment process. Although this is well known for the uptake of apoptotic cells (Fadok et al., 1998; Meszaros et al., 1999), this surprisingly also held true for the uptake of presumably live cells. We cannot formally exclude that even Annexin V-negative cells were already proapoptotic thereby exposing vitronectin or lectin ligands. However, the fact that the cells were very motile argued against this hypothesis, because one of the earliest events of apoptosis is loss of migration (Savill et al., 2002).

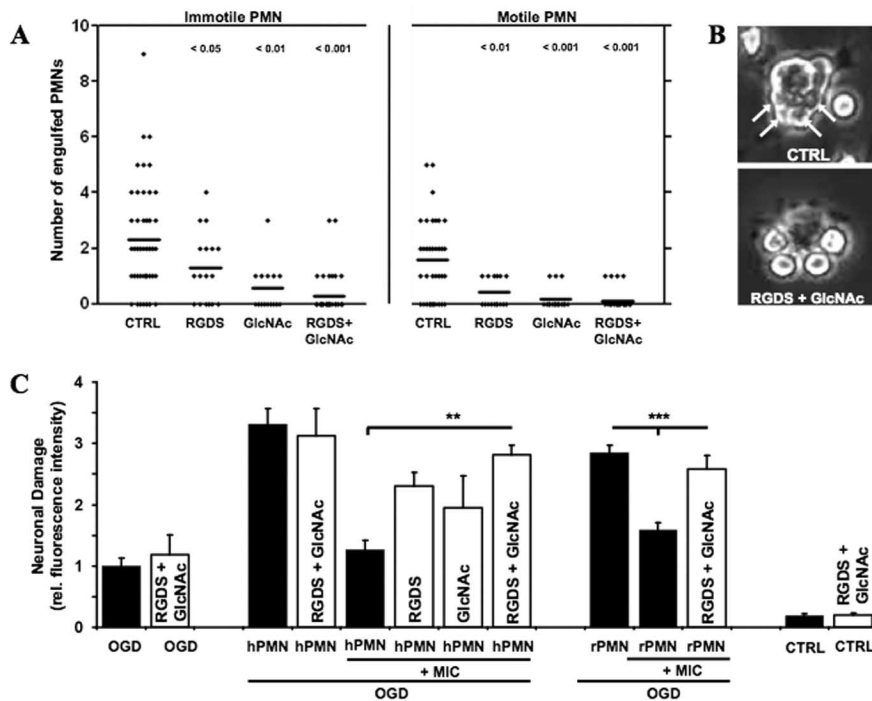


Figure 8. Blockage of the engulfment process of PMNs by microglia worsens the outcome of neuronal viability after OGD. **A**, Microglia were preincubated with RGDS (1 mM) or GlcNAc (20 mM) or both for 20 min before PMNs were added to the microglia. Time-lapse microscopy was performed to distinguish the engulfment of immotile and motile PMNs by the microglia. Column scatterplots show the number of PMNs engulfed by microglia under the indicated conditions. Significance values are shown above the columns. **B**, The images show representative microglia that were exposed to PMNs. The arrows on the top image display the engulfed PMN within the microglia. The bottom image shows PMNs that adhere to the microglia without being internalized. **C**, Microglia were preincubated with RGDS (1 mM) and GlcNAc (20 mM) or both for 20 min before they were applied together with either human-derived (hPMN) or rat-derived (rPMN) PMN onto OGD-treated OHCs. Quantification of neuronal death in CA1–3 was determined by PI incorporation after 24 h [$^{**}p < 0.01$, hPMN plus MIC (OGD) vs hPMN plus MIC plus RGDS/GlcNAc (OGD); $^{***}p < 0.001$, rPMN plus MIC (OGC) vs rPMN plus MIC plus RGDS/GlcNAc (OGD); $n = 5–7$ /bar]. Error bars indicate SEM. CTRL, Control; MIC, microglia.

Our study also indicates that interference with the phagocytosis process by RGDS and GlcNAc abolished the neuroprotective function of microglia. It is well conceivable that dying PMNs mediate neurotoxicity by the release of toxic intracellular compounds (Denes et al., 2007; Weston et al., 2007), and that, consequently, prompt phagocytosis of apoptotic PMNs by microglia might prevent the secretion of toxic compounds. In the light of these findings, we propose that clearance of PMNs from the nervous tissue might be an effective strategy to protect neurons from PMN neurotoxicity. Whether the engulfment of viable PMNs contributes to this protection remains to be determined and requires to be examined in additional studies. In our system, phagocytosis of motile (presumably viable) PMNs was even more frequent than the uptake of nonmotile cells. Therefore, it appears unlikely that this process is irrelevant for the protection we observed. How microglia turn off the neurotoxicity of a live PMN currently remains enigmatic. A possible mechanism might include active interference with cytokine secretion and production of ROS. This might be mediated by the rapid destruction of engulfed PMNs, which appears to be happening to PMNs after phagocytosis by microglia in our system. Finally, it has also been shown that macrophages release immune-regulatory cytokines such as TGF- β (Savill et al., 2002) after uptake of apoptotic PMNs. A similar process might also be exhibited by microglia after uptake of PMNs, with TGF- β mediating neuroprotection by reducing the general inflammatory responses. Future studies are required to verify whether the processes observed in our *ex vivo* model are truly active and physiologically relevant *in vivo*. If so, future therapies

might aim achieving neuroprotection by supporting microglia activation, thereby rapidly eliminating infiltrating PMNs from the ischemic lesion site.

References

- Arai H, Furuya T, Yasuda T, Miura M, Mizuno Y, Mochizuki H (2004) Neurotoxic effects of lipopolysaccharide on nigral dopaminergic neurons are mediated by microglial activation, interleukin-1 β , and expression of caspase-11 in mice. *J Biol Chem* 279:51647–51653.
- Arumugam TV, Granger DN, Mattson MP (2005) Stroke and T-cells. *Neuromol Med* 7:229–242.
- Baldauf K, Reymann KG (2005) Influence of EGF/bFGF treatment on proliferation, early neurogenesis and infarct volume after transient focal ischemia. *Brain Res* 1056:158–167.
- Banati RB, Graeber MB (1994) Surveillance, intervention and cytotoxicity: is there a protective role of microglia? *Dev Neurosci* 16:114–127.
- Barone FC, Hillegass LM, Price WJ, White RF, Lee EV, Feuerstein GZ, Sarau HM, Clark RK, Griswold DE (1991) Polymorphonuclear leukocyte infiltration into cerebral focal ischemic tissue: myeloperoxidase activity assay and histologic verification. *J Neurosci Res* 29:336–345.
- Beray-Berthaut V, Palmier B, Plotkine M, Margail I (2003a) Neutrophils do not contribute to infarction, oxidative stress, and NO synthase activity in severe brain ischemia. *Exp Neurol* 182:446–454.
- Beray-Berthaut V, Croci N, Plotkine M, Margail I (2003b) Polymorphonuclear neutrophils contribute to infarction and oxidative stress in the cortex but not in the striatum after ischemia-reperfusion in rats. *Brain Res* 987:32–38.
- Chan A, Hummel V, Weilbach FX, Kieser BC, Gold R (2006) Phagocytosis of apoptotic inflammatory cells downregulates microglial chemoattractive function and migration of encephalitogenic T cells. *J Neurosci Res* 84:1217–1224.
- Connolly Jr ES, Winfree CJ, Springer TA, Naka Y, Liao H, Yan SD, Stern DM, Solomon RA, Gutierrez-Ramos JC, Pinsky DJ (1996) Cerebral protection in homozygous null ICAM-1 mice after middle cerebral artery occlusion. Role of neutrophil adhesion in the pathogenesis of stroke. *J Clin Invest* 97:209–216.
- del Zoppo GJ, Becker KJ, Hallenbeck JM (2001) Inflammation after stroke: is it harmful? *Arch Neurol* 58:669–672.
- Denes A, Vidyasagar R, Feng J, Narvainen J, McColl BW, Kauppinen RA, Allan SM (2007) Proliferating resident microglia after focal cerebral ischaemia in mice. *J Cereb Blood Flow Metab* 27:1941–1953.
- Dinkel K, Dhabhar FS, Sapolsky RM (2004) Neurotoxic effects of polymorphonuclear granulocytes on hippocampal primary cultures. *Proc Natl Acad Sci USA* 101:331–336.
- Dirnagl U, Iadecola C, Moskowitz MA (1999) Pathobiology of ischaemic stroke: an integrated view. *Trends Neurosci* 22:391–397.
- Fadok VA, Voelker DR, Campbell PA, Cohen JJ, Bratton DL, Henson PM (1992) Exposure of phosphatidylserine on the surface of apoptotic lymphocytes triggers specific recognition and removal by macrophages. *J Immunol* 148:2207–2216.
- Fadok VA, Warner ML, Bratton DL, Henson PM (1998) CD36 is required for phagocytosis of apoptotic cells by human macrophages that use either a phosphatidylserine receptor or the vitronectin receptor ($\alpha v \beta 3$). *J Immunol* 161:6250–6257.
- Fassbender K, Ragooschke A, Kuhl S, Szabo K, Fatar M, Back W, Bertsch T, Kreisler S, Hennerici M (2002) Inflammatory leukocyte infiltration in focal cerebral ischemia: unrelated to infarct size. *Cerebrovasc Dis* 13:198–203.
- Feng G, Mellor RH, Bernstein M, Keller-Peck C, Nguyen QT, Wallace M, Nerbonne JM, Lichtman JW, Sanes JR (2000) Imaging neuronal subsets

- in transgenic mice expressing multiple spectral variants of GFP. *Neuron* 28:41–51.
- Feuerstein G, Wang X, Barone F (1998) Cerebrovascular disease: pathophysiology, diagnosis and management. Oxford: Blackwell Scientific.
- Feuerstein GZ, Wang X (2001) Inflammation and stroke: benefits without harm? *Arch Neurol* 58:672–674.
- Fordyce CB, Jagasia R, Zhu X, Schlichter LC (2005) Microglia Kv1.3 channels contribute to their ability to kill neurons. *J Neurosci* 25:7139–7149.
- Giulian D, Vaca K, Corpuz M (1993) Brain glia release factors with opposing actions upon neuronal survival. *J Neurosci* 13:29–37.
- Hallenbeck JM, Dutka AJ, Tanishima T, Kochanek PM, Kumaroo KK, Thompson CB, Obrenovitch TP, Contreras TJ (1986) Polymorphonuclear leukocyte accumulation in brain regions with low blood flow during the early postischemic period. *Stroke* 17:246–253.
- Harris AK, Ergul A, Kozak A, Machado LS, Johnson MH, Fagan SC (2005) Effect of neutrophil depletion on gelatinase expression, edema formation and hemorrhagic transformation after focal ischemic stroke. *BMC Neurosci* 6:49.
- Hayashi Y, Tomimatsu Y, Suzuki H, Yamada J, Wu Z, Yao H, Kagamiishi Y, Tateishi N, Sawada M, Nakanishi H (2006) The intra-arterial injection of microglia protects hippocampal CA1 neurons against global ischemia-induced functional deficits in rats. *Neuroscience* 142:87–96.
- Hayward NJ, Elliott PJ, Sawyer SD, Bronson RT, Bartus RT (1996) Lack of evidence for neutrophil participation during infarct formation following focal cerebral ischemia in the rat. *Exp Neurol* 139:188–202.
- Heinel LA, Rubin S, Rosenwasser RH, Vasthare US, Tuma RF (1994) Leukocyte involvement in cerebral infarct generation after ischemia and reperfusion. *Brain Res Bull* 34:137–141.
- Huang Y, Liu J, Wang LZ, Zhang WY, Zhu XZ (2005) Neuroprotective effects of cyclooxygenase-2 inhibitor celecoxib against toxicity of LPS-stimulated macrophages toward motor neurons. *Acta Pharmacol Sin* 26:952–958.
- Jean WC, Spellman SR, Nussbaum ES, Low WC (1998) Reperfusion injury after focal cerebral ischemia: the role of inflammation and the therapeutic horizon. *Neurosurgery* 43:1382–1397.
- Jordan JE, Zhao ZQ, Vinten-Johansen J (1999) The role of neutrophils in myocardial ischemia-reperfusion injury. *Cardiovasc Res* 43:860–878.
- Kawai T, Akira S (2006) Innate immune recognition of viral infection. *Nat Immunol* 7:131–137.
- Kim WK, Ko KH (1998) Potentiation of *N*-methyl-D-aspartate-mediated neurotoxicity by immunostimulated murine microglia. *J Neurosci Res* 54:17–26.
- Kitamura Y, Takata K, Inden M, Tsuchiya D, Yanagisawa D, Nakata J, Taniguchi T (2004) Intracerebroventricular injection of microglia protects against focal brain ischemia. *J Pharmacol Sci* 94:203–206.
- Kochanek PM, Hallenbeck JM (1992) Polymorphonuclear leukocytes and monocytes/macrophages in the pathogenesis of cerebral ischemia and stroke. *Stroke* 23:1367–1379.
- Kohl A, Dehghani F, Korf HW, Hailer NP (2003) The bisphosphonate clodronate depletes microglial cells in excitotoxically injured organotypic hippocampal slice cultures. *Exp Neurol* 181:1–11.
- Kreutzberg GW (1996) Microglia: a sensor for pathological events in the CNS. *Trends Neurosci* 19:312–318.
- Lalancette-Hebert M, Gowing G, Simard A, Weng YC, Kriz J (2007) Selective ablation of proliferating microglial cells exacerbates ischemic injury in the brain. *J Neurosci* 27:2596–2605.
- Lehnardt S, Lehmann S, Kaul D, Tschimmel K, Hoffmann O, Cho S, Krueger C, Nitsch R, Meisel A, Weber JR (2007) Toll-like receptor 2 mediates CNS injury in focal cerebral ischemia. *J Neuroimmunol* 190:28–33.
- Lim MC, Brooke SM, Sapolsky RM (2003) gp120 neurotoxicity fails to induce heat shock defenses, while the overexpression of hsp70 protects against gp120. *Brain Res Bull* 61:183–188.
- Matsuo Y, Onodera H, Shiga Y, Nakamura M, Ninomiya M, Kihara T, Kogure K (1994) Correlation between myeloperoxidase-quantified neutrophil accumulation and ischemic brain injury in the rat. Effects of neutrophil depletion. *Stroke* 25:1469–1475.
- Meszaros AJ, Reichner JS, Albina JE (1999) Macrophage phagocytosis of wound neutrophils. *J Leukoc Biol* 65:35–42.
- Miljkovic-Lolic M, Silbergleit R, Fiskum G, Rosenthal RE (2003) Neuroprotective effects of hyperbaric oxygen treatment in experimental focal cerebral ischemia are associated with reduced brain leukocyte myeloperoxidase activity. *Brain Res* 971:90–94.
- Minghetti L, Levi G (1998) Microglia as effector cells in brain damage and repair: focus on prostanoids and nitric oxide. *Prog Neurobiol* 54:99–125.
- Minghetti L, Visentin S, Patrizio M, Franchini L, Ajmone-Cat MA, Levi G (2004) Multiple actions of the human immunodeficiency virus type-1 Tat protein on microglial cell functions. *Neurochem Res* 29:965–978.
- Mitrasinovic OM, Grattan A, Robinson CC, Lapusta NB, Poon C, Ryan H, Phong C, Murphy Jr GM (2005) Microglia overexpressing the macrophage colony-stimulating factor receptor are neuroprotective in a microglial-hippocampal organotypic coculture system. *J Neurosci* 25:4442–4451.
- Morioka T, Kalehua AN, Streit WJ (1991) The microglial reaction in the rat dorsal hippocampus following transient forebrain ischemia. *J Cereb Blood Flow Metab* 11:966–973.
- Neumann J, Gunzer M, Gutzeit HO, Ullrich O, Reymann KG, Dinkel K (2006) Microglia provide neuroprotection after ischemia. *FASEB J* 20:714–716.
- Prestigiacomo CJ, Kim SC, Connolly Jr ES, Liao H, Yan SF, Pinsky DJ (1999) CD18-mediated neutrophil recruitment contributes to the pathogenesis of reperfusion but not nonreperfusion stroke. *Stroke* 30:1110–1117.
- Qin L, Liu Y, Wang T, Wei SJ, Block ML, Wilson B, Liu B, Hong JS (2004) NADPH oxidase mediates lipopolysaccharide-induced neurotoxicity and proinflammatory gene expression in activated microglia. *J Biol Chem* 279:1415–1421.
- Rapalino O, Lazarov-Spiegler O, Agranov E, Velan GJ, Yoles E, Fraidakis M, Solomon A, Gepstein R, Katz A, Belkin M, Hadani M, Schwartz M (1998) Implantation of stimulated homologous macrophages results in partial recovery of paraplegic rats. *Nat Med* 4:814–821.
- Rogove AD, Tsirka SE (1998) Neurotoxic responses by microglia elicited by excitotoxic injury in the mouse hippocampus. *Curr Biol* 8:19–25.
- Ruoslahti E (1996) RGD and other recognition sequences for integrins. *Annu Rev Cell Dev Biol* 12:697–715.
- Savill J, Dransfield I, Gregory C, Haslett C (2002) A blast from the past: clearance of apoptotic cells regulates immune responses. *Nat Rev Immunol* 2:965–975.
- Segal AW (2005) How neutrophils kill microbes. *Annu Rev Immunol* 23:197–223.
- Shaked I, Tchoresh D, Gersner R, Meiri G, Mordechai S, Xiao X, Hart RP, Schwartz M (2005) Protective autoimmunity: interferon-gamma enables microglia to remove glutamate without evoking inflammatory mediators. *J Neurochem* 92:997–1009.
- Sharkey J, Butcher SP (1995) Characterisation of an experimental model of stroke produced by intracerebral microinjection of endothelin-1 adjacent to the rat middle cerebral artery. *J Neurosci Methods* 60:125–131.
- Stolzing A, Grune T (2004) Neuronal apoptotic bodies: phagocytosis and degradation by primary microglial cells. *FASEB J* 18:743–745.
- Stoppini L, Buchs PA, Muller D (1991) A simple method for organotypic cultures of nervous tissue. *J Neurosci Methods* 37:173–182.
- Streit WJ (2002) Microglia as neuroprotective, immunocompetent cells of the CNS. *Glia* 40:133–139.
- Takahashi K, Rochford CD, Neumann H (2005) Clearance of apoptotic neurons without inflammation by microglial triggering receptor expressed on myeloid cells-2. *J Exp Med* 201:647–657.
- Tang LL, Ye K, Yang XF, Zheng JS (2007) Apocynin attenuates cerebral infarction after transient focal ischaemia in rats. *J Int Med Res* 35:517–522.
- Tang SC, Arumugam TV, Xu X, Cheng A, Mughal MR, Jo DG, Lathia JD, Siler DA, Chigurupati S, Ouyang X, Magnus T, Camandola S, Mattson MP (2007) Pivotal role for neuronal Toll-like receptors in ischemic brain injury and functional deficits. *Proc Natl Acad Sci USA* 104:13798–13803.
- Ullrich O, Diestel A, Eyupoglu IY, Nitsch R (2001) Regulation of microglial expression of integrins by poly(ADP-ribose) polymerase-1. *Nat Cell Biol* 3:1035–1042.
- Wang Q, Tompkins KD, Simonyi A, Korthuis RJ, Sun AY, Sun GY (2006) Apocynin protects against global cerebral ischemia-reperfusion-induced oxidative stress and injury in the gerbil hippocampus. *Brain Res* 1090:182–189.
- Weston RM, Jones NM, Jarrott B, Callaway JK (2007) Inflammatory cell infiltration after endothelin-1-induced cerebral ischemia: histochemical and myeloperoxidase correlation with temporal changes in brain injury. *J Cereb Blood Flow Metab* 27:100–114.
- Yanaka K, Camarata PJ, Spellman SR, McCarthy JB, Furcht LT, Low WC, Heros RC (1996) Neuronal protection from cerebral ischemia by synthetic fibronectin peptides to leukocyte adhesion molecules. *J Cereb Blood Flow Metab* 16:1120–1125.
- Yrjanheikki J, Tikka T, Keinänen R, Goldsteins G, Chan PH, Koistinaho J (1999) A tetracycline derivative, minocycline, reduces inflammation and protects against focal cerebral ischemia with a wide therapeutic window. *Proc Natl Acad Sci USA* 96:13496–13500.

Preparation of a tissue-like cortical primary culture from embryonic rats using Matrigel and serum free Start V Medium

Holger Braun^{a,*}, Claudia Bühnemann^b, Jens Neumann^a, Klaus G. Reymann^{a,b}

^a Leibniz Institut für Neurobiologie, Projektgruppe Neuropharmakologie, Brenneckestrasse 6, D-39118 Magdeburg, Germany

^b FAN gGmbH, Leipziger Str. 44, D-39120 Magdeburg, Germany

Received 21 February 2006; received in revised form 24 March 2006; accepted 28 March 2006

Abstract

To address the scientific quest for unravelling signalling pathways crucial in CNS development and function, cell culture systems have to be developed that are mimicking the physiological state of brain cells more efficiently. Here, we describe a method for cultivation of a virtual three-dimensional structure consisting of neural stem cell-derived cell types by using Matrigel as surface substrate and Start V as a serum free medium. We demonstrate that free floating dissociated cells form attached neurospheres from which cells start migration to surrounding areas and develop a virtual three-dimensional cell structure composed of neurons, glia and neural stem cells. Neuronal precursor cells differentiate into cholinergic and GABAergic cells and express vesicle proteins. Further, neuronal cells are interwoven with Nestin positive stem cells and GFAP positive astrocytes. Additionally, oligodendrocytes and microglia can also be detected in this neural tissue-like structure. As an example for studying cell migration we added externally microglial cells (BV2) and performed a confocal time lapse study. It revealed, that co-cultivated microglial cells migrated towards neurospheres within 14 h. Thus, the described method provides a serum free, tissue-like primary cell culture system of neural cells useful for the investigations of basic cell–cell interactions under in vitro conditions.

© 2006 Elsevier B.V. All rights reserved.

Keywords: Primary cortical culture; Matrigel; Start V Medium; Neurosphere; Migration; Serum free

1. Introduction

Primary cultures consisting of dissociated neurons or astrocytes prepared from hippocampal or cortical tissue present widely used in vitro models for neurophysiological and neuropharmacological applications. The various research areas include protein expression studies of receptor-proteins (Brown et al., 1997), axonogenesis (Dotti and Banker, 1987; Mandell and Banker, 1998; Hayashi et al., 2002; Oliva et al., 2003), signalling pathways (Grewal et al., 2000), intraneuronal transport phenomena (Davis et al., 1987) and toxicity studies (Keilhoff and Erdo, 1991). The feasibility of cultivation of dissociated neuronal cells prepared from embryonic rats was firstly demonstrated by Banker and Cowan (1977, 1979). At the beginning neurons were co-cultivated with tissue explants. Then, feeder cell layer were developed as a crucial nutrient source for the survival of cultivated neurons (Dichter, 1978). Later, co-cultivation

was withdrawn and replaced by either serum free media or media supplemented with serum (Xie et al., 2000; Romijn, 1988; Brewer, 1995). However, since dissociated cell cultures of hippocampal or cortical origin are composed of neurons and glial cells, strongly proliferating astrocytes will displace non-proliferating neurons. To impede this, cytostatic drugs, as for example AraC (cytosine arabinoside) were added to growing cells (Hertz et al., 1982, 1989; Waagepetersen et al., 1998).

Primary cultures offer the opportunity for visualizing many processes like axonogenesis or synaptogenesis on the level of single cells. Immunocytochemical methods are frequently used for this purpose. For applying modern immunofluorescent methods it is inevitable to grow the cells on glass cover slips to prevent quenching or autofluorescence effects. Therefore, coating the cover slips is needed for successful cell attachment and growth. Various compounds, as for example poly-L-lysine (PLL), laminin or poly-L-ornithine are described for coating procedures (Kondratyev et al., 1989; Pons et al., 2001; Rubin et al., 2002). Here, we describe the cultivation of primary cortical neural cells isolated from embryonic rats on cover slips coated with the extracellular matrix Matrigel. Cells were grown

* Corresponding author. Tel.: +49 391 6263781.

E-mail address: Holger.Braun@ifn-magdeburg.de (H. Braun).

under serum free conditions using the neuronal differentiation medium Start V without adding any cytostatics. Matrigel is a solubilized basement membrane preparation extracted from the Engelbreth–Holm–Swarm (EHS) mouse sarcoma and consisting of laminin, collagen IV, heparan sulfate, proteoglycans, entactin and nidogen (Kleinman et al., 1982). After polymerisation at room temperature Matrigel produces a biologically active matrix resembling the extracellular matrix produced by mammalian cells. Start V Medium was especially designed for culturing of neuronal cells without adding serum. Here, we report that Matrigel and Start V Medium allow a quick and easy preparation of primary cultures from neural tissues. We demonstrate that initially dispersed single cells form neurospheres which give rise to a virtual three-dimensional cell structure composed of neurons, astrocytes and oligodendrocytes as well as neural stem cells and microglia. Furthermore, as an example for studying cell–cell contacts we demonstrate the interaction of microglial cells added from outside with our primary culture.

2. Material and methods

2.1. Cell culture

Male and female rats were paired for 3 days. Positive vaginal plaque test was dated as day E0. On day E18 the pregnant female was deeply anesthetised by chloroform and decapitated. The uteri were dissected from the abdomen and transferred to a sterile petri dish with ice cold PBS. Embryos were removed and immediately decapitated. The skulls were collected into ice cold Hanks-buffer (Biochrom; Berlin, Germany) and can be stored on ice for at least 1 h without harmful effect on later cell culture.

Embryonic brains were removed from the skull by performing a longitudinal incision and subsequent removal of the brain from the skull using tweezers. Both hemispheres of the cortex were removed from the remaining brain stem and transferred into DMEM (Dulbecco's Modified Eagle Medium; Biochrom) with 10% FBS (Biochrom). Cortical tissue from 6 animals was mechanically dissected by using 5 ml pipettes and subsequently Pasteur pipettes. Tissue pieces were centrifuged ($320 \times g$ for 2 min) and resuspended in Hanks-buffer without Ca^{2+} and Mg^{2+} (Biochrom). For further removing of bivalent metal ions, 1 ml EDTA/PBS (1%, w/v; Biochrom) was added. After centrifugation, brain tissue was resuspended again in 6 ml Hanks-buffer and 2 ml Trypsin/EDTA solution (0.25%/0.02%, Biochrom) was added. Trypsinisation of cells was performed under gentle agitation for 2–3 min at room temperature and reaction was stopped by adding of 4 ml DMEM with 10% FBS. After centrifugation the proteolytically digested tissue was resuspended in DMEM with 10% FBS and squirted twice through a syringe equipped with a 23 gauge needle. Following final centrifugation cells were resuspended in DMEM with 10% FBS and counted using a Neubauer hemicytometer. Afterwards, 1.3×10^6 cells/well (2 ml/well) were seeded on Matrigel (Becton Dickinson, Heidelberg, Germany) coated glass cover slips.

Coating the cover slips with Matrigel was performed according to suggestions of the manufacturer. Cells need only a thin layer of polymerized Matrigel. Best polymerisation and best cell grow is achieved by coating the cover slips with undiluted Matrigel. However, this is very cost-intensive and acceptable cell grow also occurs by diluting the Matrigel 1:35 with ice cold culture media, e.g. DMEM. For that, Matrigel has to be thawed in advance on ice. The best way to do this is transferring the vial with Matrigel directly from -20°C into ice and keeping the box with ice at $4-7^\circ\text{C}$ overnight.

It is important to pipette the Matrigel rapidly, since polymerization can already happen in the tip of the pipette. Once the Matrigel is diluted it should be stored on ice. The diluted Matrigel is dropped onto the cover slips (calculate $500 \mu\text{l}$ for 30 mm cover slips). Culture plates with coated cover slips were then stored in the cell culture incubator for at least 15 min (longer incubation times even over few hours are not problematic). The Matrigel-containing media was removed immediately before seeding the cells. Matrigel stock solution can be refreezed several times.

Cells were grown under standard conditions, i.e. 37°C and 5% CO_2 . DMEM with 10% FBS was changed by 1 ml Start V Medium (Biochrom) 24 h later. After 48 h 1 ml Start V Medium per well (6 well plate) was added additionally. Starting from that point medium was changed every 48 h by fresh Start V Medium.

2.2. Immunocytochemistry

Cortical primary cultures were fixed for at least 10 min by 4% paraformaldehyde. After washing in PBS and blocking with 10% donkey serum (Sigma, Deisenhofen, Germany), primary antibodies were applied overnight at room temperature in PBS containing 1% donkey serum. Cells were analysed by immunocytochemistry using following antibodies: monoclonal mouse antibodies to neuronal nuclear antigen (NeuN, 1:200, Chemicon, Temecula, CA, USA), glial fibrillary acidic protein (GFAP, 1:200, Chemicon), nestin (1:200, BD Transduction Laboratories, San Jose, CA, USA), β III tubulin (1:1000, Promega, Mannheim, Germany), CNPase (1:1000, Abcam, Cambridge, UK), GABA (1:500, Sigma), Ox 42 (1:200, Serotec, Düsseldorf, Germany) and SV2 (1:200, Developmental Hybridoma Bank, Iowa City, IA, USA), polyclonal goat antibodies to DCX (1:300, Santa Cruz Biotechnology, Santa Cruz, CA, USA), and choline acetyltransferase (ChAT, 1:100, Chemicon) and polyclonal rabbit antibodies to glutamate decarboxylase (GAD65/67, 1:500, Sigma) and NG2 (1:300, Chemicon).

Primary antibodies were visualized by Cy2 or Cy3 conjugated secondary antibodies, e.g. donkey anti-mouse, donkey anti-goat and donkey anti-rabbit (1:500, Dianova, Hamburg, Germany) for 2 h at room temperature. Nuclei were counterstained by DAPI (1:15,000, Mobitec, Göttingen, Germany). To show antibody specificity, cells were stained by secondary antibodies only. Adhered cells were dehydrated by increasing concentrations of ethanol (50–100%), briefly submerged in xylol and mounted in DPX (Fluka, Buchs, Switzerland).

Confocal analysis was performed using a LSM 5 Pascal laser-scanning microscope (Zeiss, Jena, Germany) and Axiovision 2.05 software (Zeiss).

2.3. Culture of microglia cell-line BV2

The BV2 microglia was cultured in DMEM supplemented with 10% FBS, 1% Pen/Strep (Biochrom), 1% L-Glutamin (Biochrom) at a density not exceeding 5×10^5 cells/ml and maintained in 5% CO₂ at 37 °C. To harvest BV2 microglia, cells were trypsinated (Trypsin/EDTA), then centrifuged ($500 \times g$ for 5 min) and resuspended in Neurobasal Medium (Gibco, Eggenstein, Germany). Cell concentration was determined by counting cells in a Neubauer hemicytometer and viability was assessed by trypan blue staining (0.4% trypan blue in PBS, Sigma). BV2 microglia was added to 10 day old cortical primary cultures in an effector-to-target cell (E/T) ratio of 0.3/1. Viability of supplemented BV2 microglia was confirmed by prior staining with CTO (Invitrogen, Karlsruhe, Germany).

2.4. Time-lapse imaging by confocal laserscanning microscopy

BV2 microglia was labelled with 10 μ M CTO and added to DIV10 aged cortical culture prepared from transgenic B6.Cg-TgN (Thy1-YFP) 16Jrs mice (green fluorescent neurons). This mouse strain was created by The Jackson Laboratory (USA) and purchased from Charles River (Sulzfeld, Germany). Imaging was performed by using a confocal laserscanning microscope (Zeiss LSM 510 Meta under control of axiovision software and a 20 \times Neofluar air lens, NA 0.5). Images were recorded

every 45–60 s, reading the red and green channel simultaneously. Imaging was performed over 14 h permanently at the same spot without obvious bleaching or inhibition of cell motility.

3. Results and discussion

We prepared primary cortical neurons from E18 rat embryos and cultivated them on Matrigel coated glass cover slips and Start V Medium. Under these conditions dissociated and initially free floating cells start to aggregate and form neurospheres attached to the surface of cover slips (Fig. 1A and B). After removing serum, as a result of changing DMEM medium to Start V Medium, cells start to migrate from these neurospheres and form a network of neuronal cells (Fig. 1C and D). As reported by others, we also found that addition of serum during the first 24 h increases the survival and proliferation of neuronal cells (Leemhuis et al., 2004). However, if cells are continuously cultured in serum, the continuous proliferation of astroglial cells leads to suppression of neuronal cells (Xie et al., 2000).

Neurospheres, developing shortly after seeding of dissociated cells, are composed mainly of neuroblasts double-labelled by DCX and β III tubulin (Fig. 2A). Both markers are also expressed in processes originating from neurospheres (Fig. 2B). These processes are used by cells for migration into surrounding areas (Fig. 1B and C). Immunostaining of DCX and β III tubulin revealed the complex structure of a neuronal network developing over a period of 5–7 days of culturing. It has to be mentioned that the density of this network varies inside of one well. Even at culture day 7 regions with lower and higher cell density can be identified (Fig. 2D and E).

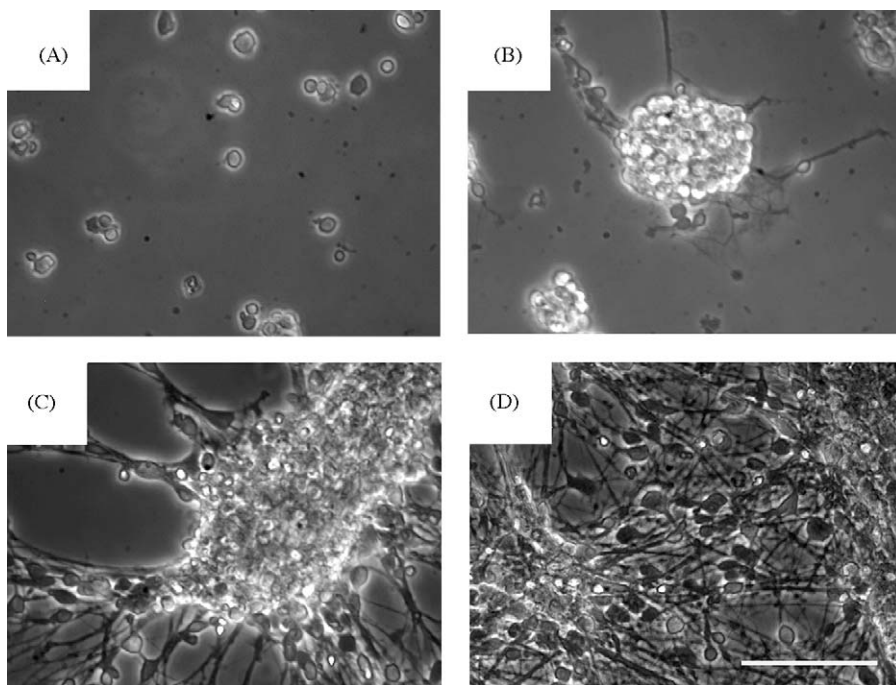


Fig. 1. Phase contrast pictures of a cortical primary culture. (A) 50 min after seeding of dissociated cells. (B) 22 h after seeding neurospheres have been formed. (C) Migration of neural precursors from neurospheres into the surrounding area 2 days after seeding. (D) After 7 days a dense network of neuronal cells is formed. Scale bar: 100 μ m.

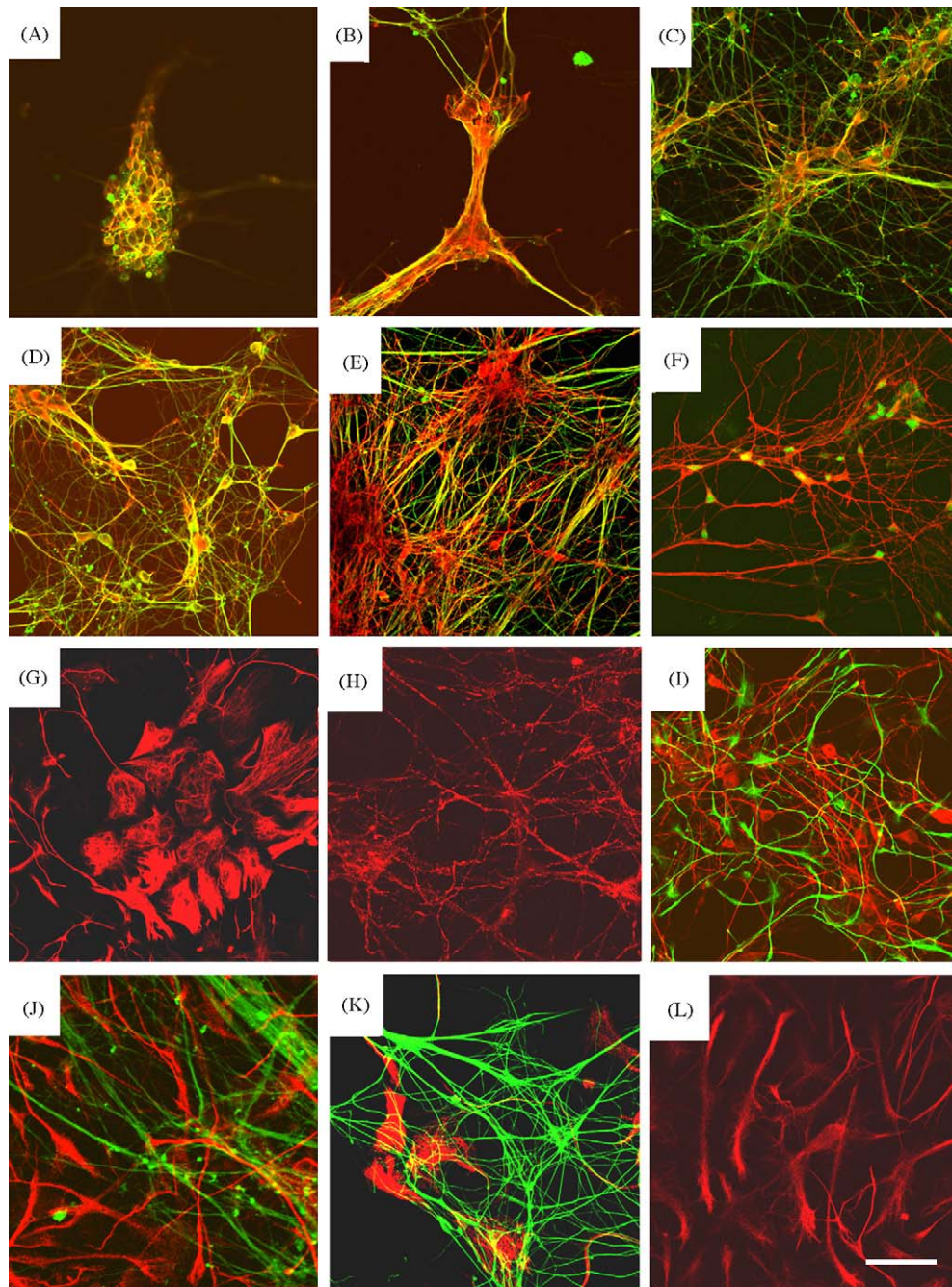


Fig. 2. Confocal analysis of immunocytochemical stained cultures. Cultures were fixed either 2 days after seeding (A–C) or 7 days after seeding (D–L). (A–E) DCX (red) and β III tubulin (green) positive neurospheres. A network of different densities is formed between neurospheres (C–E). Few of the DCX positive neurons (red) in the network are co-labelled with NeuN (green, F). (G) Nestin positive stem cells appear in different morphologies and sizes. (H) Many neurons are positive for the vesicle marker SV2 indicating the existence of synapses. (I and J) Nestin processes are interwoven with DCX and β III tubulin processes. But there is no co-localization between DCX (red) and Nestin (green, I) as well as Nestin (red) and β III tubulin (green, J). (K) Nestin positive cells (red) are often found located beneath the neuronal network consisting of β III tubulin positive cells (green). (L) The expression of GFAP demonstrates the presence of astrocytes. Scale bar: 50 μ m in all pictures except B and G (100 μ m). (For interpretation of the references to colour in this figure legend, the reader is referred to the web version of the article.)

DCX is described *in vivo* to be a marker for young, mainly migrating neuroblasts found exclusively in the subventricular zone (SVZ) of the lateral ventricle and in the subgranular zone (SGZ) of the dentate gyrus (Brown et al., 2003; Rao and Shetty, 2004). In our primary culture system DCX can be detected even in an established network of neuronal cells (Fig. 2E). Time lapse videos demonstrated that in areas with high cell densi-

ties as shown in Figs. 1D and 2E only little cell movement can be observed (not shown). Nevertheless DCX is still abundantly expressed in neurons located in these areas. This suggests that DCX might be expressed *in vivo* in regions outside of SVZ and SGZ but that the level of expression in more mature neurons is not sufficient for detection by immunohistochemistry. Interestingly, DCX positive neurons can be co-labelled with NeuN, a

classical marker for mature neurons (Fig. 2F). This observation is in line with other *in vivo* findings, detecting also DCX positive cells outside of the SVZ, and about 8% of these obviously migrating neurons were double-labelled with NeuN (Yang et al., 2004). The functional maturation of the neuronal network is further supported by expression of SV2, a protein specifically expressed on synaptic vesicles (Fig. 2H).

Non-neuronal cells are difficult to identify by phase-contrast microscopy. However, immunocytochemistry revealed the existence of both GFAP positive astroglia (Fig. 2L) and nestin positive neural stem cells (Fig. 2G). Nestin cells are found in different sizes and morphology, but mainly these stem cells are either of flattened morphology located beneath the neuronal network (Fig. 2K) or rounded and elongated cells that are interwoven with neuronal cells (Fig. 2I and J). Besides nestin positive cells are also present in just formed neurospheres (not shown). Interestingly, we did not find any co-expression of nestin positive cells with DCX or β III tubulin markers (Fig. 2I–K), indicating an abrupt down-regulation of nestin expression when neural stem cells start to differentiate into neurons.

After 7 days of cultivation neuronal cells contain subpopulations of neurons as for example cholinergic (Fig. 3A) and GABAergic neurons (Fig. 3B and C). Finally, we were interested in the existence of oligodendrocytes and microglia and indeed, both cell populations were present. Immunostaining with antibodies recognizing oligodendrocytic marker proteins NG2 (Fig. 3D) and CNPase (Fig. 3E) revealed cells with typical oligodendrocytic morphology. Ox 42, an antibody recognizing the cell surface marker CD11b/c present on microglia and macrophages, discovered the presence of microglial cells

exhibiting a morphology of very large and flattened cells (Fig. 3F). The occurrence of microglia in primary cultures was first demonstrated by Jordan and Thomas (1987).

Matrigel promotes differentiation and migration of many cell types by providing a three-dimensional substrate for cell growth (Grant et al., 1985; Hadley et al., 1985; Kubota et al., 1988) and supported *in vivo* peripheral nerve regeneration (Madison et al., 1985). Further, it was demonstrated, that regulator proteins of proliferation like sonic hedgehog (SHH) directly interact with heparan sulfate proteoglycans and laminin (Pons et al., 2001; Rubin et al., 2002). Both proteoglycan components are part of the Matrigel composition. Therefore, Matrigel coating creates much more optimal conditions for cell growth than coating with laminin or other substrates alone. In fact, both phase contrast and confocal laserscanning microscopy clearly demonstrated the three-dimensional structure composing of neuronal and glial cells as well as stem cells and microglia. Thus, the primary cell culture of cortical cells described here should be considered as a neural tissue-like structure arising from dispersed cells rather than being a simple mixture of dissociated cells. By using Start V Medium we were able to grow this culture for at least 3 weeks under serum free conditions and without the usage of inhibitors for mitosis like AraC.

In order to evaluate the usefulness of such a culture for the investigation of cell–cell contacts, we added fluorescent labelled BV2 cells to a 10 day old primary culture prepared from transgenic B6.Cg-TgN (Thy1-YFP)16Jrs mice embryos. Migratory activity of CTO-labelled microglial cells (BV2) invading into neurospheres was analysed by time lapse confocal imaging over 14 h (Fig. 4).

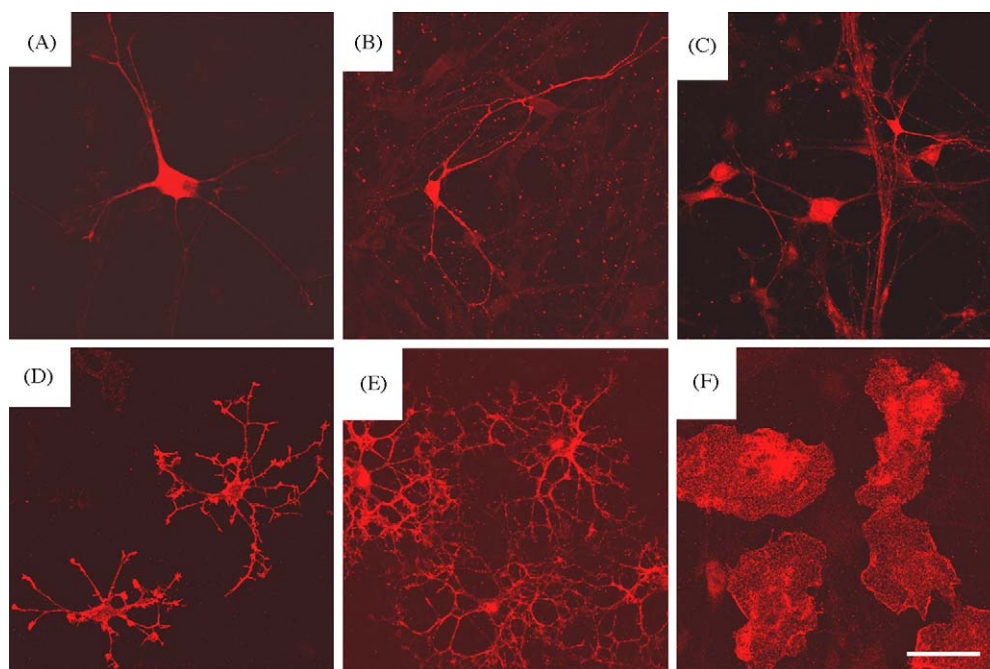


Fig. 3. Confocal imaging of 7 days old cortical primary cultures. (A–C) Neurons of different subtypes could be detected by expression of choline acetyltransferase (A) and markers for GABAergic neurons illustrated by immunostaining against GABA (B) and Glutamate decarboxylase (GAD65/67, C). (D and E) Oligodendrocytic precursor cells were identified by NG2 (D) and CNPase (E) expression. (F) Microglia cells were detected by Ox42 immunostaining. Scale bar: 30 μ m in all pictures except C (50 μ m).

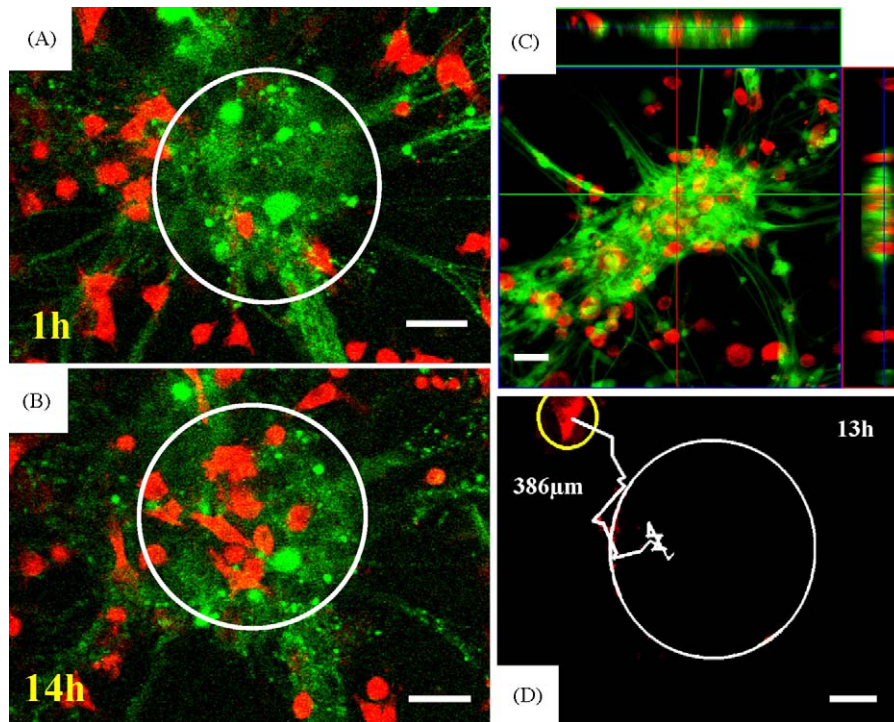


Fig. 4. Migration of microglia into neurospheres of cortical primary cultures. BV2 microglia were labeled with CTO (red) and then added directly to cortical primary cultures prepared from transgenic B6.Cg-TgN (Thy1-YFP)16Jrs mice (neurons: green). Co-cultures were recorded by time-lapse confocal laserscanning microscopy. (A) Begin of recording 1 h after application of BV2 microglia. White circle indicates the extension of the neurosphere. (B) End of recording 14 h after application. (C) 14 h after application Z-stacks of neurospheres were performed. Image shows BV2 microglia inside the neurosphere. (D) The white line indicates the representative migration pathway of a microglial cell over a time frame of 13 h. Scale bar: 50 μm (A–D). (For interpretation of the references to colour in this figure legend, the reader is referred to the web version of the article.)

An artificial tissue-like culture prepared in the way described in this paper will have several advantages and disadvantages compared to organotypic slice cultures (Chechneva et al., 2005). The latter more preserve the cellular architecture while the primary culture is easier to handle and single cells are more susceptible to various kinds of investigation. Taken together, Matrigel and Start V Medium can be applied for the rapid establishment of a serum free, tissue-like primary culture of cortical cells useful for studying effects of growth factors, expression patterns of marker proteins, synapse formation and functions as well as cell–cell interactions under in vitro conditions.

Acknowledgements

This work was supported by a grant from the State of Sachsen-Anhalt FKZ: 3594M/0405M. We thank C. Ladwig for excellent technical assistance. Further, we thank K. Gruss for the gift of GABA antibody and K. Braun for providing operation time at the Zeiss LSM 510 Meta.

References

- Banker GA, Cowan WM. Rat hippocampal neurons in dispersed cell culture. *Brain Res* 1977;126:397–442.
- Banker GA, Cowan WM. Further observations on hippocampal neurons in dispersed cell culture. *J Comp Neurol* 1979;187:469–93.

- Brown JP, Couillard-Desperes S, Cooper-Kuhn CM, Winkler J, Aigner L, Kuhn HG. Transient expression of doublecortin during adult neurogenesis. *J Comp Neurol* 2003;467:1–10.
- Brown MD, Banker GA, Hussaini IM, Gonias SL, VandenBerg SR. Low density lipoprotein receptor-related protein is expressed early and becomes restricted to a somatodendritic domain during neuronal differentiation in culture. *Brain Res* 1997;747:313–7.
- Brewer GJ. Serum-free B27/neurobasal medium supports differentiated growth of neurons from the striatum, substantia nigra, septum, cerebral cortex, cerebellum, and dentate gyrus. *J Neurosci Res* 1995;42:674–83.
- Chechneva O, Dinkel K, Schrader D, Reymann KG. Identification and characterization of two neurogenic zones in interface organotypic hippocampal slice cultures. *Neuroscience* 2005;136:343–55.
- Dichter MA. Rat cortical neurons in cell culture: culture methods, cell morphology, electrophysiology and synapse formation. *Brain Res* 1978;149:279–93.
- Dotti CG, Banker GA. Experimentally induced alteration in the polarity of developing neurons. *Nature* 1987;330:254–6.
- Davis L, Banker GA, Steward O. Selective dendritic transport of RNA in hippocampal neurons in culture. *Nature* 1987;330:477–9.
- Grant DS, Kleinman HK, Leblond CP, Inoue S, Chung AE, Martin GR. The basement-membrane-like matrix of the mouse EHS tumor: II. Immuno-histochemical quantification of six of its components. *Am J Anat* 1985;174:387–98.
- Grewal SS, Horgan AM, York RD, Withers GS, Banker GA, Stork PJ. Neuronal calcium activates a Rap1 and B-Raf signaling pathway via the cyclic adenosine monophosphate-dependent protein kinase. *J Biol Chem* 2000;275:3722–8.
- Hadley MA, Byers SW, Suarez-Quian CA, Kleinman HK, Dym M. Extracellular matrix regulates Sertoli cell differentiation, testicular cord formation, and germ cell development in vitro. *J Cell Biol* 1985;101:1511–22.

- Hayashi K, Kawai-Hirai R, Ishikawa K, Takata K. Reversal of neuronal polarity characterized by conversion of dendrites into axons in neonatal rat cortical neurons in vitro. *Neuroscience* 2002;110:7–17.
- Hertz L, Juurlink BJJ, Fosmark H, Schousboe A. Astrocytes in primary cultures. In: Pfeiffer SE, editor. *Neuroscience Approached Through Cell Culture*. Boca Raton: CRC Press; 1982. p. 175–86.
- Hertz E, Yu ACH, Hertz L, Juurlink BJJ, Schousboe A. Preparation of primary cultures of mouse cortical neurons. In: Shahar A, De Vellis J, Vernadakis A, Haber BA, editors. *Dissection and Tissue Culture Manual for the Central Nervous System*. New York: Liss; 1989. p. 183–6.
- Jordan FL, Thomas WE. Identification of microglia in primary cultures of mixed cerebral cortical cells. *Brain Res Bull* 1987;65:153–9.
- Keilhoff G, Erdo SL. Parallel development of excitotoxic vulnerability to *N*-methyl-D-aspartate and kainate in dispersed cultures of the rat cerebral cortex. *Neuroscience* 1991;43:35–40.
- Kleinman HK, McGarvey ML, Liotta LA, Robey PG, Tryggvason K, Martin GR. Isolation and characterization of type IV procollagen, laminin, and heparan sulfate proteoglycan from the EHS sarcoma. *Biochemistry* 1982;23:6188–93.
- Kondratyev AD, Zotova EE, Loginov BV, Tsirenina ML, Melnik EI, Severin ES. Production and immunohistochemical characterization of primary cultures of human embryo brain cells. *Neuroscience* 1989;32:261–8.
- Kubota Y, Kleinman HK, Martin GR, Lawley TJ. Role of laminin and basement membrane in the morphological differentiation of human endothelial cells into capillary-like structures. *J Cell Biol* 1988;107:1589–98.
- Leemhuis J, Boutillier S, Barth H, Feuerstein TJ, Brock C, Nürnberg B, et al. Rho GTPases and phosphoinositide 3-kinase organize formation of branched dendrites. *J Biol Chem* 2004;279:585–96.
- Madison R, da Silva CF, Dikkles P, Chiu TH, Sidman RL. Increased rate of peripheral nerve regeneration using bioresorbable nerve guides and a laminin-containing gel. *Exp Neurol* 1985;88:767–72.
- Mandell JW, Banker GA. Selective blockade of axonogenesis in cultured hippocampal neurons by the tyrosine phosphatase inhibitor orthovanadate. *J Neurobiol* 1998;35:17–28.
- Oliva Jr AA, James CD, Kingman CE, Craighead HG, Banker GA. Patterning axonal guidance molecules using a novel strategy for microcontact printing. *Neurochem Res* 2003;28:1639–48.
- Pons S, Trejo JL, Martinez-Morales JR, Marti E. Vitronectin regulates Sonic hedgehog activity during cerebellum development through CREB phosphorylation. *Development* 2001;128:1481–92.
- Rao MS, Shetty AK. Efficacy of doublecortin as a marker to analyse the absolute number and dendritic growth of newly generated neurons in the adult dentate gyrus. *Eur J Neurosci* 2004;19:234–46.
- Romijn HJ. Development and advantages of serum-free, chemically defined nutrient media for culturing of nerve tissue. *Biol Cell* 1988;63:263–8.
- Rubin JB, Choi Y, Segal RA. Cerebellar proteoglycans regulate sonic hedgehog responses during development. *Development* 2002;129:2223–32.
- Xie C, Markesbery WR, Lovell MA. Survival of hippocampal and cortical neurons in a mixture of MEM+ and B27-supplemented neurobasal medium. *Free Radical Biol Med* 2000;28:665–72.
- Yang HK, Sundholm-Peters NL, Goings GE, Walker AS, Hyland K, Szele FG. Distribution of doublecortin expressing cells near the lateral ventricles in the adult mouse brain. *J Neurosci Res* 2004;76:282–95.
- Waagepetersen HS, Bakken IJ, Larsson OM, Sonnewald U, Schousboe A. Comparison of lactate and glucose metabolism in cultured neocortical neurons and astrocytes using ¹³C-NMR spectroscopy. *Dev Neurosci* 1998;20:310–20.

The Power of Single and Multibeam Two-Photon Microscopy for High-Resolution and High-Speed Deep Tissue and Intravital Imaging

Raluca Niesner,^{*†} Volker Andresen,[‡] Jens Neumann,[§] Heinrich Spiecker,[‡] and Matthias Gunzer^{*}

^{*}Helmholtz Centre for Infection Research, Junior Research Group Immunodynamics, D-38124 Braunschweig, Germany; [†]Institute of Physical and Theoretical Chemistry, Technical University of Braunschweig, D-38106 Braunschweig, Germany; [‡]LaVision Biotec GmbH, 33607 Bielefeld, Germany; and [§]Institute for Applied Neuroscience, 39120 Magdeburg, Germany

ABSTRACT Two-photon microscopy is indispensable for deep tissue and intravital imaging. However, current technology based on single-beam point scanning has reached sensitivity and speed limits because higher performance requires higher laser power leading to sample degradation. We utilize a multifocal scanhead splitting a laser beam into a line of 64 foci, allowing sample illumination in real time at full laser power. This technology requires charge-coupled device field detection in contrast to conventional detection by photomultipliers. A comparison of the optical performance of both setups shows functional equivalence in every measurable parameter down to penetration depths of 200 μm , where most actual experiments are executed. The advantage of photomultiplier detection materializes at imaging depths $>300 \mu\text{m}$ because of their better signal/noise ratio, whereas only charge-coupled devices allow real-time detection of rapid processes (here blood flow). We also find that the point-spread function of both devices strongly depends on tissue constitution and penetration depth. However, employment of a depth-corrected point-spread function allows three-dimensional deconvolution of deep-tissue data up to an image quality resembling surface detection.

INTRODUCTION

Fluorescence microscopy is an important tool in biomedical research for the study of tissues, cells, and even subcellular structures with high spatial and temporal resolution (1). As a result, the dynamics of live cells form the focus of many approaches. To avoid alterations induced by isolation from their natural environment, observing cellular behavior in living animals has become the preferred method for these analyses (2). The possibility of investigating cells in their natural environment is considered to be crucial for understanding their functions and behavior (2–4). Conventional wide-field or confocal intravital fluorescence microscopy can be applied to investigate blood flow in superficial vessels (3) or the migration of cells in subcapsular zones of peripheral lymph nodes (5). Often, however, the biologically most interesting phenomena such as T-cell activation happen 100–400 μm below the surface of relevant tissues in mice. The excitation wavelengths typically used in confocal microscopy hardly allow the examination of cells this deep in living tissue

or whole animals. As a result of significant scattering and absorption occurring in optically dense samples, only a few times 10 μm can be investigated at the microscopic level. Therefore, cutting the object into slices is often the only method to obtain information about cell dynamics inside (6,7).

The invention of multiphoton microscopy (MPM) (8) represents a breakthrough in tissue and intravital studies. It substantially enlarges the penetration depth to a couple of hundred micrometers, thus enabling noninvasive imaging with subcellular resolution in intact animals (9). In addition to its larger penetration depth, MPM provides inherent optical sectioning, reduced photobleaching and photodamage outside the focal plane, and convenient excitation of UV-absorption bands of intrinsic fluorophors (7). Despite its subcellular resolution, MPM is also able to record simultaneous activity of multiple neurons in vivo by means of field detection of calcium currents (10). Although it has been widely used in neurology since its introduction more than 15 years ago (8), only in the last 5 years have immunologists also “discovered” MPM for their questions. Since then a huge number of publications (recently reviewed (4,9,11,12)) found multiple novel insights into the biophysics of cell migration and cell-cell communication under different conditions. Thus, given the obvious success of the technology, it can be expected that many more groups will start to set up MPM capabilities. To this end, a very informative review has summarized the advances and problems of MPM in the immunology field so far (11).

The most important drawback of MPM is probably that the two-photon-excitation efficiency of most fluorophors is very low compared to single-photon excitation, resulting in a small

Submitted December 5, 2006, and accepted for publication May 29, 2007.

R.N. and V.N. contributed equally to this work. R.N., V.A., and M.G. performed experiments, conceived the work, and wrote the paper. J.N. provided vital material. R.N., V.A., H.S., and M.G. analyzed and interpreted the data. M.G. supervised the work.

Address reprint requests to Matthias Gunzer, PhD, Helmholtz Centre for Infection Research, Junior Research Group Immunodynamics, Inhoffenstrasse 7, D-38124 Braunschweig Germany. Tel.: 49-531-6181-3130; Fax: 49-531-6181-3199; E-mail: mgunzer@helmholtz-hzi.de; or to Raluca Niesner, PhD, Technical University of Braunschweig, Institute of Physical and Theoretical Chemistry, Hans-Sommer Strasse 10, D-38106 Braunschweig, Germany. Tel.: 49-531-391-5346; Fax: 49-531-391-5396; E-mail: raluca.niesner@tu-bs.de.

Editor: Petra Schwille.

© 2007 by the Biophysical Society

0006-3495/07/10/2519/11 \$2.00

doi: 10.1529/biophysj.106.102459

number of emitted photons (13). This in turn leads to long image acquisition times that are often on the order of seconds, restricting observation of living samples and dynamic processes within them with a high temporal resolution. A common approach to overcome this problem is to increase the excitation laser power to generate more fluorescence and use faster scanning methods such as acousto-optical deflectors (9,11). But because the nonlinear photo damage rises faster than the number of excited molecules with increasing laser power (7), crossing a critical power level does not make sense. Thus, the only method to increase the number of fluorescence photons per time without raising photodamage is to parallelize the excitation process. Simultaneous excitation with N foci results in N times more excited molecules, which in turn enables N times quicker acquisition or much gentler imaging.

We employ here a multiphoton scanhead that makes use of reflecting mirrors to split an incoming infrared laser beam into a line of up to 64 beamlets (14). This scanhead makes it possible to generate up to 64 times more fluorescence light out of a sample compared to single-beam scanning systems without the danger of photo- or thermotoxicity. Consequently, scanning can be made up to 64 times faster, allowing real-time observation of image planes deep inside the sample with low power in each single focus. Because this setup is dependent on charge-coupled device (CCD)-camera field detection, it is necessary to evaluate its optical performance. The reference detection device here is a point detector (photomultiplier tube, PMT), which is used by switching the beam path inside the same scanhead to generate only a single excitation beam. Both methods are directly compared in terms of resolution, maximum penetration depth, and signal/noise ratio (SNR).

Another serious problem of tissue two-photon microscopy is the significant decrease of the optical resolution with increasing penetration depth. Novel approaches apply point-spread function (PSF) engineering by means of deformable mirrors, which, however, is technically challenging (15). Our experiments show that this is based on degradation of the excitation PSF caused by the transit through optically dense samples that feature a strongly varying refraction index. This prevents the resolution of small details deeper inside the sample. We demonstrate that the level of degradation of the PSF is strongly dependent on the type of tissue imaged and that application of a depth-dependent PSF for three-dimensional deconvolution completely restores maximum image quality.

METHODS

Multifocal two-photon microscope

All experiments were carried out using a specialized two-photon microscope that is based on a commercial scan head (TriMScope, LaVision BioTec, Bielefeld, Germany, Supplementary Fig. 1). We used either CCD cameras or photomultipliers for detection (14).

Agarose films

A 4% (wt %) aqueous suspension of agarose (Merck, Darmstadt, Germany) was boiled and then mixed with a 0.002% suspension of fluorescent polystyrene beads (emission maximum 440 nm and 515 nm, Invitrogen, Karlsruhe, Germany). The volume ratio of the suspensions was 7:3. The still-fluid mixture was quickly pipetted onto a glass slide and cooled down to room temperature to solidify.

Preparation of lymph nodes

A total of 25 μ l of a 2% suspension of green fluorescent polystyrene beads was injected into the footpad of 8-week-old BALB/c mice (Harlan, Germany). Overnight, the beads moved into the popliteal lymph nodes. Mice were sacrificed, and the lymph nodes were isolated and used for experiments concerned with the analysis of spatial resolution.

Preparation of brain slices

Organotypic hippocampal brain slices (OHBS) were prepared as described (30) from 10-day-old transgenic B6.Cg-TgN (Thy1-YFP)16Jrs mice (Jackson, distributed by Charles River, Wilmington, MA), which express EYFP at high levels in subsets of neurons, including the pyramidal cells of the hippocampus (31). Hippocampi were dissected and transversely sliced into a 500- μ m or a 700- μ m thickness on a McIlwain tissue chopper (The Mickle Laboratory Engineering, Surrey, UK). OHBS were immediately fixed with 4% PFA for 40 min at room temperature and were maintained in 30% sucrose. OHBS were then cryosectioned to suitable thickness as described (30). Before usage, OHBS were rinsed in phosphate-buffered saline (PBS) for 3×10 min.

To determine the ePSF in OHBS, we kept 100 μ l of a suspension of fluorescent beads (as used above within agarose) on each side of OHBS for 3–4 h at 37°C. This 100 μ l of suspension was obtained by diluting a 2 wt % stock suspension of beads 1:1000 with water and adding 15 vol % DMSO. Under these conditions we could not observe any damage to the morphology of the samples. After the incubation with bead suspension, the OHBS were washed so that no bead clusters remained on the sample surface.

Intravital microscopy

Mice were prepared for intravital microscopy using Isofluran-based intubation narcosis and gentle exposure of the inguinal lymph node as described (5). Blood-flow measurements were performed on blood vessels above the inguinal lymph node. For blood staining, anesthetized mice were injected i.v. with 100 μ l Rhodamine-6G (1.25 mM in 0.9% NaCl). Subsequently, spleen cells stained with CFSE (5 μ M) or CTO (5 μ M) were also injected i.v. Imaging was performed until 1h after injection, when the Rhodamine signal was beginning to decay.

The animal experiments were approved by the Gewerbeaufsichtsamt Braunschweig under file number 509.42502/07-04.04 and were performed in accordance with current guidelines and regulations.

RESULTS

For single-beam imaging, PMTs were used to detect the fluorescence, whereas in multibeam mode CCD cameras were employed. Consequently, the comparison between these two different methods is also a comparison of the optical performance between a pixel-by-pixel and a field-detection device.

Calibration and benchmarking of the measurement system

The optical performance of an imaging system for biological tissues is defined by its maximum spatial (lateral and axial) resolution, the maximum penetration depth, and the depth-dependent signal/noise ratio (ddSNR). Thus, we first investigated these parameters using an agarose gel as a model for a homogeneous sample.

The spatial resolution of a laser-scanning microscope is determined by the dimensions of the effective (detected) point-spread function (ePSF) of a punctiform object with dimensions below the resolution limit. The rigorous mathematical description of the PSF is complicated (16–19). A commonly accepted procedure is to approximate the two-photon ePSF by simpler three-dimensional peak functions such as the two-dimensional Gauss-Lorentz distribution or the asymmetrical three-dimensional Gauss distribution (16). Indeed, the experimental ePSFs measured with our setup could be fitted by asymmetrical three-dimensional Gauss functions. The ePSFs were measured by collecting the local three-dimensional fluorescence signal of small labeled polystyrene beads whose diameter (100 nm) was below the resolution limit of our setup.

To characterize the resolution of the single-beam PMT compared to the multibeam CCD setup, we performed ePSF measurements with both methods in thick agarose gels. This was done at different excitation wavelengths in the range of 720–920 nm, with two different types of labeled beads (fluorescence maximum at 440 and 515 nm), at different penetration depths, and with two different lenses, i.e., a 20× high-working-distance water-immersion objective (NA = 0.95) and a 100× low-working-distance oil-immersion objective (NA = 1.4). The lateral and axial dimensions of the ePSFs were determined from one-dimensional Gaussian fits of the respective x , y , and z profiles. Thereby, we considered the maximum extension of the ePSF in each direction for evaluation.

In conformity with the diffraction theory (16), both the lateral and the axial resolution decreased with increasing excitation wavelength, whereas neither the emission wavelength nor the penetration depth had a measurable effect on the spatial resolution (Supplementary Table 1).

The dimensions of the theoretical PSF, calculated using paraxial approximation, corresponded very well to the spatial resolution measured in agarose. At an excitation wavelength of 800 nm, the calculated axial resolution was 347 nm, and the lateral resolution 1.47 μm , whereas the measured values were (lateral) 344 ± 14 nm and (axial) 1.41 ± 0.09 μm , respectively (Fig. 1, *A* and *B*).

The maximum penetration depth in agarose measured using the 20× objective was larger than 900 μm , i.e., the thickness of the sample, for both setups. The spatial resolution in this depth measured using green fluorescent beads (fluorescence maximum at 515 nm) excited at 780 nm amounted to

364 ± 12 nm (lateral) and 1.42 ± 0.02 μm (axial) for the multibeam CCD setup and to 363 ± 16 nm (lateral) and 1.44 ± 0.07 μm (axial) for the single-beam PMT setup. Thus, in agarose the loss of resolution caused by imaging depth was less than 2.5%.

The spatial resolution measured with a high-NA objective in agarose at 780-nm excitation wavelength (fluorescence maximum 515 nm) was 207 ± 7 nm (lateral) and 814 ± 31 nm (axial) for the multibeam CCD setup and 209 ± 10 nm (lateral) and 817 ± 16 nm (axial) for the single-beam PMT setup. These values correspond to already published results using the same or similar lenses (20,21). The maximum penetration depth was limited to 100 μm by the working distance of the objective.

Despite its very high spatial resolution, the 100× objective is inadequate for imaging biological samples because of its short working distance and the need for oil immersion. Thus, all further experiments were performed with the more appropriate 20× water-immersion objective.

For directly comparing the spatial resolution of the single- and multibeam excitation mode, we used the CCD camera as detector for both modes to rule out differences introduced by the detection method. We performed ePSF measurements in agarose using 3-mW laser power in the focus of each beam and 12- μs pixel time. Independent of the number of laser beams (1, 2, ... 64) used, all experiments yielded the same axial and lateral resolution. By using the 20× objective combined with a twofold magnification of the fluorescence image, a pixel resolution of 161 nm on the CCD chip and of 141 nm on the reconstructed PMT image was obtained. For the 100× objective, the pixel resolution was 65 nm on the CCD chip and 56 nm on the PMT image. The steps between two consecutive optical slices were adjusted to 300 nm in all ePSF measurements.

Spatial resolution decreases with imaging depth and sample complexity

Transparent media such as agarose are advantageous for characterization of the maximum optical performance of imaging devices. However, there are large differences between this ideal model and genuine probes. To test the influence of optical density and refraction-index variation, we performed ePSF experiments on two tissue types of particular interest, i.e., OHBS and lymph nodes. Fig. 1, *C* and *D*, depicts representative results for depth-dependent ePSFs in OHBS, whereas *E* and *F* show typical values in the lymph node. The xy region considered for evaluation was relatively small (15×15 μm^2) because the heterogeneous surface (nonplanar in the range of several micrometers), which is typical for brain slices and lymph nodes, affects penetration depth and resolution. Only when one is measuring small xy regions is the imaging depth nearly uniform over the whole image.

The spatial resolution in biological samples was strongly influenced not only by the penetration depth but also by the

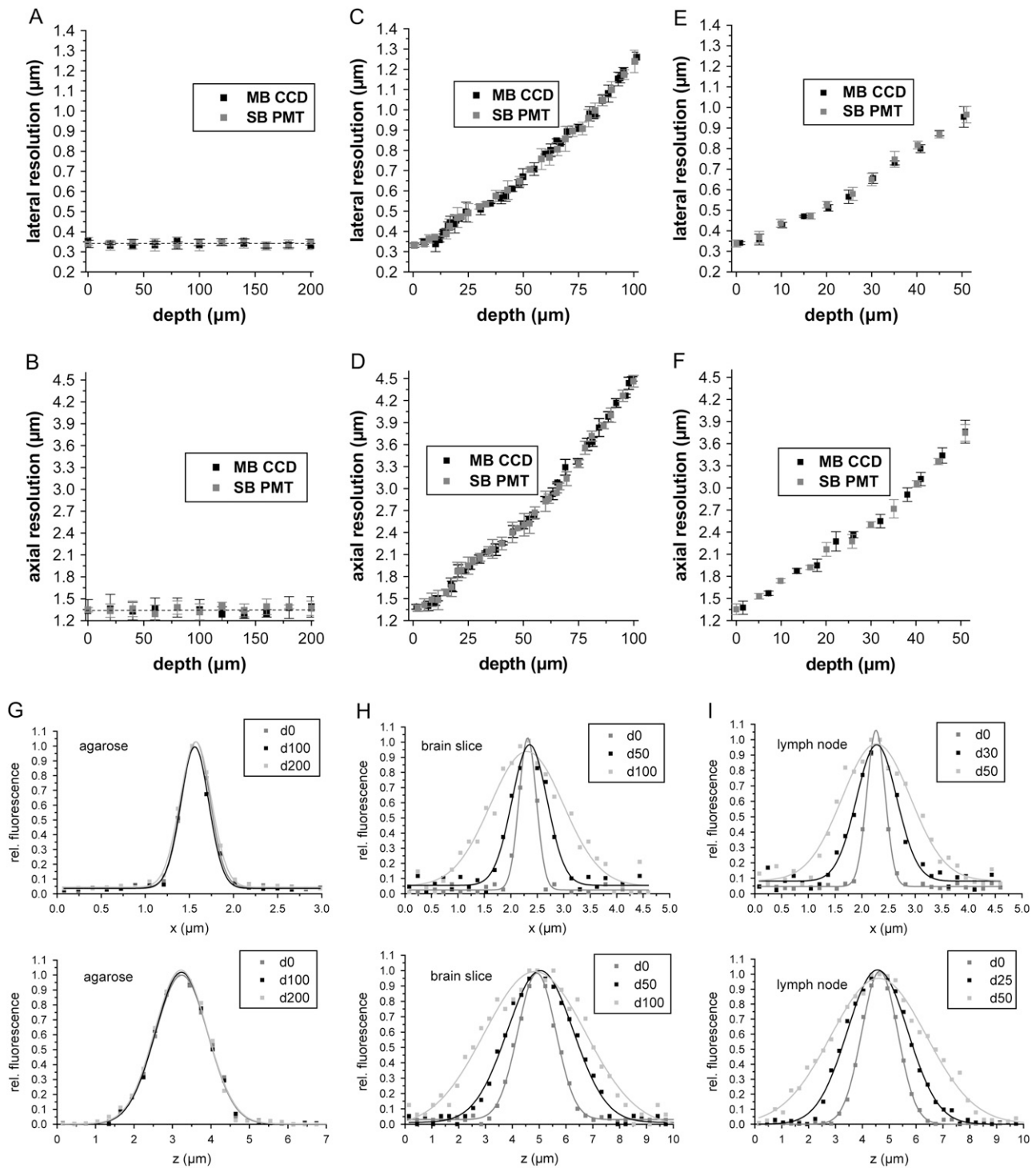


FIGURE 1 Dependence of the spatial (lateral and axial) resolution on the penetration depth measured in (A and B) agarose, (C and D) brain tissue, and (E and F) lymph nodes with both the single-beam PMT and the multibeam CCD setup. Typical lateral and axial profiles of experimental ePSF are shown in three different depths for (G) agarose, (H) brain tissue, and (I) lymph node. The ePSF were measured using green fluorescent beads (emission maximum 515 nm) excited at 800 nm. Each value of the spatial resolution was calculated as the average over 6–15 data points.

tissue constitution, which varied strongly even within the same sample (Figs. 1 and 2). To quantify this effect, we comparatively measured the dependence of the spatial resolution on the penetration depth in lymph nodes and OHBS in regions con-

taining either mainly axons or somata. Representative results are depicted in Fig. 2. Importantly, the decrease in resolution was independent of the detection device. Laser powers of 3 mW/beam were used in all ePSF experiments within biological

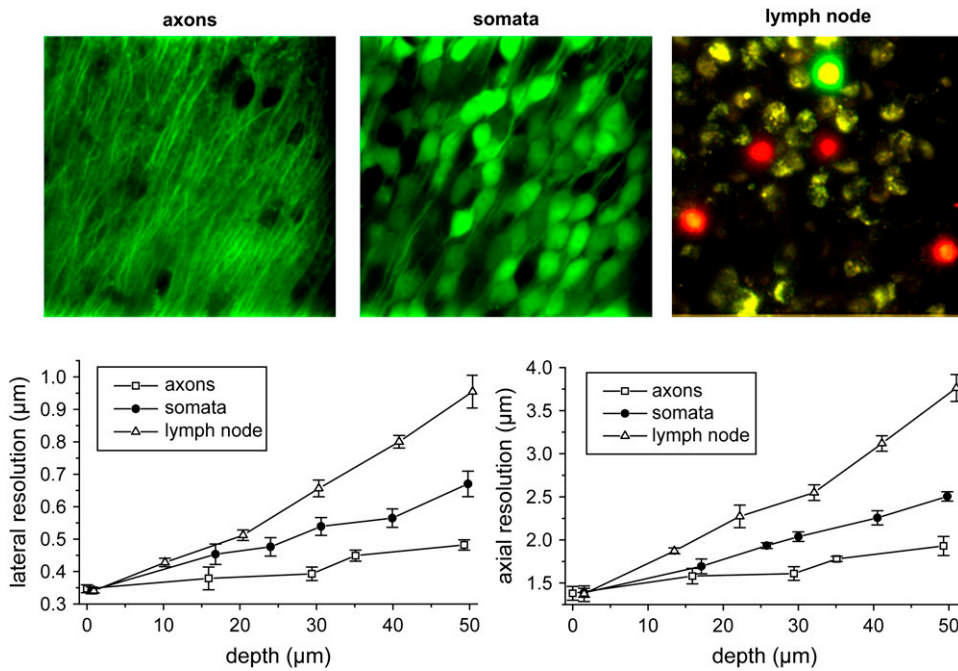


FIGURE 2 Dependence of the spatial resolution on the penetration depth in lymph nodes and in brain slice regions containing axons and somata, respectively. The ePSF experiments were performed with green fluorescent beads (emission maximum 515 nm) using the multibeam CCD setup at 800 nm excitation wavelength. Images show representative pictures of brain slices from Thy-1-EYFP transgenic animals or lymph nodes from wt animals where red and green leukocytes had been adoptively transferred before imaging. Please note the abundance of cell bodies in lymph nodes (either from transferred red or green cells or from endogenous autofluorescent cells) and brain regions with somata, whereas axon-rich brain areas display a relatively low number of (*black*, i.e., EYFP-negative) cell bodies.

samples, no matter which detection method was used. The pixel time for CCD-based measurements ranged between 12 and 21 μ s, whereas that for PMT measurements was between 70 and 160 μ s/pixel. Thus, the PMT images were acquired by scanning significantly more slowly to collect enough signal per pixel.

Deconvolution with depth-dependent ePSF

Mathematical postprocessing of fluorescence images leads to a considerable gain of information and optical quality. One of the most efficient techniques is the three-dimensional deconvolution of raw data, i.e., z -stacks of fluorescence images, with corresponding PSFs (22). Currently, three-dimensional deconvolution is performed using a constant PSF either calculated from the technical data of the microscope or evaluated from the fluorescence three-dimensional signal of a punctiform object, usually measured in an ideal sample such as agarose. However, we observed that the PSF was not a constant parameter but rather was strongly influenced by the constitution of the sample and by the penetration depth (Fig. 2). This insight gave rise to the question of whether a three-dimensional deconvolution performed with a depth-dependent PSF typical for the imaged sample would lead to an improvement of the postprocessed data as compared to the currently used three-dimensional deconvolution techniques.

Thus, we imaged a region of a 78- μ m-thick OHBS that was fixed between two coverslips, from both sides. In this way, we collected two mirrored three-dimensional stacks of the same region, so that the first image (Fig. 3 *F*) at the surface of one stack corresponded to the last image (Fig. 3 *C*),

i.e., deepest layer, of the other. This allowed imaging the same region within a biological tissue either through 75 μ m of overlying tissue (the usual approach in deep tissue *in vivo* imaging) or directly from the other side. Thus, we could also produce the same picture without any tissue layer disturbing the image, giving the optimal result obtainable within this sample. Moreover, we measured the depth-dependent ePSF in both three-dimensional stacks, so that for each fluorescence image the corresponding ePSF was known (Fig. 3, *A–C*, *F*). The ePSF used for deconvolution was averaged within each xy plane but was specifically taken in each z -position.

As expected, increasing penetration depth degraded both the resolution and the optical quality of the fluorescence images (Fig. 3, *A–C*). Even if images *C* and *F* in Fig. 3 show the same OHBS area, because of scattering, the quality of image *C* collected through 75 μ m of tissue is considerably lower than that of image *F*, which was collected through only 3 μ m of tissue from the opposite side of the sample.

By three-dimensional deconvolution based on the ePSF measured in agarose, which corresponded to the calculated PSF, the amount of detail was not evidently larger than that in the original image (Fig. 3, *C* and *D*), although the noise increased dramatically (Fig. 3, *D* and *G*). Three-dimensional deconvolution based on the penetration depth-dependent ePSF of brain tissue delivered an even higher optical quality than the direct image of the same area, which was collected through only 3 μ m of tissue (Fig. 3, *E* and *F*). Thus, postprocessing using the depth-corrected PSF can generate images from planes deep inside tissue with a resolution comparable to that obtained by imaging near the surface.

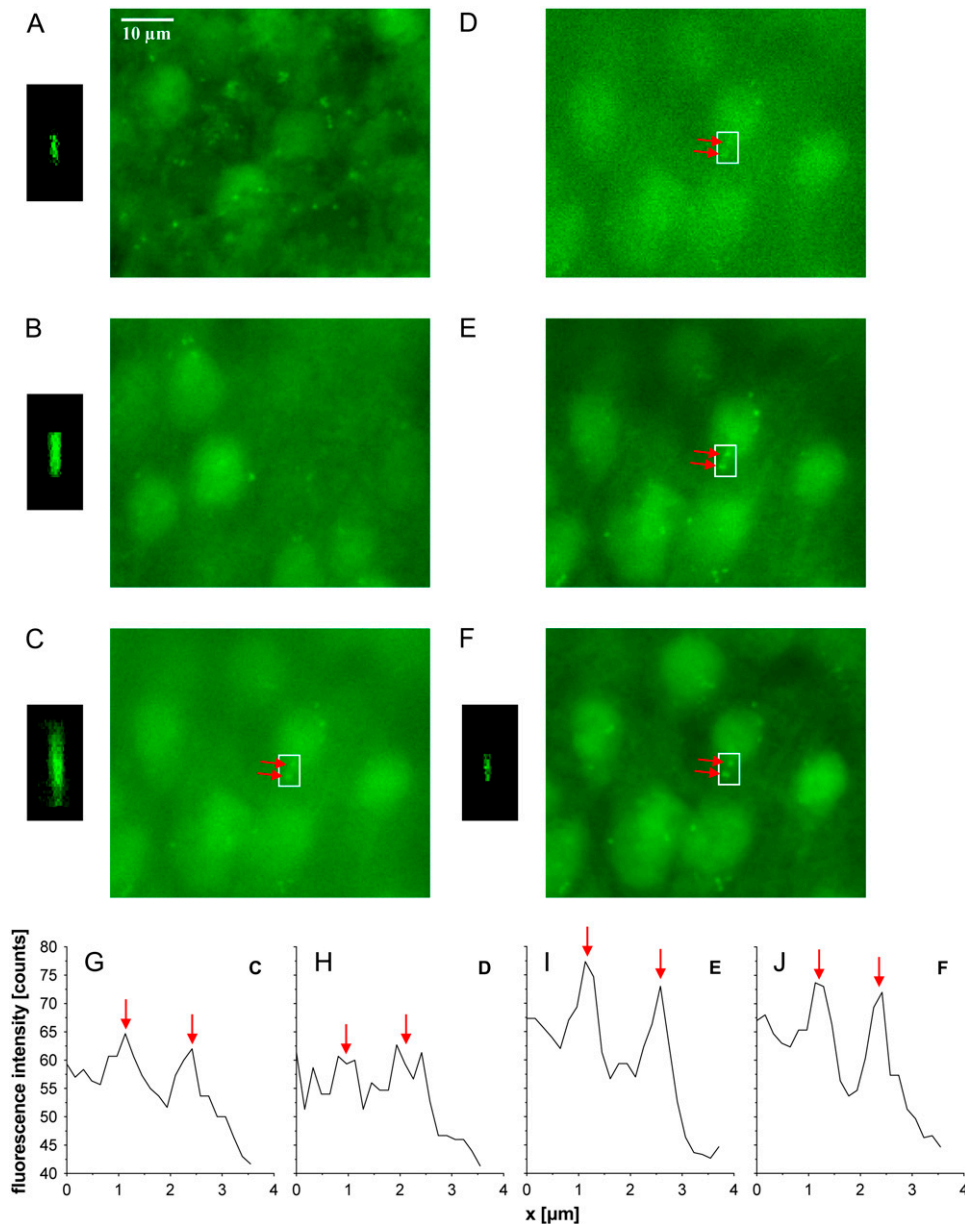


FIGURE 3 Deconvolution with depth-dependent ePSF allows restoration of images from deep tissue layers to the quality level of surface data. Fluorescence images of a 78- μm -thick brain slice and corresponding xz cross sections of the in situ measured ePSF: (A) at the surface, (B) in 37 μm depth, and (C) in 75 μm depth. (D) Three-dimensional deconvolved image of C using the ePSF measured at the surface (identical to the ePSF measured in agarose). (E) Three-dimensional deconvolution of C using the ePSF measured in 75- μm depth. (F) The same layer as C but imaged from the other side of the brain slice, i.e., through a brain tissue layer of only 3 μm thickness. The diagrams G, H, I, and J represent intensity profiles along a line through the two bright spots indicated by red arrows in the images C–F. For optimal deconvolution, the heights of maxima as well as height of the minimum have to be as close as possible to the “perfect” image in F. The experiments were performed using the multibeam CCD setup at an excitation wavelength of 800 nm. The z -step between two consecutive optical slices was 500 nm.

Maximum penetration depth and SNR

Many relevant biological phenomena happen at a considerable depth within highly scattering biological tissues. Thus, the maximum penetration depth at which useful dynamic, high-resolution images can still be generated is a central feature of tissue imaging devices.

Thus, we measured the maximum penetration depth in OHBS, both with the multibeam CCD and with the single-beam PMT setup. The maximum penetration depth reached ~ 500 μm for the single-beam PMT setup and ~ 300 μm for the multibeam CCD setup. Consequently, the fluorescence signal strongly decreased with increasing penetration depth independent of the detection device. However, this decrease was more rapid for the multibeam CCD than for the single-beam PMT system (Fig. 4 A).

It is evident that the maximum penetration depth is reached when the fluorescence signal decreases to the level of the background noise and, thus, cannot be distinguished from it any more. The parameter that defines the relation between the fluorescence signal and the background noise is the SNR, which in maximum penetration depth reaches the value 1 (SNR = 1) by definition.

With the multibeam CCD setup, the SNR value of 1 was reached at 310 μm depth, whereas with the single-beam PMT setup this happened at 510 μm depth (Fig. 4 B). It is noteworthy that down to a penetration depth of ~ 150 μm the SNR values were similar for both setups, and the reduction of the SNR was moderate; i.e., the SNR decreased 45% in both systems within the first 150 μm of penetration into the sample. Loss of SNR was accelerated at higher depths. In the

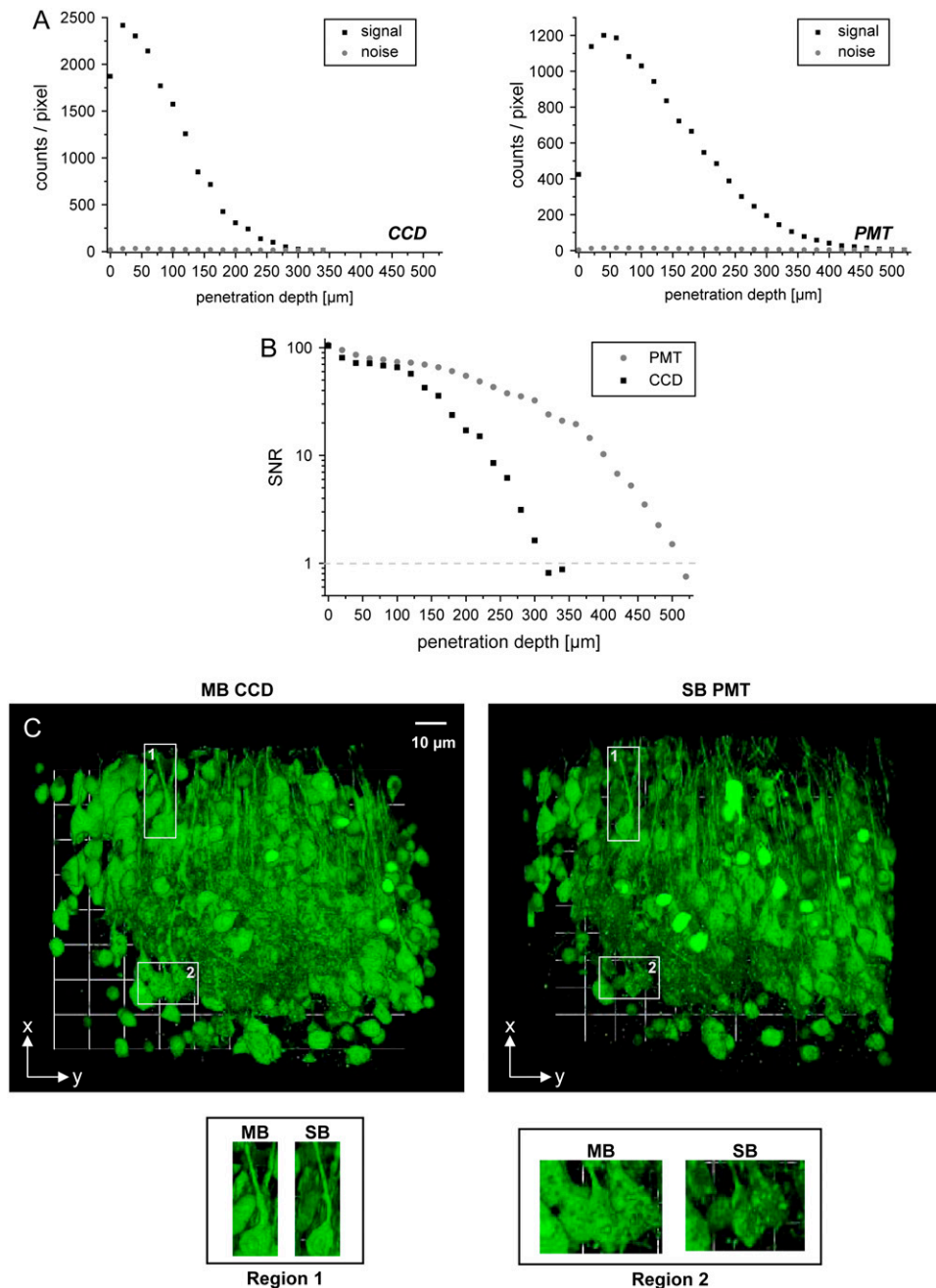


FIGURE 4 (A) Dependence of the fluorescence signal and of the background noise on the penetration depth measured with the multibeam CCD or single-beam PMT setup. Because of the truncation of the PSF at the sample surface, the fluorescence signal in this depth is lower than that at 20 μm depth. (B) Dependence of the SNR on the penetration depth. The z -step between two consecutive optical slices was 2 μm (imaged region $300 \times 300 \mu\text{m}^2$). (C) Comparison between the multibeam CCD and the single-beam PMT setup on the example of a three-dimensional reconstruction of an EYFP brain slice region. A Thy-1-EYFP brain slice of 166 μm thickness was imaged either with the multifocal CCD or the single-beam PMT setup and subsequently voxel-rendered with a 1- μm z -spacing. The small images show zoomed views of two identical regions in both stacks, revealing almost identical optical performance and content. The excitation wavelength was 920 nm in all experiments.

range 150–300 μm depth, 96% of the SNR was lost with CCD and only 71% with PMT detection (Fig. 4 B). This was the main reason for the higher penetration depth of the PMT detection method. Consequently, within depths of 150–200 μm , CCD and PMT performed equally well. As a result, images obtained from both devices in this region show a comparable degree of optical content and resolution (Fig. 4 C). Fluorescence images of a 166- μm -thick sample of a brain slice obtained with the single-beam PMT setup appeared only slightly crisper (Fig. 4 C).

A laser power of 2 mW/beam was chosen for all SNR experiments. The pixel time used for CCD-based imaging

was 6 μs /pixel (pixel size $322.5 \times 322.5 \text{ nm}^2$), and that for single-beam excitation with a PMT as detector amounted to 5 μs /pixel (pixel size $293 \times 293 \text{ nm}^2$). The scanned sample region was $300 \times 300 \mu\text{m}^2$ in both cases.

Imaging speed

Thus, the main advantage of the single-beam PMT setup over the multibeam CCD device is the larger penetration depth in strongly scattering samples because of a better SNR gradient (Fig. 4). However, besides imaging in deep tissue, visualizing the dynamics of biological phenomena represents

an equally important challenge for bioimaging (11,23). In terms of imaging speed, the multibeam CCD technique is evidently superior to the state-of-the-art PMT method. To obtain images of equal quality and dynamic range, a $150 \times 150 \mu\text{m}^2$ area was imaged within 5000 ms with the single-beam PMT setup and within only 83 ms with the multibeam CCD setup. Thus, CCD detection has a clear advantage over the single-beam PMT when high imaging speed is relevant. A laser power of 2 mW/beam and pixel times of $0.4 \mu\text{s}$ (pixel size $322.5 \times 322.5 \text{ nm}^2$) for the CCD and $27 \mu\text{s}$ (pixel size $293 \times 293 \text{ nm}^2$) for the PMT were used, similar to the SNR experiments. Imaging depths between 0 and $50 \mu\text{m}$ were taken into account.

To quantify the speed of the multibeam CCD system at the outermost limit, we imaged the fluorescence of blood flow in vessels of living mice two- and three-dimensionally, in one color and in two different spectral channels, simultaneously (Fig. 5). Although for the single-color experiments only one CCD camera was necessary, for the dual-color experiments fluorescence was imaged onto two synchronized CCD cameras after being spectrally separated by a dichroic mirror.

By this approach, individual cellular and subcellular fragments of blood (erythrocytes, white cells, and platelets) could be visualized in almost natural (i.e., round) shape, and many individual steps of white cells rolling on the surface of vessels were captured (Fig. 5 A, *movies 1* and *2*). In rolling cells, subcellular structures could sometimes be resolved, making it possible to observe barrel rolling of the cell body over the vessel surface (Fig. 5 C, *movie 5*).

Because the applied intravital dye Rhodamine-6G slowly diffused out of the blood vessels, it also stained cells in the surrounding connective tissue. Thus, this approach allowed simultaneous visualization of the $\sim 100\times$ slower autonomous three-dimensional movement of cells in tissue, next to the fast transport of cells in blood vessels (Fig. 5 B, *movie 3*). The two-color image sequence shows individual rolling steps of cells in different colors separated from other cellular blood components that were still well resolved and appeared in yellow (Fig. 5 C, *movies 5* and *6*). Three-dimensional rendering allowed reconstruction of whole cell bodies in the free bloodstream. However, because of the fast transport, these cells appeared distorted (Fig. 5 D, *movies 3, 4, and 7*). In addition, in two-color three-dimensional experiments, we reached the border of technical feasibility with this setup because after spectral separation the SNR in both channels was close to the value of 1, making it difficult to separate the signal from background noise.

DISCUSSION

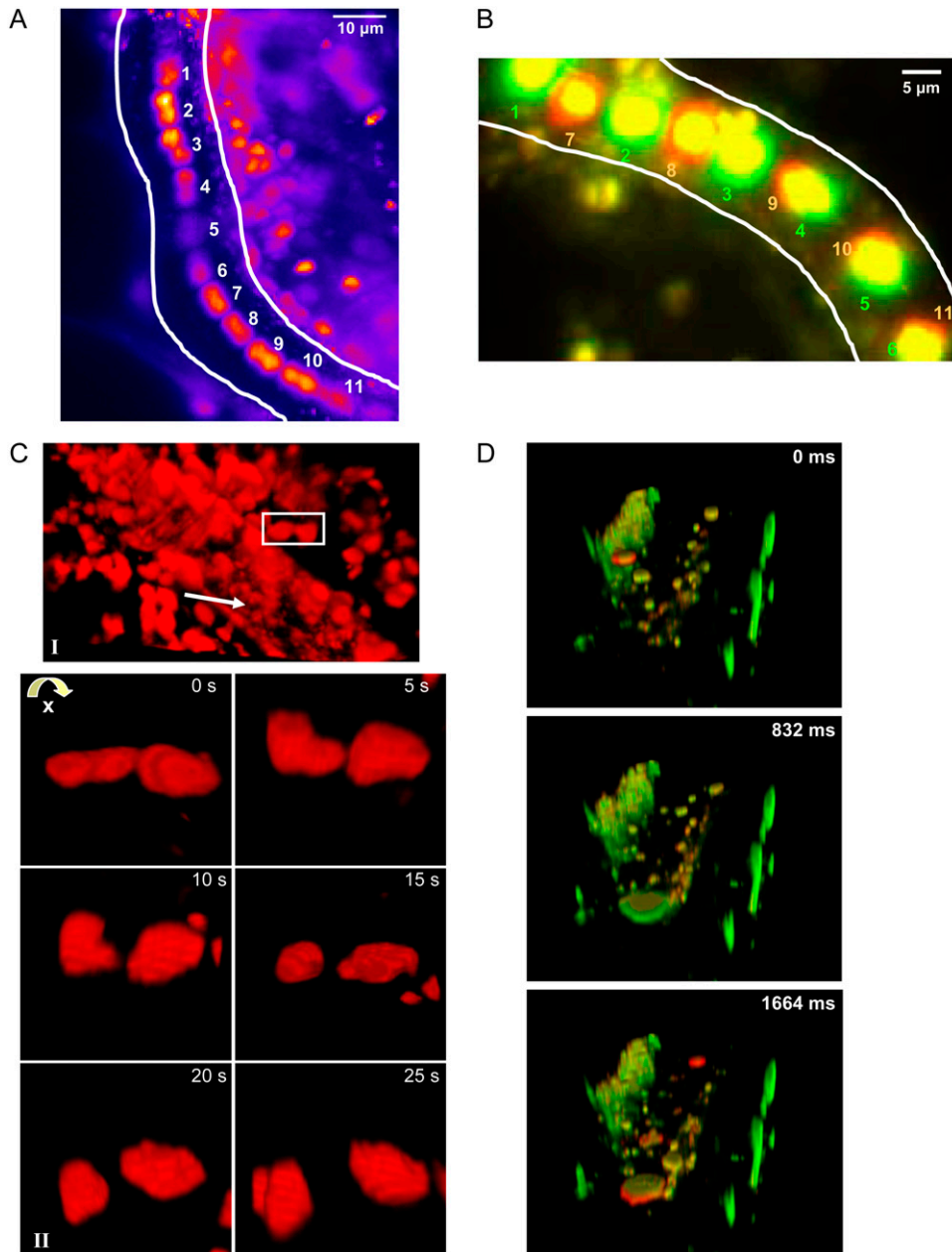
MPM of live cells in explanted tissues or living animals today is a rapidly developing field (6). Consequently, imaging hardware is also developing apace. In particular, tunable Ti:Sa lasers as light source have seen an enormous improvement from early machines, which covered a com-

plete laboratory desk and required an expert to change the wavelength, to contemporary travel-bag-sized turn-key systems that provide a wide tuning range and easy-to-use computer interfaces for control. Also, the output power of these lasers has increased dramatically. Current models provide $>2 \text{ W}$ average power at 800 nm emission, and the most recent developments will provide as much as 2.5–3 W including $>1 \text{ W}$ at wavelengths of $>900 \text{ nm}$.

As a result, conventional single-beam scanheads have built-in attenuators that decrease the laser power reaching the sample, typically by 99%, to avoid bleaching and thermal sample destruction. The multibeam scanhead used in this study distributes the available laser power onto up to 64 beams, which is only 1.7% per beam. This is still enough for efficient two-photon excitation but below the destructive level for most applications. Consequently, the laser generally runs at full power, and thus, much more fluorescence light per time is generated.

However, multifocal illumination requires whole-field detection of the fluorescence with a CCD camera. Thus, it was necessary to compare the optical performance of this method with the usually applied PMT detection of single-beam scanning setups. It was generally assumed that detection with a CCD would be inferior to PMT detection because there is no method to suppress scattered photons (11). We were, therefore, surprised to find that neither the ePSF nor the loss of resolution with imaging depth showed differences for both detection devices down to imaging depths of $200 \mu\text{m}$ in optically dense tissue. Our experiments show that the development of the SNR is responsible for the differences in maximum penetration depth. Although the SNR value for the CCD decayed more rapidly than that of the PMT, it was still well above 1 at $200 \mu\text{m}$, where signals are lost in the background noise. Only in very deep regions ($>310 \mu\text{m}$) was the CCD no longer able to differentiate signals, a point that was not reached for the PMT until $500 \mu\text{m}$ imaging depth. Because the majority of imaging studies record cellular movements at $100\text{--}200 \mu\text{m}$ below the surface, e.g., of lymph nodes (24–26) or the brain (27,28), our work shows that in this area CCD detection is equivalent to PMT detection. Additionally, CCD detection will benefit from more powerful lasers, which will enhance the SNR and thus make it possible to reach deeper regions, although this can not be expected for PMT because of phototoxicity issues. Because the scanhead used here can run PMT or CCD detection, it is not necessary to choose one system. Instead, the optimal detection device can be used for each problem under investigation.

Our study also demonstrates that the resolution of two-photon imaging in biological tissues is a function not only of imaging depth but also of the environment where imaging is performed. In brain areas where axons are predominant, loss of resolution was much less pronounced than in areas with high numbers of somata. The most difficult tissues studied here were lymph nodes, which destroyed the depth-dependent two-photon ePSF very rapidly. This argues for the concept



Time delay between two consecutive z -stacks was 5 s. Images were taken from movies 3 and 4. (D) Three-dimensional representations of the dual-color fluorescence of a blood vessel in a mouse prepared as described above at three different time points. The time delay between two consecutive z -stacks was 800 ms. The z -stacks used for the three-dimensional representations contained 16 frames each, separated by $2 \mu\text{m}$. Images were taken from movie 7. In all experiments: minimum exposure time = 28 ms, excitation wavelength = 800 nm. The minimum delay between two consecutive images was limited by the readout time of the CCD chip.

that tissues with a predominance of cell nuclei, such as brain in regions with somata but especially lymph nodes, where $>1 \cdot 10^6$ nuclei are located within $\sim 1 \mu\text{l}$ volume, are particularly difficult for deep-tissue imaging. Thus, it was very encouraging to find that poor-quality images from deep regions could be deconvolved efficiently to an image quality that can usually be obtained only directly below the surface of tissues.

We demonstrate here that this deconvolution is possible only if an ePSF that corresponds to the imaged tissue and, especially, the imaged depth is used for image restoration. Deconvolution based on a general ePSF calculated for the optical setup produced unusable results, as already attempted elsewhere (29). Unfortunately, currently available deconvolution software does not account for depth-dependent PSF. In addition, mathematical deconvolution is still very time

FIGURE 5 Imaging blood flow in mice in real time with a multibeam CCD setup. Dual-color images were detected simultaneously with two independent CCD cameras based on color splitting by a 570-nm-cutoff dichroic mirror. (A) Time projection over 11 single-color two-dimensional fluorescence images of a blood vessel and surrounding tissue stained by i.v. injection of Rhodamine-6G. The time delay between two consecutive numbers was 50 ms. Shown is a cell doublet rolling on the surface of the vessel (*white outlines*). Images were taken from movies 1 and 2. (B) Time projection of 11 dual-color two-dimensional fluorescence images of a blood vessel (*white outlines*) stained with Rhodamine 6G (*yellow*). Spleen cells previously stained either with CFSE (*green*) or CTO (*red*) and additionally injected into the mouse are represented green and red, respectively, because they were detected by only one of the two CCD cameras. The fact that blood cells stained with Rhodamine-6G only appear yellow indicates their simultaneous detection in both cameras and thus proves the synchronicity of the system. The green numbers indicate the position of a CFSE-stained cell at six different time points, whereas the red numbers indicate the position of a CTO-stained cell at five subsequent time points. The time delay between two consecutive numbers is 50 ms. Images were taken from movies 5 and 6. (C I) Three-dimensional visualization of the fluorescence of a blood vessel and surrounding tissue-resident cells, which were stained with Rhodamine 6G as described above. (C II) Image series representing the two cells framed in C I at six different time points during a 180° rotation around the x axis. The z -stacks used for the three-dimensional representation contained 21 frames each, separated by $1 \mu\text{m}$.

consuming, making it difficult to reconstruct multichannel, multistack time series. Software development to overcome these barriers would thus be desirable. Future work needs to show whether typical tissue-type- and depth-related ePSFs can be obtained and used for deconvolution or whether ePSFs must always be specifically determined for the investigated sample. Even if this turns out to be necessary for optimal image quality, it is not required to provide artificial sub-resolution particles within the sample. Instead, our experience shows that the use of small endogenous structures as a reference is possible.

Finally, we could demonstrate the potential of fast two-photon imaging. This allowed us to visualize autonomous movements of perivascular cells in time and space. The identity of these cells is currently unclear. Based on their shape and size, macrophages or lymphocytes appear likely. It will be very interesting to see the change in migratory behavior of these cells when a local trigger, e.g., injury or infection, occurs.

However, even this setup was not able to reconstruct the three-dimensional shape of freely flowing blood cells satisfyingly. This was based on reaching the technical limits. At the given staining protocol and illumination regime, single erythrocytes or leukocytes did simply not produce enough fluorescence photons to allow for even shorter illumination time, which would be the basis for more rapid *z*-stacks. Thus, future developments should improve the brightness of labels. Also higher laser power or the use of even more beams in parallel will enable faster image acquisition times. Finally a rapid and reliable *z*-stepper could be obtained by fixing the distance between object and lens and shift the focal plane by moving the tube lens rather than the objective. This would avoid motion and compression artifacts and allow for rapid *z*-scanning.

In summary, we have shown here that multifocal illumination opens the way to fast, yet highly accurate, two-photon microscopy. Future developments will prove the power of this approach for biomedical research.

SUPPLEMENTARY MATERIAL

To view all of the supplemental files associated with this article, visit www.biophysj.org.

This study was supported by the Deutsche Forschungsgemeinschaft (SPP 1160 (GU 769/1-1 and GU 769/1-2) to M.G.) and by the German Ministry for Education and Research (BMBF, Bioprofile) to M.G., H.S., and V.A. We thank Christof Maul for critical reading of the manuscript.

V.A. and H.S. work for LaVision Biotec GmbH, Bielefeld, Germany, which produces the multiplexing scan-head TriMScope used in the experiments presented in this work.

REFERENCES

- Lichtman, J. W., and J. A. Conchello. 2005. Fluorescence microscopy. *Nat. Methods*. 2:910–919.
- Sumen, C., T. R. Mempel, I. B. Mazo, and U. H. von Andrian. 2004. Intravital microscopy; visualizing immunity in context. *Immunity*. 21: 315–329.
- von Andrian, U. H., and C. M'Rini. 1998. In situ analysis of lymphocyte migration to lymph nodes. *Cell Adhes. Commun.* 6: 85–96.
- Halin, C., M. J. Rodrigo, C. Sumen, and U. H. von Andrian. 2005. In vivo imaging of lymphocyte trafficking. *Annu. Rev. Cell Dev. Biol.* 21:581–603.
- Gunzer, M., C. Weishaupt, A. Hillmer, Y. Basoglu, P. Friedl, K. E. Dittmar, W. Kolanus, G. Varga, and S. Grabbe. 2004. A spectrum of biophysical interaction modes between T cells and different antigen presenting cells during priming in 3-D collagen and in vivo. *Blood*. 104:2801–2809.
- Cahalan, M. D., I. Parker, S. H. Wei, and M. J. Miller. 2002. Two-photon tissue imaging: seeing the immune system in a fresh light. *Nature Rev. Immunol.* 2:872–880.
- König, K. 2000. Multiphoton microscopy in life sciences. *J. Microsc.* 200:83–104.
- Denk, W., J. H. Strickler, and W. W. Webb. 1990. Two-photon laser scanning fluorescence microscopy. *Science*. 248:73–76.
- Helmchen, F., and W. Denk. 2005. Deep tissue two-photon microscopy. *Nat. Methods*. 2:932–940.
- Hasan, M. T., R. W. Friedrich, T. Euler, M. E. Larkum, G. G. Giese, M. Both, J. Duebel, J. Waters, H. Bujard, O. Griesbeck, R. Y. Tsien, T. Nagai, A. Miyawaki, and W. Denk. 2004. Functional fluorescent Ca²⁺ indicator proteins in transgenic mice under TET control. *PLoS Biol.* 2:E163.
- Germain, R. N., M. J. Miller, M. L. Dustin, and M. C. Nussenzweig. 2006. Dynamic imaging of the immune system: progress, pitfalls and promise. *Nature Rev. Immunol.* 6:497–507.
- Reichardt, P., and M. Gunzer. 2006. The biophysics of T lymphocyte activation in vitro and in vivo. *In Cell Cell Communication in the Nervous and Immune System*. B.Schraven, E.Gundelfinger, and C.Seidenbecher, editors. Springer-Verlag, Berlin. 199–218.
- Larson, D. R., W. R. Zipfel, R. M. Williams, S. W. Clark, M. P. Bruchez, F. W. Wise, and W. W. Webb. 2003. Water-soluble quantum dots for multiphoton fluorescence imaging in vivo. *Science*. 300:1434–1436.
- Nielsen, T., M. Fricke, D. Hellweg, and P. Andresen. 2001. High efficiency beam splitter for multifocal multiphoton microscopy. *J. Microsc.* 201:368–376.
- Rueckel, M., J. A. Mack-Bucher, and W. Denk. 2006. Adaptive wavefront correction in two-photon microscopy using coherence-gated wavefront sensing. *Proc. Natl. Acad. Sci. USA*. 103:17137–17142.
- Gu, M. 2000. *Advanced Optical Imaging Theory*. Springer, Berlin.
- Hell, S. W., G. Reiner, C. Cremer, and E. H. K. Stelzer. 1993. Aberrations in confocal fluorescence microscopy induced by mismatches in refractive index. *J. Microsc.* 196:391–405.
- Török, P., and F.-J. Kao. 2002. Point-spread function reconstruction in high-aperture lenses focusing ultra-short laser pulses. *Optics Comm.* 213:97–103.
- Squire, J., and M. Müller. 2001. High resolution nonlinear microscopy: A review of sources and methods for achieving optimal imaging. *Rev. Sci. Instrum.* 72:2855–2867.
- Kano, H., H. van du Voort, M. Schrader, G. van Kempen, and S. W. Hell. 1996. Avalanche photodiode detection with object scanning and image restoration provides 2–4 fold resolution increase in two-photon fluorescence microscope. *Bioimaging*. 4:187–197.
- Diaspro, A., G. Chirico, F. Federici, F. Cannone, S. Beretta, and M. Robello. 2001. Two-photon microscopy and spectroscopy based on a compact confocal scanning head. *J. Biomed. Opt.* 6:300–310.
- Conchello, J. A., and J. W. Lichtman. 2005. Optical sectioning microscopy. *Nat. Methods*. 2:920–931.
- Kurtz, R., M. Fricke, J. Kalb, P. Tinnefeld, and M. Sauer. 2006. Application of multiline two-photon microscopy to functional in vivo imaging. *J. Neurosci. Methods*. 151:276–286.

24. Bajenoff, M., B. Breart, A. Y. Huang, H. Qi, J. Cazareth, V. M. Braud, R. N. Germain, and N. Glaichenhaus. 2006. Natural killer cell behavior in lymph nodes revealed by static and real-time imaging. *J. Exp. Med.* 203:619–631.
25. Castellino, F., A. Y. Huang, G. tan-Bonnet, S. Stoll, C. Scheinecker, and R. N. Germain. 2006. Chemokines enhance immunity by guiding naive CD8+ T cells to sites of CD4+ T cell-dendritic cell interaction. *Nature*. 440:890–895.
26. Qi, H., J. G. Egen, A. Y. Huang, and R. N. Germain. 2006. Extrafollicular activation of lymph node B cells by antigen-bearing dendritic cells. *Science*. 312:1672–1676.
27. Nimmerjahn, A., F. Kirchhoff, and F. Helmchen. 2005. Resting microglial cells are highly dynamic surveillants of brain parenchyma in vivo. *Science*. 308:1314–1318.
28. Davalos, D., J. Grutzendler, G. Yang, J. V. Kim, Y. Zuo, S. Jung, D. R. Littman, M. L. Dustin, and W. B. Gan. 2005. ATP mediates rapid microglial response to local brain injury in vivo. *Nat. Neurosci.* 8:752–758.
29. Shimizu, K., K. Tochio, and Y. Kato. 2005. Improvement of transcutaneous fluorescent images with a depth-dependent point-spread function. *Appl. Opt.* 44:2154–2161.
30. Neumann, J., M. Gunzer, H. O. Gutzeit, O. Ullrich, K. G. Reymann, and K. Dinkel. 2006. Microglia provide neuroprotection after Ischemia. *FASEB J.* 20:714–716.
31. Feng, G., R. H. Mellor, M. Bernstein, C. Keller-Peck, Q. T. Nguyen, M. Wallace, J. M. Nerbonne, J. W. Lichtman, and J. R. Sanes. 2000. Imaging neuronal subsets in transgenic mice expressing multiple spectral variants of GFP. *Neuron*. 28:41–51.